
# Politecnico di Torino

Master's of Science in Environmental and Land Engineering
A.a. 2021/2022
Graduation Session December 2021

# Modeling the Role of the Cryosphere in the Definition of Ground Temperature in an Alpine Permafrost Area

In collaboration with Arpa Piemonte

**Supervisor:**
Prof. Jost von Hardenberg
**Co-supervisors:**
Dr. Christian Ronchi
Dr. Luca Paro

**Candidate:**
Yara Hammoud

# Acknowledgements

I would like to express my sincere gratitude to my thesis supervisor Prof. Jost von Hardenberg for accepting me to work on this thesis under his supervision. His invaluable expertise in the topic and research methodology inspired my work throughout the thesis. His continuous support, counseling and encouragement cleared the way for me to be able to work on my own under the shadow of his knowledge.

I would like to thank Dr. Christian Ronchi and Dr. Luca Paro for giving me the opportunity to work under their co-supervision in collaboration with ARPA Piemonte. Their valuable presence and assistance was a foundation for the success of this work.

My ultimate gratitude and endless appreciation goes to my parents, Hanadi and Kassem, for their irreplaceable support and motivation during the whole journey. Thank you for all that you have done to allow this achievement to happen. Your presence in my life is something I will always cherish.

# Abstract

The abundant existence of permafrost in the Alpine region leads to the need to understand permafrost characteristics in the area, given the context of rapid climate change and its potential impacts on permafrost and its containing environments. Understanding the processes involved in permafrost degradation and active layer thickening requires studying the governing energy regime. This is done by properly tuning and applying physically based models to simulate the occurring processes and to model the parameters of interest, such as the snow cover and surface soil temperature. The focus of this research work is to appropriately model the thermodynamical processes governing the evolution of the cryosphere, namely the snow layer and to investigate its role in defining the ground temperature in the presence of permafrost. It aims to provide a better understanding of the role of the surface energy balance in a permafrost-dominated area, at Passo del Monte Moro, Italian Alps.

The study is done at a point-scale by utilizing a state-of-the-art hydrological model (GEOtop), with a complete representation of the thermodynamical processes controlling the evolution of the snow layer. In its full configuration, GEOtop is a complete distributed hydrological model, with coupled water and energy budgets, while here it used in its 1D mode at a single point. The evaluation extends over the period from August 2012 till August 2018. Initial setting of the model was achieved by including the accurate sky view factors and topographic aspects of the area. Studying the thermodynamic processes and setting the physical parameters in each module aided the proper tuning of the model. The model results are assessed against measured snow depth and surface ground temperature at Passo del Moro monitoring station, and they show good agreement for most years included. The initial realization of model results shows that the accuracy of meteorological input data is an integral part of a successful simulation of the snow depth. This was overcome by correcting the precipitation input data by different methods, using real snowfall and wind speed data, leading to great improvement in the accuracy of model results. A sensitivity analysis is also done to determine the most important parameters affecting GEOtop model outcomes. The highlighted parameters that resulted are the threshold temperature for discriminating rain and snowfall, the parameterization equation of incoming longwave radiation and a snowfall correction factor, all having important impacts on snow depth variations including the accumulation and melting trends.

**Keywords**: Hydrological Models, Permafrost, Surface Energy Balance, Snow Depth, Ground Surface Temperature, Precipitation

# Contents

# Table of Figures

# Table of Tables

# Chapter 1

## Introduction and Motivation

The cryosphere plays a vital role in moderating Earth's climatic system, including its main components such as the snow layer and the permafrost. Considering its spatiotemporal dynamic nature, its implications on atmospheric, hydrological, and hydro-geological modelling are important. Accurately demonstrating the snow cover in models at all scales is an essential, yet challenging part of modelling owing to the complication of the snow physics (Dong, 2018). The snow cover system is numerically defined by several non-linear processes that interact among each other. The quantification of these processes mathematically is not a simple task and is an integral part of modeling in the context of climate change.

This chapter presents an extensive literature review, discussing the relation of the cryosphere with the surface energy balance, the hydrological cycle and the economy in general. A specific focus is given to the snow layer and to the permafrost, specifically in high mountain and remote areas. The impacts of climate change on the cryosphere are also presented. Attention is given to the Alpine region climatic conditions and consequences of climate changes on permafrost in that area.

## 1.1 Snow and the Climate

Snow covers on average around 46 million square kilometers of surface every year, forming the greatest component of the cryosphere by extension, and most of which is located within the Northern Hemisphere (NSIDC, 2020). It plays a huge role in regulating the global surface energy balance (SEB) and governing earth's hydrological cycle (Liston, 1999). The global radiation balance in turn drives Earth's atmospheric circulation system, and thus the whole climate.

The unique physical properties and other characteristics of snow are the reason behind its major control over the climate. Snow generally has very high albedo values, varying between 80 and 90 percent, as compared to other natural surfaces on earth. For instance, surfaces with trees, plants or bare soil reflect not more than 25% of incoming sunlight (Kotak et al., 2015). Another vital characteristic of snow is its thermal conductivity. Snow is one of the best natural insulators, having a significantly lower thermal conductivity than most other natural substances. When surfaces like land, inland waters or man-made constructions are covered with snow, the heat allowed to flow from them to the atmosphere is highly decreased. The value of this parameter is significant in several fields of study, like studies related to climate modelling, permafrost areas and most importantly in predicting the changes in snow precipitation in the context of climate change (Sturm et al., 1997). The seasonality of snow appears in its spatial and temporal variability which is yet another factor considerably affecting the climate. This means that the area covered by snow and the depth of snow changes noticeably between seasons and inter-annually. One example with major global impacts is the Northern Hemisphere, where the area of the average monthly snow cover varies from 7% to 40% during the yearly cycle. This results in making the snow cover the fastest varying large-scale surface component on earth (Hall, 1988).

Regarding the relation between the snow cover and the climate, a positive snow feedback exists: the warming of the climate causes decline in the snow cover areas, which in turn reduces the albedo or reflectance of the earth surface, and consequently increases the energy absorbed by the earth, hence increasing the temperatures even more. Cess et al. (1991) suggest that other feedbacks such as cloud interaction and longwave incoming radiation may also interfere in the snow feedback and cause amplification of the warming.

The temperature of ground below a snow cover is a function of many aspects of the overlying snow such as the time of snowfall, the duration of events, the depth of the snow layer, the accumulation and compaction of this layer and the melting process involved (Zhang et al., 2000). The low thermal conductivity of snow renders it a great natural insulator falling between the atmosphere and the ground below it. Despite this, other characteristics of the snow like the date of snowfall and time of melting govern whether it will act as a cooler warmer to the ground below it (Luetschg et al., 2008).

The snow layer undergoes accumulation, compaction and melting processes on a seasonal basis. Snow densification or compaction may lead to change of the type of snow into firn and then ice crystals thus changing some of its properties (Meyer et al., 2020). This transformation occurs gradually over time and differently over space and is eventually one other complication of the nature of snow. The snowmelt occurrence leads to release of latent heat by which the snow in this case acts as a heat sink (Zhang et al., 2005). The snowmelt process intervenes in the hydrological cycle through providing surface water and may have harmful effects on it such as risks of flooding and erosion (Zeinivand and De Smedt, 2009). Alterations in the cryosphere directly affect the hydrological cycle in the area by shifting the discharge maxima in time (Beniston et al., 2018). This means that for snow in mountain areas, not only the concerned area will be affected, but also farther areas due to changes in water availability and water storage. Consequences on agriculture and hydropower production also prevail, hence indirectly affecting the socioeconomic system in mountain areas.

Mountain areas are the most prone to the accelerated environmental changes and the cryosphere has the greatest share of responsibility in this regard (Gobiet et al., 2014). For example, the European mountain cryosphere, among several other regions in the world, is faced with temperature warming which leads to a shift from snow precipitation to liquid precipitation in some cases, and thus induces the movement of the seasonal snow lines to higher elevations. This situation also results in a shorter period of the snow season. In the Alps region, numerous studies have reported a decrease in snow depth over the years, varying between significant reductions at low heights and less major declines at high elevations (Marty, 2008; Scherrer et al., 2013; Matiu et al., 2021). While the major cause for the snow depth reduction is the warming of Earth, it has been suggested that atmospheric circulation patterns at the large scale also have an impact on the snow depth in European mountains (Bednorz 2004). One example is the North Atlantic Oscillation, where its warm phase is one of the factors causing lower depths of snow in European Alps (Gobiet et al., 2014).

## 1.2 Permafrost Overview

Permafrost is a part of the lithosphere and can be defined as ground material having a temperature that remains at or below 0 °C at least for two consecutive years. Permafrost areas occupy around 20 million square kilometers of Earth's surface, seafloor and glacial areas (Gruber, 2012; Murton, 2021), and it can exist on land or below oceans. A considerable part of existing permafrost is located in mountain areas such as the European Alps. Its temperatures can be as low as around -10 °C like in the Arctic. The upper layers are known to have considerable amounts of ground ice. Permafrost layers can exist with a wide variety of depths, ranging from a few meters to as thick as 1400 m (Romanovsky et al., 2002). A permafrost layer can be either continuous where it fully covers a specific area, or discontinuous where some parts are thawed during some times of the year mainly due to average temperatures. The thermal state at the surface of permafrost is a result of climatic and microclimatic processes. It is governed by the main components of Earth's energy balance which are incoming shortwave radiations, outgoing shortwave and longwave radiations, and latent and sensible heat fluxes (Stocker-Mittaz, Hoelzle, and Haeberli, 2002). The climate has powerful impacts on the spatial and temporal distribution of permafrost around the world, and permafrost responds in several ways to climatic changes that are faced in the recent years. On the other hand, permafrost existence also has a great effect on the environment holding it. It interferes in the water and energy budgets. The hydrological cycle in permafrost areas becomes a lot different than other areas. It has an impact on microclimatology and water storage as well. Permafrost existence lowers the ability of soil water flow vertically and decreases the amount of water possible to be stored (Vorosmarty et al., 2001).

### 1.2.1 Permafrost-Atmosphere Interactions

The active layer is the top part of the permafrost that thaws during summer seasons and freezes up again during winter months. When defining permafrost, this layer is technically not included in the permafrost but is directly above it. It is the main layer that interacts with the atmosphere in a mutual manner. This layer incorporates most of the hydrological processes. It controls the groundwater flow processes, gas exchanges and vegetation conditions. The active layer is regulated mainly by air temperature, but also by other elements such as snow cover or other surface cover, organic layer thickness and soil water content (Zhang et al., 2005). The set of interactions that occurs between these elements results in many changes in the active layer. Permafrost has high sensitivity to climate changes. Studying the thermal state of permafrost has been increasing for the past years, and further studies

aim at understanding the existing volumes of permafrost ice (Beniston et al., 2018). Permafrost interacts not only with the atmosphere but with the climate as a whole, with surrounding ecosystems and eventually with human infrastructures. The importance of studying permafrost variations is mainly because of the safety issues it provokes to human infrastructure, hydrologic cycle and the ecosystem, but also partly because of the fact that the active layer is an excellent indicator of climate change as well (Smith and Riseborough, 1996).

Atmospheric warming in the past years has caused considerable degradation in permafrost extent, known as permafrost thaw, as well as an increase in the thickness of the active layer (Serreze et al., 2002). The upper part of the permafrost has the most ice content and this leads to pronounced effects of the slightest thaw of permafrost. Alterations in the active layer thickness have vast impacts on the SEB and on the hydrologic cycle. This raises major concern when considering permafrost in mountains and sloping areas due to the risks of slope stability that it provokes.

The impact of the active layer thickness changes extends also to interfering with the carbon exchange between land and the atmosphere. It is worth mentioning that permafrost layers contain massive amounts of stored organic carbon and methane which are released upon thawing of the permafrost. Carbon contained in permafrost sums up to about twice the amount of carbon existing in the atmosphere (Natali et al., 2021). This carbon was formed tens of thousands of years ago from organic materials (debris of animals and plants) and has been stored in permafrost which provides a cold environment suitable for protecting this organic carbon. Thaw of permafrost allows the decomposition and release of organic carbon into the atmosphere, contributing to the well-known and all-time environmental problem of greenhouse gas emissions (Chen, Liu, and Moore, 2020). The rise in atmospheric temperature induces permafrost thaw which in turn releases considerable amounts of carbon and methane previously stored in it. Consequently, the amplification of the global temperature warming means that a positive feedback mechanism loop by permafrost exists. In areas like the Artic which used to be a carbon sink, there is a major concern of it turning into an emitter of carbon and other greenhouse gases due to the increased rate of permafrost thawing in the area (Schuur et al., 2015).

Furthermore, ecological and biogeochemical processes that occur throughout land containing permafrost are all altered when the active layer thickness is modified (Jorgenson et al., 2001). This means that the growth rate and spatial extent of existing vegetation in the area is also altered, changing

the whole ecosystem productivity. Ecosystem diversity is also strongly impacted. Permafrost declination means the melting of the ground ice within the layer. This increases the water table which has adverse effects on trees or other plants in the area (Jin et al., 2020). In the Arctic for instance, the thaw of permafrost affects the existing lakes and alters their ecosystems and creates new water bodies as well. Release of organic matter upon permafrost thaw can be dissolved or particulate matter and combined with other factors such as the existing stratification, this could control the amount of greenhouse gases released in opposition to that dropped in the downstream flows (Vonk et al., 2015). This presents a problem to the downstream existing aquatic systems and urges more research to quantify the magnitude of these effects on the underwater ecosystems.

### 1.2.2 Alpine Permafrost

The climate in the Alpine region of Europe is subject to huge variabilities in space and in time, and climate features in the area are essential study topics, having impacts on the local and global climate. The Alpine mountains are characterized by unique climatic gradients, recurrent heavy precipitation events and the distinctive snow and ice cover with its immense power on regulating all phenomena occurring in the region. Permafrost underlies around 6000 square kilometers in the Alps, which sums up to more than the area occupied by glaciers. The abundant presence of permafrost underlain areas in the Alpine region affects the evolution of other systems in the area.

Permafrost in the Alps region is distinguished by having high spatial variability, and this is mostly due to the topography of the mountains there (Gruber and Haeberli, 2007), properties of the surface and the ground (Schneider et al., 2012; Nan, Li, and Liu 2002). The elevation, slope of the mountains, and the aspect are all factors that interfere in the incoming shortwave radiation onto the permafrost zone thus intensifying the spatial variability of permafrost at high elevations. The snow cover is also one main actor among those which affect the permafrost conditions through its insulation characteristic and the meltwater provided onto the permafrost (Park et al., 2015). The microclimate also affects the thermal stability of the permafrost, promoting the spatial variability in its characteristics. The type of the surface overlying the permafrost layer has an effect on its thermal state as well. For example, snow cover would have high albedo values while vegetation or bare soil would have low albedo values and would provide less insulation to the permafrost layer (Froese et al., 2008).

Studies on permafrost variations due to climate change have been thriving for many years now (Haeberli and Beniston, 1998; Jorgenson et al., 2010; Schuur et al., 2015; McGuire et al., 2018). The driver behind this research is the risk that permafrost thaw and active layer thickness reduction impose on the hydrologic cycle and corresponding water availability, slope stability, human infrastructure, tourism, economic sector in densely populated mountain areas, and the ecosystems. The significance of permafrost in highly elevated areas like the Alps extends to numerous aspects. First is the sensitivity of the hydrologic cycle in mountains to even small changes in the permafrost due to climate change (Swenson et al., 2012). Permafrost can modify the hydrological cycle in many ways, including mainly surface and subsurface water fluxes (Walvoord et al., 2012). Thaw of permafrost provokes earlier runoff and shorter time of tolerance to rainfall events. Other processes like evapotranspiration and water storage are also altered. This has an impact on the sediment flow budget and geomorphological processes in mountainous areas (Gruber and Haeberli, 2007). The most direct impact of permafrost presence and variations on humans is related to natural hazards caused by slope instabilities and debris movement due to permafrost thaw (Dramis et al., 1995). The Alps contain large touristic areas which need to be maintained and protected to avoid disasters. The presence of permafrost at or around these regions poses risks to the safety of these environments. This makes the expansion of these sites more difficult from the construction point of view and urges continuous maintenance of the infrastructure already existing.

Existing engineering structures in the Alps and specifically in permafrost areas are already affected by permafrost thaw and active layer thickness variations. Usually, any subsurface alterations imply risks on existing structures and mountain areas in the Alps are highly prone to such dangers. The impacts expected could be soil creep leading to subsidence and raising problems on safety of structures, which might have differing design safety factors than the current situation urges (Bommer, Phillips, and Arenson, 2010). The topography in high altitude areas is already challenging to engineering practices of construction due to dominance of course sediments. Hillslope susceptibility to landslides is highly increased due to permafrost thaw. This is technically explained by geotechnical changes in the characteristics of materials forming the slopes, some of which include decline in cohesion effects (Patton, Rathburn and Capps, 2019). Several landslides, debris flow and rockfall events have been reported over the years due to permafrost thaw (Dramis et al., 1995; Huscroft et al., 2003; Haeberli et al. 2017; Patton, Rathburn and Capps, 2019). These are becoming more and more problematic as they tend to increase in frequency and occur regularly following thaw events. As the intensity of permafrost

thaw is increasing, the magnitude of such natural hazards escalates as well. Mitigation efforts for avoiding slope instabilities and consequent natural hazard are highly needed in touristic areas such as in the Alps.

Permafrost ecosystem is a combination of the cryogenic ecosystem in high mountains in the Alps, along with the occurring variations related to water and heat exchange processes (Walker et al., 2003). Presence of permafrost is an important factor in the ecological balance of alpine systems, having the power to affect the life cycle and quality of vegetation in Alpine pastures. Permafrost ecosystems are highly sensitive to permafrost degradation that occurs due to climate warming, especially when it has high ice content (Li et al., 2017). The main links between permafrost degradation and the ecosystem are the water and heat exchanges that occur with the soil that beholds the vegetation. Characteristics of the soil are altered, such as the soil water content, and consequently the nutrient concentration and distribution (Yang et al., 2010). This in turn modifies the life cycle of all species that are inhabited in these cold environments and leads to ecosystem succession and eventually its degradation.

The relation between permafrost and vegetation is an interdependent one, whereby both have effects on each other (Yi, Woo and Arain, 2007). Presence of permafrost imposes low temperatures in the ground where the roots of vegetation extend, and it limits their extension into deeper layers, while at the same time aiding in accumulation of organic materials in that area. Permafrost is also a vital provider of soil moisture for the vegetation. As for the role of vegetation in this mutual relation, the vegetation can act as a shading cover for the underlying permafrost, reducing the risk of permafrost thaw and allowing permafrost cooling (Runyan and D'odorico, 2012). Other advantages to the presence of vegetation above permafrost exist, such as the fixation of soil reducing the risks of erosion and moderating the soil-vegetation water balance (Qin et al., 1987). An alarming factor in regard to the permafrost ecosystem in mountain areas is its relation to greenhouse gases. A study by Kittler et al. (2017) has shown that the uptake capacity of permafrost to carbon dioxide has decreased over years.

## 1.3 Climate Change Impacts on the Cryosphere

The cryosphere is a sensitive system to climate changes and mainly to the warming in temperatures, and its state poses critical feedbacks on the climatic system as well. Cryosphere includes all ice bodies such as sea or lake ice, permafrost, snow cover and glaciers (Goodison et al., 1999). Studies have

shown degradation in all cryosphere bodies due to climate warming (Robinson, Dewey and Heim, 1993; Zhang et al., 2003; Vuille et al., 2008; Murton, 2021).

Research on the high mountain cryosphere and its relationship with climate change has been studied since decades ago and has increased a lot in the recent years (Barry, 1985; Fitzharris et al., 1996; Atkinson et al., 2006; Huss et al., 2017; Adler et al., 2019; Murton, 2021). The aim is always to evaluate the extent of changes in the cryosphere, to quantify its impacts on several aspects of life and to predict the future changes that might occur. Problematic issues include reduction in depth of snow cover, glacier retreat, ice sheets melting, permafrost degradation and active layer increase in thickness.

Etzelmüller et al. (2020) found that over the past 20 years permafrost areas across Europe have warmed not only at the surface, but as deep as 50 m and more. The temperature changes detected range between 0.4 °C and 1.5 °C. A more alarming indicator is the thickness of active layer, which was found to have increased by 10% at some sites, and by a staggering 200% at other sites, as compared to the beginning of the study 20 years earlier. The biggest changes in the active layer were seen in the Alps region. The implications of this in the Alps mainly rise from the threats on infrastructure, natural hazards especially close to densely populated or touristic areas, and the impact on the water supply and runoff downstream. This intensifies the need of broadening the knowledge about permafrost presence, its extent, its thermal conditions, and its ice content. A study by Duvillard et al. (2019) estimates the damages to ski resorts in the French Alps that occurred because of permafrost thaw in the area. Out of around 1000 human-made structures, 24 were severely damaged and the estimate of maintenance costs consequently required sums up to be in the order of millions of euros.

### 1.3.1 Climate Change in the European Alps

For the past decades, the alpine region has experienced changes in its climate, both on a decadal scale and following the patterns of the long-term global climate change. In the period between around the year 1900 up until the year 2000, the annual mean temperature in the European Alps region has increased by around 2 °C (Auer et al., 2007). The temperature rise was mainly concentrated in the period after the year 1980, which was a result of greenhouse gas emissions combined with water vapor during that period. This rate of increase was about two times that in the northern hemisphere as an average. It is remarkable that this temperature change was not spatially varying in the Alpine region. However, changes in precipitation in that period occurred spatially as well. Little precipitation

increases where seen in the north-western area of the Alpine region, whereas the south-eastern parts faced a reduction in precipitation amounts (Brunetti et al., 2006).

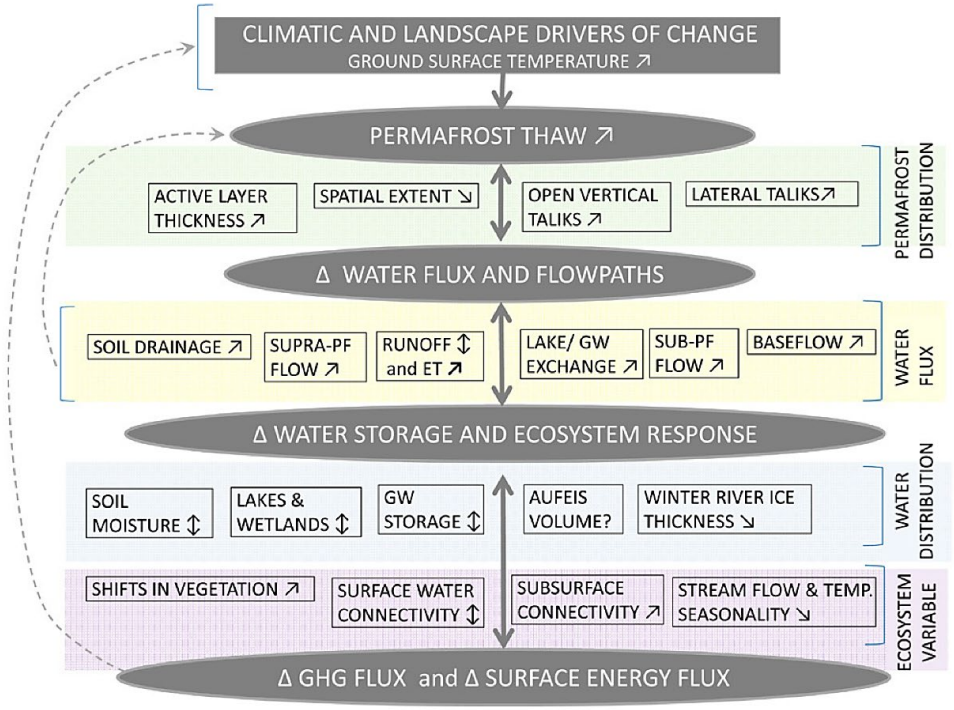


Figure 1 Impacts of Permafrost thaw on the hydrological cycle (Bui, Lu and Nie, 2020)

A foremost concern is the influence of temperature changes on permafrost in the Alps. As mentioned before, permafrost underlies a great part of the European Alps including high mountain areas. Degradation of permafrost changes the surface and subsurface water fluxes, alter groundwater flow regimes and water storage, increases supra-permafrost flow, causes time shifts in runoff expected, interferes in greenhouse gas fluxes at the surface and alters the energy balance (Bui, Lu and Nie, 2020). A detailed description of the impacts of permafrost thaw mainly on water fluxes and its responses to climate change is presented in *Figure 1*. Problematic issues that could arise include slope instability, mass movements, landslides, debris flow and alteration of sediment transfer. A study by Stoffel, Tiranti and Huggel (2014) presents several cases of mass movements that have occurred in different regions of the Alps. A pattern of events has shown that debris flow and landslides are more likely to occur in spring and fall seasons than in summer, due to the unprecedented heavy precipitation events that are experienced during these months. The rate of movement of permafrost and glaciers governs the volumes of debris associated in these natural hazards. The current movement rates and the simulated

future ones might cause larger impacts than ever seen before (Chiarle et al., 2021). Natural hazards are expected to increase in frequency as well.

Climate change has also shown effects on precipitation and temperature extremes in the Alps (Gobiet et al., 2014). Extreme rainfall events are distinctively dangerous due to their potential to cause natural hazards and damages to human infrastructures. Unexpected high amounts of precipitation cause huge volumes of runoff which can turn into floods in some areas. In populated areas, man-made structures might not be designed to handle such amounts of rainfall and would thus fail to cope with extreme precipitation events. This would mean huge losses on the societal and economic levels. Several events of extreme rainfall were recorded in the Alps region (Norbiato et al., 2007; Awan and Formayer, 2017). Observations over the past years show more intense precipitation in the Alps, such as in the Italian Alps during the last century (Turco et al., 2013).

Thus, this subject is of high relevance in the Alps region and studying the reasons behind these occurrences is also vital for future reference. Studies have shown that causes of precipitation extremes in the Alps are mainly due to orographic mechanisms, which means precipitation events that are caused by high moisture concentrations in the atmosphere (Gobiet et al., 2014). The original problem is the warming of the air which increases its capacity to hold moisture. Other possible factors for heavy precipitation episodes exist and are generally related to the complicated processes that occur within the hydrological cycle. Pall, Allen and Stone (2007) suggest that alterations in the atmospheric stratification could be another possible factor.

Extreme temperatures in the Alps are also a major concern due to the impact that temperature has on the cryosphere in this area. The last 2 decades have experienced unexpectedly warm seasons (Brönnimann et al., 2018). Studies have linked the drought periods in the Mediterranean area to winters with low rainfall amounts in south of Europe. Atmospheric circulation then pushes the phenomenon to the north of Europe leading to summers with very high temperatures in Europe (Vautard et al., 2007). Such changes are expected to occur in the future and probably more severely, yet they are still hard to predict accurately and require more and more research and simulations to be done.

As climate change is expected to continue and escalate even if immediate action was taken, research always aims to anticipate future climatic behaviors. This is critically important in the cases of extreme

precipitation and extreme temperatures (Zappa and Kan, 2007). The use of regional and global climate models allows continuous efforts to be made in this regard. Predicting future weather extremes is an essential part of planning infrastructure construction especially in touristic regions in the Alps. Regional climate models have been used to anticipate seasons with extreme temperatures (Coppola et al., 2021). The simulations might not be able to quantify exactly the temperatures to be expected, yet statistical measures can give clues about the times of when to expect heat waves (Beniston, 2007).

As part of the cryosphere, glaciers in the Alps region are also highly affected by climate change. Observations have detected glacier retreats and fragmentation for many years now (Sommer et al., 2020). The impacts of rapid degradation are strongly negative downstream the glaciers. High risks of natural hazards are imposed in the region where the retreats occur. These include activation of avalanches and occurrence of landslides with vast amounts of materials involved. Fast formation of new lakes is also one of the associated consequences. The disadvantage of these rapidly formed lakes is predominantly linked to their thermal energy. The result is a positive feedback process whereby further melting of the glacier is induced and more lakes are formed. Other natural hazards could be related to huge rockfalls that occur due to glacier retreats when glaciers are present in a sloping area.

### 1.3.2 Permafrost Monitoring

In the most recent research on permafrost there are currently some major concerns including the search for advanced methods to evaluate the extent of permafrost thaw and monitor the processes occurring. There is also the constant search for mitigation and more importantly adaptation solutions to minimize the negative impacts of permafrost thaw on human infrastructure components, the hydrological cycle, the greenhouse gas permafrost feedback and on ecosystems.

Since the 1980s, research has been done for the sake of delineating and predicting the existing permafrost areas and several models have been proposed for the regionalization of permafrost (Sellman et al., 1980; Nelson and Outcalt, 1987; Granberg and Vachon, 1998). As climate change impacts have become more pronounced and the need for monitoring their impacts arose, research on methods for monitoring permafrost and active layer variations commenced. At first, measuring the ground temperatures and checking the depth changes of the active layer were the methods used to measure the extent of permafrost thaw (Smith and Riseborough, 1996, Smith et al., 2005). Measurements of temperature in permafrost layer were done either manually on monthly or quarterly

basis. After that, measurements were possible by dataloggers connected to weather stations and gave more frequent data recordings.

The use of geophysical techniques later on made a huge advancement in the research field of permafrost and active layer monitoring, allowing to gain insight on the spatial distribution of permafrost, it geophysical properties and its temporal variations. Properties like electrical resistivity, dielectric permittivity and seismic wave velocities in the tested media were key factors in the success of geophysical methods (Kneisel et al., 2008). Some of the most used methods until this day are electrical resistivity tomography, frequency and time domain electromagnetic induction, seismic refraction tomography and ground penetrating radars. Improvements are continuously provided for better spatial representations, more advanced monitoring, and enhanced data processing methods for permafrost sites (Hauck, 2013; Mewes et al., 2017; Sudakova et al., 2021). A study by Lindner et al. (2021) presents the results of years of passive seismic monitoring of a permafrost site in a region in the Alps. The study shows that variations in velocity on a seasonal basis imply the freeze and thaw cycle of the active layer, and a more general trend in decrease of velocity over the years suggest permafrost degradation. This proves the relevance and effectiveness of using passive seismology for monitoring permafrost thaw and performing future predictions. Monitoring of submarine permafrost has been less focused on in the past years but is also advancing with time. A study by Overduin et al. (2012) employed the direct current electric resistivity method to monitor the delineation change in permafrost and its degradation. It proves the efficacy of electrical resistivity methods in monitoring submarine permafrost.

The fact that most permafrost is present in high-mountain areas which could be remote and difficult to reach for applying direct techniques of their measurement, and the fact that they usually spatially extend over large areas, urges the employment of remote sensing techniques for monitoring permafrost thaw and consequent natural hazards (Kääb et al., 2005). Airborne and spaceborne remote sensing technologies are very efficient in these cases. Image classification techniques are used to monitor processes in areas of permafrost or glacier and changes can be detected. Examples of most used remote sensing techniques to monitor permafrost thaw are optical stereo data which are used to produce digital terrain models, laser scanning or synthetic aperture radar (Kääb, 2008). Geographic information systems are combined with remote sensing techniques for the purpose of assessing natural hazards and their risks in remote mountainous areas. A recent study by Gao et al. (2020) proposes a

monitoring and classification method to monitor the spatial distribution of permafrost and its variations. It deploys a passive microwave remote sensing technology and is based on a dual-index algorithm. The results reinforce the importance of remote sensing technologies for monitoring applications and present the potential of improvement that these methods possess. Another study by Park, Kim and Kimball (2016) was the first to utilize satellite microwave remote sensing technologies to observe freeze and thaw cycles for the aim of inferring permafrost extent.

Other new techniques for monitoring permafrost degradation have been applied. Anders et al. (2020) examine the use of terrestrial laser scanning point clouds for computing the extent of thaw subsidence in Arctic permafrost. Another study by Seppi et al. (2019) utilizes thermal and kinematics monitoring of permafrost containing ice into an integrated method to investigate the creeping of permafrost and thus its degradation. Oldenborger and LeBlanc (2018) stress the importance of gathering information about water that is unfrozen in permafrost layers in order to better understand the evolution of permafrost. For this goal, electrical resistivity techniques were employed.

### 1.3.3 Adaptation Methods

As mentioned before, the cryosphere is facing considerable changes due to climate change and imposes impacts on other systems and especially on human-made ones. Permafrost thaw and deepening of the active layer pose great risks to neighboring infrastructure, slope stability, ecosystems and eventually imposes a burden on the economic sector. Countless studies have shown that permafrost degradation has already occurred to a large extent, and active layer thicknesses have increased considerably. This urges action to be taken in a sense to adapt to the impacts that have already taken place due to climate change, thus calling for efforts to be put into adaptation planning.

Plenty of infrastructure were built on ground underlain by permafrost, while not accounting for future impacts of climate change. Degradation of permafrost in these areas implies huge threats to their infrastructures. The aim of adaptation methods and adaptation policies is to help cope with the effects of climate change on such structures and to ensure their integrity. Transportation infrastructure is one of the vital man-made systems socially and economically, and any threats to its integrity must be handled immediately. Ground subsidence and cracking induced by permafrost degradation are examples of the threats to the structural capacities of roads. There are several categories of suggested adaptation methods for infrastructure built on degrading permafrost. These can be categorized into

methods that aim to reduce the heat intake into the permafrost layer, techniques that work by extracting heat from permafrost, and structural methods that act by modifying the design of the structure itself to be able to handle geo-mechanical changes underneath it. Examples of the methods that prevent heat intake by the permafrost, which are techniques that have been implemented, are the passive cooling methods (Doré, Niu and Brooks, 2016). Passive cooling can be achieved by placing surfacing materials characterized by high albedo. These surfaces will cover previously dark paved ones and can considerably decrease the amount of heat transferred to the underlying permafrost layer, which will limit the degradation of permafrost. Polystyrene insulation sheets are also used to prevent heat intake as well. It is worth noting that such methods are used only to delay the rapid degradation of permafrost and cannot totally limit it. For sloping embankments, sun-sheds are used to slow the thaw and to protect the stability of the slopes. The second type is the technologies used to extract heat from the ground in permafrost areas. These include technologies like air convection embankments which constitute a layer of medium-sized aggregates that allows convection in the embankment. Other technologies in this category are air ducts and thermosyphons. The last category includes structural renewal designs that provide more stable and resilient structures. These are mainly employed when preventing the degradation itself is not possible or unfeasible. This could be achieved by integrating geosynthetic reinforcing materials that provide resistance to faults, cracks and subsidence.

Another form of adaptation to changes in permafrost caused by climate change is improving the monitoring networks and hazard mapping applications in areas at risk. A study by Flynn et al. (2019) evaluates the efficacy of hazard mapping in providing information for adaptation policymakers. Increasing the awareness of not only the community planners but also the public in general is a vital step throughout the adaptation process. Planning construction and maintenance should be made with enough information in hand and with knowledge of future expected situations.

## 1.4 Motivation and Research Questions

Understanding the processes involved in permafrost degradation and active layer deepening for the aim of predicting its future behaviors and protecting affected communities is a scientific research topic of concern today (Colombo et al., 2019; Bui, Lu and Nie, 2020; Wani et al., 2021). This is especially true for permafrost existing in high-mountain regions like in the Alpine area, where there is the challenge of a more complex topography. Permafrost thaw imposes massive changes in the hydrological cycle, at the surface and in the subsurface (Woo et al., 2008), puts ground and slope

stability under risk, causes natural hazards including rockfall and debris flow (Stoffel, Tiranti and Huggel, 2014), modifies run-off, changes the ecosystem (Jin et al., 2020) and can contribute to the emission of greenhouse gases (Schuur et al., 2015). The Alps region contains large communities and the impacts of climate change on permafrost negatively affect the livelihood of humans. Modeling of the snow cover and soil surface temperature is a very effective way to analyze permafrost evolution and consequences on the environment. This can be achieved only through properly tuning physically based models to simulate the occurring processes. The accuracy of the data input into models also plays an immense role in the quality of the results and thus this is of major concern in such applications.

This research work aims to provide a better understanding of the role of the surface energy balance (SEB) in a permafrost-dominated area in Passo del Monte Moro, Macugnaga, in the Italian Alps. The main focus is to appropriately model the thermodynamical processes governing the evolution of the cryosphere, namely the snow layer, to investigate its role in defining the ground temperature in the presence of permafrost. The study is done at a point-scale, in a permafrost-dominated area in Passo del Monte Moro, Macugnaga, by utilizing a state-of-the-art hydrological model (GEOtop), with a complete representation of the thermodynamical processes controlling the evolution of the snow layer. In its full configuration, GEOtop is a complete distributed hydrological model, with coupled water and energy budgets, while here it used in its 1D mode at a single point. Through proper tuning of the model, analysis and improvement of the input data and performing simulations, GEOtop was used to model the snow cover and soil surface temperature. The efficacy of this research prevails first in properly setting the model GEOtop for accurate simulations of the snow depth in the Alps region, using simple meteorological data commonly available in measuring stations. This gives potential to future predictions of snow depth in order to analyze the associated permafrost behavior to be expected.

The research questions that were addressed in this work are:

1. What are the main factors for the proper modeling of the snow cover and ground surface temperature in high mountain areas?
2. What is the impact of meteorological data accuracy in modelling of the snow depth and ground temperature in permafrost areas?

### 1.4.1 Thesis Structure

The thesis report is structured as follows:

- In Chapter 2 an overview of hydrological models and their applications is presented. The relevance of hydrological modelling in high mountain areas with permafrost is explained as well. This chapter also describes the model GEOtop, highlighting the most relevant modules and equations.
- In Chapter 3 the research methodology is explained. The methods used for GEOtop model calibration including the relevant modules are mentioned. The input data correction methods are also explained in detail.
- In Chapter 4 the results of the research work are presented, discussed and interpreted. The results consider the calibration phases as well as 3 scenarios corresponding to input data corrections, and a sensitivity analysis on model parameters.
- In Chapter 5 the key findings of the research work are highlighted. In addition, some future research improvements and recommendations are given.

# Chapter 2

## Hydrological Models

Assessing the impacts of climate change requires utilizing models to simulate physical processes and predict future behaviors. In permafrost areas where the presence of permafrost alters the hydrologic cycle immensely and interferes with the surface energy balance, hydrological models are used to evaluate climate change effects. There exists a variety of hydrological models, each having its own functionality, strengths, and drawbacks. In mountain areas, the shortage in data availability due to difficult climatic conditions, and the complex topography lead to critical hydrological systems that require intricate choices of models for their simulation (He et al., 2009). The addition of permafrost to such a complicated environment adds to the complexity of the surface and subsurface hydrological system, not to mention that it also alters the energy budget as well. Thus, hydrological models are sometimes coupled with energy and mass balance models in order to simulate their interrelations and interactions.

This chapter includes an overview on hydrological modeling along with its usability, complexities, and limitations. The ability of coupling hydrological models with other model types is important, specifically for permafrost applications, and is discussed in this chapter. A focus on hydrological models' utilization in permafrost-containing areas is also included. For the purposes of this research work, the model GEOtop, a distributed model of the hydrological cycle coupled with mass and energy balances, is chosen and is used to simulate the snow depth above the permafrost layer and the ground temperature directly overarching the permafrost layer. This chapter also includes an extensive description of the GEOtop model, focusing on the relevant equations to the snow module and energy and water balances.

## 2.1 Review and Recent Applications

Climate change has forced most natural scientific study areas to shift focus to trying to quantify, monitor, assess and predict its impacts. The field of hydrology is closely related to climate change issues as the water cycle is hugely altered due to temperature increase. The integration of hydrological modeling with other scientific areas was essential for studies concerning the changing climate. In permafrost areas, hydrological modeling is critical and its coupling with other modeling types such as mass and energy balance is very useful for a more comprehensive study of permafrost evolution.

### 2.1.1 Basics of Hydrologic Modeling

Hydrological modeling goes back to the 1850s where it started with the rational method which was deployed to calculate peak discharge (Mulvany, 1850). Since then, all the physical knowledge of the hydrological cycle that is present now has started to build up, like Darcy's law, Fick's law, and others. Advancements in hydrological modelling were then introduced, like distributed physical models, stochastic hydrological models and 2D and 3D modelling of surface, groundwater, and infiltration processes (Dhami and Pandey, 2013). The importance of modeling is the huge computational ability that it provides while applying the physical and mathematical concepts of hydrology. Among their variety of purposes, hydrological models can be used for water resource management, modeling of groundwater flow, urban planning, flood control and water management in mountain areas and permafrost-containing areas. Currently, hydrological modelling is a powerful tool for assessing the effects of climate change on many aspects of human life and the ecosystem.

Hydrologic models present a scaled-down simulation of real-life systems that allows quantifying and predicting water resources (Brooks et al., 2012). They represent the relationships between water, soil, land and the climate. Models are usually based on several factors and on naturally occurring physical processes which mainly constitute the water cycle (Jajarmizade et al., 2012). These include processes of precipitation, evapotranspiration, above-surface and groundwater flow, and many others. Hydrological models act spatially in 2D and some in 3D to account for the processes occurring horizontally and vertically, such as water flows and infiltration. They also account for the temporal changes in the systems. Improvements in this field are driven by many factors including the technologies existing today and the ability to integrate geographic information systems and remote sensing findings for the purposes of hydrologic modeling (Singh, 2018). This gives great potential in

terms of studying the impacts of climate change on large scales, in remote areas and areas with initially lower data availability. It is worth stressing that hydrologic models simulate water flows at the surface and below the surface as well, which is useful in many fields especially in permafrost-dominated areas.

There are several ways to categorize hydrological models. However, all the models can be summarized by their simulation, their temporal and spatial distribution, and the logic behind the solution process. One way to distinguish hydrologic models is according to their base, which could be either a physical process, a mathematical formulation, or an analog of a simulated process (Dingman, 2015). Hydrological models can also be categorized into deterministic models, where each parameter is described by a physically based equation, and stochastic models, which rather define their parameters according to probability and provide probability of occurrence of events and their magnitude (Shaw, 2005). Another way to differentiate hydrologic models is depending on the level of spatial detail they provide. They can be lumped, where the catchment is considered as one big body with homogeneous parameters and no internal interactions, or semi-distributed where the study area is divided into rather large segments which interact among each other and possess different parameters, or completely distributed where the area is divided into grid cells which are totally heterogeneous, each possessing its own parameter values and where the model solves the interrelations between all cells (Cunderlik, 2003). Many more ways to categorize hydrological models exist as well, like dynamic or static, linear or non-linear, and so on.

### 2.1.2 Coupled Hydrological Modeling

The field of hydrology today is integrated with numerous other scientific fields to produce a comprehensive understanding of natural systems, their interactions, their performance against climate change and to predict their future behaviours. Hydrologic models can be coupled in a one-way or two-way manner with regional climate models. Although climate simulations have focused more on global climate models in the past, today regional climate models are getting more attention and advancing due to their high relevance to applications in many fields including hydrology (Hay et al., 2006). At the catchment scale in hydrologic studies, climatological information is very essential and is required at the scale of the catchment under investigation. This is one of the reasons for the need of downscaling in climate models. A study by Hay et al. (2006) shows the effectiveness of coupling a small-scale regional climate model, which is able to predict temperature and precipitation at suitable catchment scales, with a hydrological model for the purpose of predicting daily runoff. Yu, Pollard

and Cheng (2006) created a method for coupling a course-grid regional climate model, or even a global climate model with a small-scale hydrologic model. This method allows the use of climate data for hydrological modelling of water bodies such as rivers or lakes, accounting for infiltration and runoff, while at the same time getting the feedback of the hydrological processes for more accurate studying of the climate in the area.

Hydrological models can be also coupled with land surface schemes, allowing the integration of topography effects, soil conditions and the surface energy fluxes with the surface and sub-surface hydrology. This advancement could be very important for applications such as in permafrost case as the energy fluxes play a role as important as that of the hydrologic cycle in the interactions between permafrost, the surrounding environment and the climate. A model integration by Shi et al. (2013) shows that coupling the SEB with a hydrological model improves the forecasting of total discharge and the estimation of evapotranspiration amounts and shows that the water system is highly influenced by changes in the energy fluxes. These realizations stress that coupling of hydrological models with other components is inevitable and is the road to improve this field of study, as many processes in nature are interrelated and possess two-way relationships.

Zeinivand and De Smedt (2010) tackled a similar issue which in specific targets the interrelation between snowmelt and the hydrological cycle along with flood risks. In their study they provide an approach to couple a hydrological model with a physically based one that represents snowmelt and shows its feedback on the hydrologic cycle and thus on water resource management. The snowmelt is represented by a series of processes that occur under the mass and energy balances of the snow. Many other attempts for the mass and energy balance of the hydrological cycle have been presented through well-known models, one of which is used for the purposes of this research work, GEOtop, and which will be presented in detail in the following parts.

### 2.1.3 Model Tuning

The quality of model results is highly impacted not only by the model used, but more importantly by how correctly the model is implemented. This includes the correctness of the input data, as well as the calibration or tuning of model parameters. Especially in hydrological models with coupled water and energy balances, every parameter to be set in the models has an impactful role in the complicated and inter-related formulations solved by the model and have diverse effects on the results. Improper

tuning or calibration of complex models adds to the sources of uncertainty in modelling and can affect the results inversely (Güntner, 2008).

### 2.1.4 Models Applied in Permafrost-Dominated Areas

As mentioned and stressed before, the existence of permafrost, especially in high mountain areas like the Alpine region, strongly impacts the hydrological cycle in the area. In the context of climate change, permafrost degradation and active layer thickness increase pose a more complex hydrological problem in the area. Hydrological models are inclusive and capable tools for assessing the influences of climate changes in these situations. Plenty of hydrologic models have been created and advanced for purposes of understanding permafrost interactions and behaviour, and they have proven effectiveness and accuracy (Kollet et al., 2017). Choosing a model among the many existing models is a challenge to modellers as each model has its own strengths and limitations. It is essential to note that for a successful and comprehensive simulation of permafrost, both surface and sub-surface water balances must be accounted for, and this adds to the criticality of choosing the most relevant model for the purposes of each study.

Many approaches have been implemented in surface and sub-surface hydrological models for permafrost applications. Hydrological models focused on modelling surface hydrology of permafrost seasonal changes can be solved using analytical solutions, that means by applying heat transfer equations (Hayashi et al., 2007). Another applied approach is using numerical solutions such as the finite difference method. On the other hand, models tackling the sub-surface hydrology have advanced a lot in coupling the water and heat budgets in 3D inclusive modalities, which adds an important factor in permafrost modelling that is the surface soil conditions (Sebben et al., 2013). Aside from all the advantages that hydrologic models bring to permafrost simulation, some limitations still exist. For surface hydrological models that apply heat transfer equations, the one-dimensional nature is a drawback as compared to the 3D reality of heat fluxes and exchanges. Moreover, in such models the 3 phases of water are not represented separately which also poses problems when it comes to permafrost existence and simulation. As for sub-surface hydrological modelling, their innate nature disregards the processes that occur at the surface, while in fact these processes exist and have an impact on the subsurface hydrology.

Many models have been formed to simulate permafrost and investigate its changes. There are one-dimensional models that are applied at small scales, and they utilize the heat and water budget equations while accounting for phase changes. These produce results related to depth of permafrost and allow evaluation of its degradation over time (Walvoord and Kurylyk, 2016). Other existing models can be applied on larger scales and have a spatial capacity to forecast discharges of nearby water bodies, but such models do not comprehensively represent the energy surface balance. A third kind of models is mainly one that simulates the sub-surface flows of water and of energy as well, however, might be missing to account for the atmospheric role in the SEB.

### *Topoflow Model*

Among the examples of existing models used for permafrost simulation is the model Topoflow (Schramm et al., 2007). Topoflow is a spatially distributed hydrological model which is process-based. This model accounts for the surface energy budget, the process of accumulation and melting of snow, infiltration, evapotranspiration, groundwater flow and computes the soil water content heterogeneity as well. Despite its simplicity, this model can predict the active layer thickness, although not extremely accurately, but enough for general studies in such areas.

### *AST Model*

Another model used for permafrost applications is the Advanced Terrestrial Simulator (ATS) model. This model tackles surface and sub-surface hydrology, taking into consideration the surface energy balance, freezing and degradation and surface snow complications (Coon, 2016). It provides three-dimensional simulations and results and can be used in presence of permafrost. It was one of the first models to couple surface and subsurface phenomena in permafrost applications, where it applies Richard's equation for solving in the subsurface coupled with the diffuse wave model for solving the surface processes. One of the strengths of this model is the accuracy of simulating snow processes over the temporal scale. The drawback of this model is mainly solving the non-linear systems concerned with the freeze and degradation of permafrost.

### *ECOMAG Model*

An example of a semi-distributed hydrological model is the ecological model for applied geophysics (ECOMAG) (Motovilov et al., 1999). It is physically based and can be used for simulating the water cycle and quality, in arid and cold environments. The model has been applied in permafrost-dominated areas in the Arctic. The model is structured in a way such that the hydrological part is in a separate

sub-model than that of the water quality. It is representative of both surface and sub-surface water flows, infiltration into surface soil and evapotranspiration. ECOMAG is suitable for permafrost areas since it demonstrates accurately the hydrothermal dynamics, comprising the snow cover with its accumulation, compaction and melting, as well as active layer changing aspects and vertical heat transfer. A study by Gelfan et al. (2015) proves how this model is able to produce acceptable results even within the scope of climate change for the hydrological cycle.

### *SWAT Model*

Another example of a semi-distributed and physically based model is the soil and water assessment tool (SWAT) model (Arnold, 1994). This model targets watershed modelling and is very well-known in this field. The original purpose of the model was to assess the effects of land and water use on water availability and eventually in agricultural prosperity. It can operate on a long temporal duration within periods over which the conditions of soil and land management change. It also has the advantage of modelling over large spatial areas. In addition to that, SWAT demonstrates relatively accurately the climate change and ecosystems in the area under study (Dile, Berndtsson and Setegn, 2013). Like the ECOMAG model, in permafrost-containing environments, SWAT accounts for the surface energy budget, snow dynamics, infiltration, spatial variability of soil parameters and subsurface hydrology as well. Modifications to the model can be done regarding its demonstration of the active layer evolution and dynamics, as this model accounts for them only as averages and not precisely (Bui, Lu and Nie, 2020). Moreover, one of the model limitations is the fact that it requires a high number of parameters for its calibration (Arnold et al., 2012). This makes it difficult to calibrate the model and complicates the parametrization procedure, which is why several calibration techniques have been suggested by the authors.

## 2.2 GEOtop Model

As discussed in the previous part, several hydrological models are suitable for modelling the surface energy balance, snow cover and/or soil temperature in permafrost areas. Among the existing and previously applied models, a comprehensive, inclusive, and very well-suited model for this work is chosen. For the purpose of this research work, the open-source state-of-the-art hydrological model GEOtop 2.0 (Rigon et al., 2006; Endirizzi et al., 2014), hereafter referred to as GEOtop, was employed to model the SEB in pointwise mode in order to simulate the snow cover depth and soil ground temperature. In its full configuration, GEOtop is a complete distributed hydrological model, with

coupled water and energy budgets, while here it used in its 1D mode at a single point. GEOtop is inclusive of a complete representation of the thermodynamical processes controlling the evolution of the snow layer, and accounts for all the hydrological fluxes including ones related to energy, snow, and vegetation on the surface. A detailed description of the model is presented in this part, showing its relevance and effectiveness for use in cold, high altitude, complex topography, and permafrost-dominated areas.

### 2.2.1 Model Description

In its full configuration, GEOtop is a distributed, fine-scale, gridded and terrain-based hydrological model that simulates the water and energy balances at and below the ground surface (Rigon et al., 2006; Endirizzi et al., 2014). It illustrates the water flow in a three-dimensional manner on the surface and in the sub-surface. Differently from most other hydrological models, it accounts for the energy exchanges with the atmosphere and accurately deals with the radiative fluxes at the soil surface while accounting for the complex topography. Most relevantly to permafrost modelling, GEOtop is able to demonstrate the particularly non-linear relations between the water and energy budgets while freezing and thawing processes occur (Dall'Amico et al., 2011). It also incorporates a rather recent multilayer snow module, which accurately models the evolution of the snow cover over time, including the water and heat balances in it, simulating thus their impact on the ground soil temperature. GEOtop simulator accounts accurately for the terrain topography, allowing it to be applied successfully in complex terrains.

The model can operate at both point scale or distributed. It takes as input temporal meteorological data in the hourly resolution, specific for the site studied, such as air temperature, precipitation, wind speed and others (Rigon et al., 2006). The resulting output can be customized and can contain several variables such as soil temperature at several depths, snow depth in cases of snow existence, and water content. Thus, it is able to demonstrate the evolution of soil and snow conditions in time from the given meteorological data. The model solves for these outputs by equating the water and energy flow equations. The water and heat (radiant and turbulent) fluxes at the surface with the atmosphere are accounted for as boundary conditions. This is done numerically in the sub-surface, that means the soil layer, and above surface which is represented by the snow cover.

The modelling in GEOtop occurs over a soil volume that is pre-set by the user with a specified depth. The soil column is divided into parallel layers with varying depths. The surface layers are commonly set thinner than the lower ones to account more properly for the high gradients near the surface. Dividing the surface spatially, the resulting parts are called cells.

### 2.2.2 Surface Energy Balance

The energy balance at the surface regulates the variability of the ground temperature spatially and in its evolution over time as well (Westermann et al., 2009). The energy budget is rather dependant on the interactions with the atmosphere overarching the surface. In cold environments with presence of snow, the SEB is governed by the radiation, snow cover, surface vegetation if present, soil water content and atmospheric temperature (Lunardini, 1981). GEOtop can be used to estimate fluxes supposedly important in the SEB, such as sensible heat, latent heat and heat conduction into ground surface (or snow). As mentioned before, the surface energy balance is coupled with the water balance in GEOtop. The general SEB equation can be written as in equation [ 1 ] (Oke, 2002):

$$R_n + H + LE + G - F_{surf} = 0 \quad [1]$$

where $R_n$ is the net radiation on the surface, $H$ is the sensible heat, $LE$ is the latent heat flux, $G$ is the conduction of heat by the ground or snow layer, that means the ground heat flux, and $F_{surf}$ is the surface heat flux exchanged with the atmosphere, in the snow surface layer as a result of melt or freeze of snow.

Coupling the general SEB equation with the water balance results in the equation on which GEOtop formulation of surface balance is based, as shown in equation [ 2 ]:

$$F_{surf}(T_s) = SW_n + LW_n(T_s) + H(T_s) + LE(T_s, \theta_w) \quad [2]$$

where $T_s$ is the surface temperature, which is not known, and all equation variables are a function of it except $SW_n$. $SW_n$ and $LW_n$ are the net short-wave and net long-wave radiations. The latent heat flux ($LE$) is a function of $\theta_w$ which is surface-soil moisture, playing the essential role of coupling the water and energy balances at the surface. The calculation of the turbulent fluxes, that are the latent heat and the sensible heat, is presented in Endirzzi et al. (2014).

*Shortwave Radiation*

Shortwave radiation included in the SEB equation is a net result of the balance between the incoming shortwave radiation $SW_{in}$ and the outgoing shortwave radiation $SW_{out}$. $SW_{out}$ is calculated as seen in equation [ 3 ]:

$$SW_{out} = SW_{in} \cdot \alpha \quad [3]$$

where $\alpha$ is the broadband albedo. The albedo value depends on the surface cover, which could be either with snow or without. If the surface is not covered with snow, the albedo value is calculated as a linear function of the top or near surface soil water content. In case where the surface is covered by snow, the method used in GEOtop to calculate the albedo is taken from Dickinson et al. (1993). This method accounts for several important factors that render it accurate. It considers the intra-snow-event decrease in albedo through time, that is when no fresh snow has fallen. The formulation also deliberates the albedo value by dividing the spectrum into visible and near infrared. It also takes into account the angle at which radiation is received by the surface, which is majorly due to the Mie scattering parameters, and modifies the formula accordingly (Hock, 2003). GEOtop also modifies the albedo value if the snow layer is relatively shallow, by combining the albedo of the snow and of the soil surface below it. The minimum thickness of the snow layer below which the total albedo includes the snow and soil albedo is a parameter that can be calibrated by the modeler.

The shortwave radiation incoming on a flat terrain is a function of the shortwave radiation at the top-of-atmosphere ($SW_{toa}$), and the transmissivity coefficient of atmosphere ($\tau_a$), which is known as the ratio of the incoming shortwave radiation for a clear sky to the $SW_{toa}$, and shortwave transmissivity of clouds ($\tau_c$), which is computed using incoming radiation on a flat surface, being the ratio between value in case of a cloudy sky to that in case of a clear sky. The relation is presented in equation [ 4 ]:

$$SW_{in} = SW_{toa} \cdot \tau_a \cdot \tau_c \quad [4]$$

The top-of-atmosphere shortwave radiation is analytically found as a function of azimuth and the solar height, using the method explained in Iqbal (2012). As for the atmospheric transmissivity, its value is calculated as a product of the transmission coefficients after Rayleigh scattering, after aerosols scattering, and after absorption by gases (including water vapor). The calculation of the transmission

coefficients is explained in Endirizzi et al. (2014). The cloud transmissivity is computed from the input data of incoming shortwave radiation. This same value is used as cloud cover for longwave radiation calculations.

As for the case of a complex terrain, the surface heat fluxes' computation is more complex. The incoming global SW radiation is also calculated using the formula [ *4* ], where the cloud transmissivity is calculated as seen in equation [ 5 ], where c is the cloud cover fraction:

$$\tau_c = 1 - 0.71c \qquad [\,5\,]$$

The incoming SW radiation is divided into two parts, the direct radiation from the sun received by Earth's surface, and the diffuse radiation that has been scattered by the atmosphere and is taken as isotropic. An empirical formula is used to relate the product of the atmospheric and cloud transmissivities ($\tau_a . \tau_c$) to $k_T$, which is defined as the ratio of the hourly diffuse to the global radiation (Erbs et al., 1982). The result of direct radiation is corrected for topography characteristics such as shadowing and the solar incidence angle. The diffuse radiation is a combination of hemispheric part multiplied by the sky view factor, $V_f$. This is a parameter related to the topography, which accounts for the part of the sky that is visible to the point in space where the calculations are being done. It varies from 0, which implies no sky seen from study point, to 1 which means the sky can be fully seen, which is the $V_f$ value for the case of a flat terrain. The other part is one coming from the surrounding terrain.

### *Longwave Radiation*

The longwave radiation term included in equation [ *2* ] is a net result of the balance between the incoming longwave radiation from the atmosphere $LW_{in}$ and the outgoing longwave radiation (emitted by the surface) $LW_{out}$. Each of these 2 values is computed separately. $LW_{in}$ coming from the atmosphere onto a flat terrain, in the case of a clear sky, is computed using Stefan-Boltzmann law as shown in equation [ 6 ]:

$$LW_{in,clear} = \epsilon_a(T_a, e_a) \cdot \sigma \cdot T_a^4 \qquad [\,6\,]$$

where $\epsilon_a$ (-) is the effective atmospheric emissivity for a clear sky, $T_a$ (K) is the surface air temperature, $e_a$ (bar) is the water vapor pressure, and $\sigma$ is the Stefan-Boltzmann constant that is equivalent to $5.67 \times 10^{-8}\ \mathrm{Wm^{-2}K^{-4}}$. For a complex terrain, the incoming longwave is partitioned into incoming from atmosphere, and from surrounding terrain, which is similar to that of the incoming shortwave radiation. For the case of a complex terrain, which prevails in several studies and in the case of this research study site, the incoming LW radiation from the atmosphere is calculated using the formula in equation [ *6* ] multiplied by the sky view factor, $V_f$.

However, for cloudy skies, the incoming longwave radiation formula is as presented in equation [ 7 ]:

$$\mathrm{LW_{in,cloudy\ sky}} = \epsilon_c(T_a, e_a) \cdot \sigma \cdot T_a^4$$

[ 7 ]

where $\epsilon_c$ (-) is the atmospheric emissivity in case of presence of clouds, and its value can be much higher than that of $\epsilon_a$. There are several proposed formulations to equate $\epsilon_c$. In GEOtop, it is computed as presented in equation [ 8 ] which is chosen because it does not require the computation of the cloud-cover fraction which could cause some uncertainties. Alternatively, it uses the provided incoming shortwave radiation through its cloud transmissivity value:

$$\epsilon_c = \tau_c + (1 - \tau_c) \cdot \epsilon_a$$

[ 8 ]

The outgoing longwave radiation is not related to the incoming one and is computed in a separate way but also following the Stefan-Boltzmann law, using the formula in equation [ 9 ]:

$$LW_{out} = \epsilon_s \cdot \sigma \cdot T_s^4$$

[ 9 ]

where $T_s$ (K) is the surface temperature, $\epsilon_s$ is the surface emissivity.

### 2.2.3 Heat Equation and Snow Cover

Equation [ 10 ] expresses the formulation used in GEOtop for the energy budget on a soil volume, accounting for phase changes:

$$\frac{\partial U^{ph}}{\partial t} + \nabla G + S_{en} - \rho_w \left[ L_f + c_w \left( T - T_{ref} \right) \right] S_w = 0$$

[ 10 ]

where $U^{ph}$ is the internal energy of the soil per volume (J/m$^3$), which is prone to phase changes, t is the time in seconds, G is the flux of heat conduction (W/m$^2$), $S_{en}$ (W/m$^3$) and $S_w$ (1/s) are the sink terms of energy and mass, respectively. $L_f$ is the latent heat of fusion (J/kg), T is the temperature of soil and $T_{ref}$ is the temperature taken as a reference and at which the internal soil energy is computed, both in °C. The characteristics of the water contained in the soil also play a role, such as $\rho_w$ that is the density of water (kg/m$^3$) and $c_w$ which is the specific thermal capacity (J/kg/K). G is computed using Fourier's Law and is equivalent to (equation [ 11 ]):

$$G = \lambda_T \nabla T$$

[ 11 ]

where $\lambda_T$ is the thermal conductivity (W/m/K) and it varies non-linearly with temperature. Substituting the formula of G in the heat equation [ 11 ] results in equation [ 12 ]:

$$\frac{\partial U^{ph}}{\partial t} + \nabla \cdot (-\lambda_T \nabla T) + S_{en} - \rho_w \left[ L_f + c_w \left( T - T_{ref} \right) \right] S_w = 0$$

[ 12 ]

The snow layer above soil plays an important role in the energy balance between the soil and the atmosphere. The modelling of snow in GEOtop is Eulerian, based on energy, and discretised into several layers (Endirizzi, 2007). The thermal gradients between the snow layers are well-defined. Snow metamorphism and accumulation and also accounted for in the snow model.

### 2.2.4 Model Implementation

For the purpose of this work, GEOtop is applied using its 1D mode at a point-scale. The model admits input meteorological data at an hourly timescale which is the one at which the equations would be solved. GEOtop can operate using information from at least one meteorological station and can also accept more stations. For the purposes of this research work data from only one meteorological station are used. Information regarding the longitude and latitude of the meteorological station, which is in this case the same location of the simulation point, are given to the model. Topographic information of the location is also given, such as the azimuth and elevation which are included in the

horizon file input to the model. The sky view factor which is an important parameter is also given to the model in the case of a complex terrain, which prevails in the Italian Alps location considered.

The model is forced with available meteorological data, such as air temperature, solar radiation, wind speed and direction, relative humidity, and precipitation. Corrections of all data given to the model is done a priori. The soil module in GEOtop is set by defining the available soil column, setting the number of layers, their different depths, and the corresponding temperature and pressure values in each soil layer. Numerous parameters exist and require calibration, and this research work focuses on the calibration of the snow module and all its parameters. Throughout this research work as well, the importance of the parameters is tested through sensitivity analyses.

# Chapter 3

## Research Methods

The focus of this research work is to model the snow layer and soil temperature using the model GEOtop using its 1D mode, at a point-scale. In order to provide reliable results from the modeling process, pre-processing of the data and model calibration are essential. The most impactful factors to be considered are the input data given to the model, which are vital for producing proper results, in addition to the model parameters that can be calibrated according to the site on which the study is done. Firstly, it is important to intricately check the correctness of input data and make any required corrections before giving the data to the model. Another crucial step is the parameter calibration which can be done through understanding the site properties and forcing the model with the relevant parameters.

This chapter presents the location on which the study is done, and the data collected at the location's meteorological station. It also describes the methods followed to correct the available observed precipitation data. Another part of this chapter focuses on the calibration of GEOtop model in order to model the snow cover and the ground surface temperatures. The results of the correction methods and the simulations done using GEOtop are presented and discussed in the next chapter.

## 3.1 Site and Data Available

The first part of this chapter presents the site on which the study was done, which is Passo del Monte Moro, Macugnaga, in the Italian Alps, along with the data gathered at the monitoring station at this site. Throughout the other parts of this chapter, the methods used in this study are presented, including the observed data check and correction methods, as well as the model calibration methodology.

In order to model the snow layer and soil surface temperatures in an Alpine region underlain by permafrost, the model GEOtop is run using data from a monitoring site, and snow depth and soil surface temperature observed data are used to assess the reliability of the model results. For the pointwise run of GEOtop, the run location is taken having the same coordinates of the monitoring station for which the model input data are available and data later on used for check of the quality of results are also available.

### 3.1.1 Monitoring Station

The monitoring station used in this study is the station Passo del Monte Moro, located in Macugnaga, in the Piedmont region in Northern Italy. The location is part of the Italian Alps, very close to the Italian-Swiss borders, which is underlain by permafrost. Passo del Monte Moro station is located at an elevation of 2823 m s.l.m. This monitoring station is one of five stations in Piedmont region (shown in *Figure 3*,which were installed and operated by ARPA Piemonte, taking part in the 'PermaNET – Permafrost Long-term Monitoring Network' project, which is a project included in the Alpine Space program by the European Territorial Cooperation (PermaNET Alpine Space, 2021). This program aims mainly to contribute to the installation of a permafrost monitoring network in the Alpine region, in order to provide data on permafrost distribution in the Alps, allow better water resource management, and attempt to reduce the risks of natural hazards by providing required data on permafrost evolution.

The Passo del Monte Moro station location is along the latitude 45° 59' 49,9" N, and the longitude 007° 58' 34,3" E, at an elevation of 2823 m s.l.m (*Figure 4*). The station constitutes a meteorological measurement station, as shown in *Figure 2*, as well as an underground well for performing direct measurements. The meteorological station includes a heated rain gauge, a snow gauge, an anemometer for wind speed and wind direction measurements, a radiometer for measuring radiant fluxes, a hygrometer for measuring relative humidity, and a thermometer for temperature measurements. As

for the underground part, a 30-meters-deep well exists and is equipped with 25 thermometers used to perform direct measurements of the temperature at several depths underground.

Figure 2 Passo del Monte Moro monitoring station

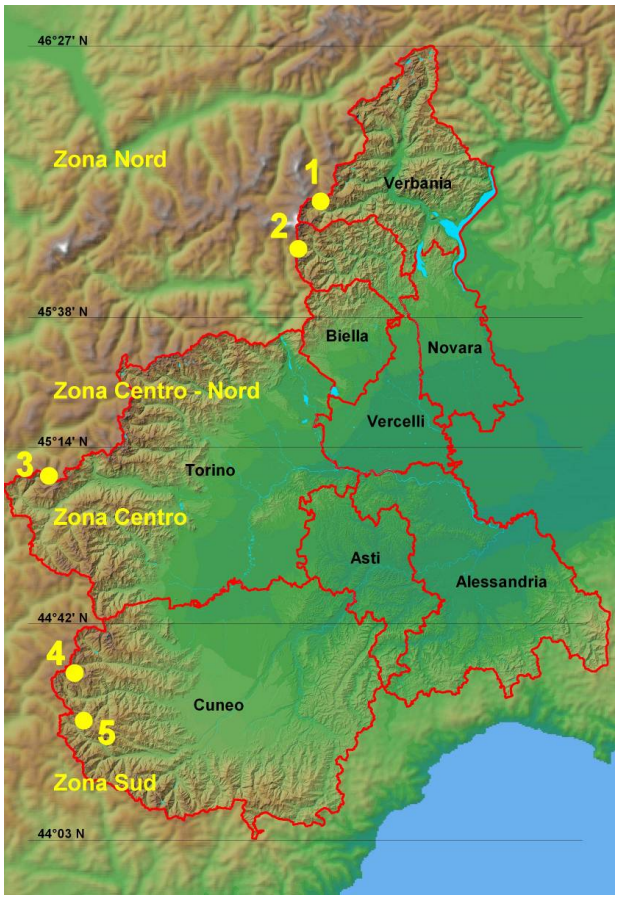


Figure 3 Map of 5 monitoring stations

### 3.1.2 Meteorological Data Available

The data collected at site and available for usage for the purposes of this research work are of variable temporal scales and available over several years. Part of the data is used as input data for running the model GEOtop, another part is used as parameters for calibrating the model, and the last part is used for assessing the accuracy of the model results by comparing the simulated values with the observed ones. The chosen period for the simulations is from August 2012 till August 2018 over which all model input data are available. Among the observed data used to assess the model results are the snow depth and the ground surface temperature. The only exception to the chosen time interval of 6 years is the data for ground (or soil) surface temperature (GST), which is available over only a short period of 2 years.

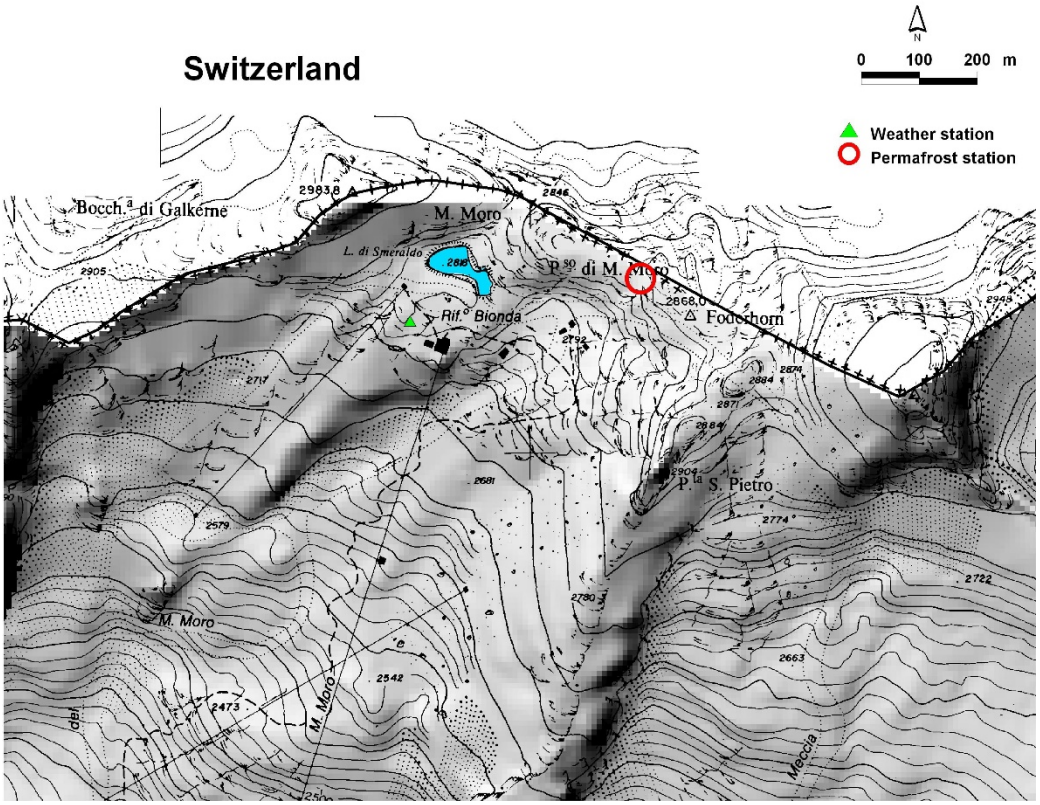

Figure 4 Elevation map of the Alps region including Passo del Monte Moro station location

The data taken from Passo del Monte Moro monitoring station and used as input in GEOtop include measurements of air temperature (°C), shortwave global solar radiation (W/m$^2$), precipitation (mm), wind speed (m/s), wind direction (°) and relative humidity (%). The air temperature and relative humidity data are recorded every 30 minutes, while all the other measurements are taken at a 10-minutes interval. However, the model GEOtop requires data at an hourly timescale, which would be the timestep at which the equations are solved. Thus, the available data are aggregated over an hourly scale, by taking the mean value for each of all the variables, except for the precipitation which is accumulated over the one-hour period.

Some pre-processing of data that was to be input to the model is performed to avoid model errors. An initial step of data pre-processing is the cleaning of data that includes removal of non-valid data, which could be present due to several reasons including equipment or human-made errors. As for the next step that concerns missing data, this is resolved by interpolating the data, as long as it is for a short and insignificant period of time. This was a very rare case in the data used and thus was applied only minimally.

## 3.2 Site Topography

GEOtop requires topographic information of the simulation point, which are used as part of the calculations it performs, namely for the partitioning of incoming and outgoing shortwave and longwave solar radiations. The calibration of the relevant parameters regarding the site topography is considered as the initial calibration step for the GEOtop model. The sky view factor, $V_f$, the azimuth and the horizon elevation are important parameters to set in GEOtop model for the simulation point and for the meteorological station in hand. In the case of this research work, the simulation point overlaps with the meteorological station location and thus these two parameters are calculated once for both.

$V_f$ is a parameter related to the topography, which accounts for the part of the sky that is visible to the point in space where the calculations are being done. It varies from 0, which implies no sky seen from study point, to 1 which means the sky can be fully seen, which is the $V_f$ value for the case of a flat terrain. $V_f$ intervenes in the calculation of the diffuse part of the outgoing SW radiation, and the incoming LW radiation. The horizon elevation and the corresponding azimuth are also used to define the topography of the simulation point in GEOtop.

For the calculation of $V_f$, horizon elevation, and azimuth at the chosen location of simulation, a package in R is employed, named 'svf: Sky View Factor from DEM RasterLayer' (Van Doninck, 2018). It utilizes the libraries Horizon, which is a part of Horizon Search Algorithm, and Raster. This model uses the longitude and latitude information to compute the horizon elevation angle and $V_f$ for a pre-chosen number of azimuth angles, using the parameter called 'nAngles'. Another parameter that can be chosen by the modeler is the maximum radius of search from the point of operation. Higher distance values would render more accurate results. For this application, the number of angles chosen was 8 and the search radius was 5,000.

## 3.3 GEOtop Calibration Methodology

The calibration of the model GEOtop is done over several main steps, tackling separately the relevant modules in GEOtop. An initial step is done to calibrate the topography module of the model, which was explained in the previous section. The main changes performed are related to the sky view factor and the horizon data, and the results of the resulting simulations are presented in *section 4.3.1*. The following steps performed in the calibration of GEOtop model are the surface energy fluxes module

calibration and the snow module calibration. The calibration methods are presented in this part and the results of the simulations are shown in *section 4.5*.

### 3.3.1 Surface Fluxes Module

The second step in GEOtop model calibration tackles the surface energy fluxes module. This module mainly controls the conditions and solutions relevant for the surface energy fluxes. These occur either between the surface and the atmosphere, or between the surface and the overlaying snow layer. The fluxes at the surface are moderated by many factors, including but not limited to the incoming radiant fluxes input to the model, the calculation of the incoming and outgoing fluxes by the model, and the atmospherical conditions existing. The two main parameters that can be tuned in the surface energy fluxes model are the LWinParameterization and the MoninObukhov parameters. The former allows the selection of the formula to be used for the calculation of the incoming longwave radiation. There are several possible formulas: Brutsaert (1975), Satterlund (1979), Idso (1981), Idso and Hodges (1981), Koenig-Langlo and Augstein (1994), Andreas and Ackley (1982), Konzelmann (1994), Prata (1996), and Dilley (1998). Each formula computes the $LW_{in}$ in a different way, and calibrating this parameter highly affects the snow depth and GST simulated results. The default form of the LWinParameterization parameter uses the formula by Dilley (1998). Some of the available formulas are forced to the model in order to analyse which one mostly represents the actual conditions at Passo del Monte Moro site.

The other impactful parameter is the MoninObukhov parameter, which controls the atmospherical stability conditions in GEOtop's simulations. This parameter represents the buoyancy effects in the lower atmospheric boundary layer and their impacts on turbulent fluxes (Grachev and Fairall, 1997). All the possible options for this parameter are available to be set in GEOtop: either accounting for both stability and instability in the atmosphere, accounting for only stability, only instability or considering only atmospheric stability. The default value in GEOtop is considering both stability and instability. The parameter can be tuned to check the modelled results that most nearly comply with the snow depth observed at the site. After the final calibration of these 2 parameters related to surface energy fluxes, the results of the snow depth simulated are compared to the observed snow depth profile and assessed.

### 3.3.2 Snow Module

As a further step towards tuning of the GEOtop model, the calibration of the snow module is performed. The snow module in GEOtop includes parameters that characterize the formation and melting of the snow cover, which in turn affect the ground surface temperature at the simulation point. The calibration is mainly done in order to optimize these parameters for the specific site Passo del Monte Moro, and which can be further applied in other similar or nearby locations. The parameters included in the calibration of the snow module are the snow irreducible water saturation, maximum snow porosity, and the visible and near infrared reflectance of fresh snow. The calibration is done by finding parameter values in literature that are suitable for Passo del Monte Moro site. They are either taken from sites with similar climatic conditions to the site in hand, or from nearby sites, in the Italian Alps or in general in the Alps region. The model is forced with the parameter values from literature and the snow depth results are compared to those with default parameters.

## 3.4 Precipitation Correction Methodology

A further part of the input data pre-processing includes checking the correctness of the actual input data. Precipitation data are one of the major hydrometeorological datasets that play a considerably important role in snow cover formation and thus in its modelling. The problem prevails mainly in cases when snowfall is part of the precipitation during winter. Especially in high elevation mountain areas and for remote meteorological stations, under-catch of snowfall is common and ranges between 20% to 50% (Rasmussen et al., 2012). Several correction methods for precipitation are provided in literature and have proved to produce improved results in terms of modelling or other applications (Mair et al., 2016; Grossi et al., 2017; Masuda et al., 2019).

### 3.4.1 Rain Gauge Errors

The rain gauge used at Passo del Monte Moro monitoring station is the PMB2/R type. It is formed of a mechanical sensor that measures the amount of precipitation, and a heater that gives the possibility to measure the water equivalent of snow precipitation as well. The resolution of the rain gauge used is 0.2 mm of rain. Systematic biases in precipitation data measured by rain gauges and heated rain gauges are common in cold mountainous areas and have several causes. Errors from rain gauges while measuring solid and liquid precipitation include 1) wind-caused biases, 2) inaccuracies due to heating of falling snow which cause some evaporation, and 3) wetting effects that lead to losses as well

(Masuda et al., 2019). Power supply problems could also be a factor causing erroneous precipitation measurements. Errors in liquid and solid precipitation measurements have been commonly documented in the Alpine region and are partly overcome by using simple correction methods (Gottardi et al., 2012; Grossi et al., 2017).

In cases of snow and precipitation fall together, the final values reported by the rain gauge represent a water equivalent result of the mixture of these two. Thus, another issue that prevails when dealing with mixed precipitation data (solid and liquid) is the discrimination between rainfall and snowfall when using the data. This is accounted for in GEOtop by applying threshold temperatures for rainfall and snowfall, which could be the same or different values. Either air or dew temperatures can be used as the threshold. The parameter threshold rain temperature specifies the temperature above which all precipitation amount is accounted for as liquid. On the other hand, the snow threshold temperature parameter sets the temperature below which all amount of precipitation is said to be snow. If the two thresholds are not equivalent, the temperatures in between the threshold are considered to have a mixture of solid and liquid precipitation. The calculation of the partitioning of falling precipitation considers a linear extrapolation between snow and liquid precipitations.

### 3.4.2 Precipitation Underestimation

As a first step in the process of correcting the available precipitation data, an attempt to check for the underestimation of precipitation in the Italian Alps, at Passo del Monte Moro site in specific, is done. The fresh snow depth (HN) measurements are available at the station and can be considered as the 'true precipitation' in cases of snowfall only, since errors in these measurements are much more accurate than heated rain gauge precipitation (Grossi et al., 2017). Therefore, HN values are used as a reference for comparing the available precipitation data. The temperature threshold below which precipitation is considered as purely snow is taken at -4 °C, considering a margin of error to avoid involving any liquid precipitation data. The observed precipitation data (mm) are available at temporal intervals of 10 minutes, while the fresh snow measurements are available at a daily scale, so the precipitation data are aggregated to the daily scale for the comparison.

In order to compare the observed precipitation to HN, the water equivalent of HN is calculated. The relation between HN and the snow water equivalent (SWE) is through the density of freshly-fallen

snow, and can ideally be calculated used the formula [ 13 ] by utilizing freshly-fallen snow depth and density measurements:

$$SWE = \rho_{snow} \cdot HN \qquad [\ 13\ ]$$

However, density measurements are quite difficult to be collected and usually rare to find, specifically in remote mountain areas like in the Italian Alps. Due to the lack of density data at the site in hand, other calculation methods should be used to get the SWE of freshly fallen snow. Various advanced empirical and semiempirical models for the calculation of SWE from available snow depth (HS) data, or from other meteorological data, exist in literature (Bocchiola and Rosso, 2007; Jonas et al., 2009; Pistocchi, 2016; Guyennon et al., 2019; Winkler et al., 2021). For instance, the model by Guyennon et al. (2019) was applied in the Italian Alps and it utilizes the day-of-year as a proxy of seasonal effects while calculating the SWE. It is an advancement of the Pistocchi (2016) model which also uses the day-of-year parameter. The improvement was through adding a quadratic term to the equation, that allows to overcome the hypothesis of a linear relation. In addition, these two models have site-specific parameters that can be calibrated according to site location in the Alps region.

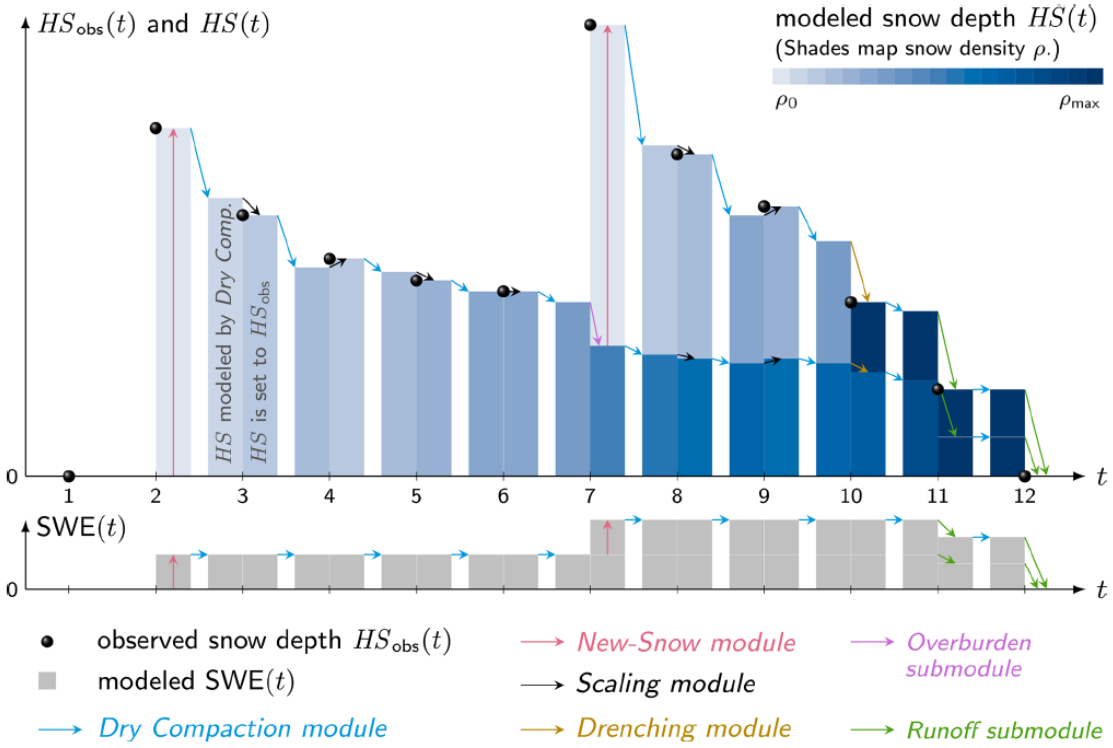


Figure 5 Schematic of DeltaSnow model (Winkler et al., 2021)

The model used for the purposes of this research work for the calculation of SWE is called ΔSnow by Winkler et al. (2021). The model is available in a package in R called Nixmass (Winkler and Schellander, 2021), which includes also other models mentioned previously. The model ΔSnow is a semi-empirical and multi-layer model that uses only timeseries of snow depth (HS) to produce the corresponding SWE values at a daily timescale. The model includes several modules including one that generates the preliminary snow layer, one for compaction in between snowfall events, and one for new snowfall over old snow depths. *Figure 5* presents the schematic that the model ΔSnow operates according to.

There are 7 parameters that can be calibrated in the model, including new snow density ($\rho_0$), maximum possible snow density ($\rho_{max}$), 2 viscosity parameters ($\eta_0$ and k), threshold deviation ($\tau$) and 2 overburden parameters ($c_{ov}$ and $k_{ov}$). For the density and viscosity parameters, values specific to the Italian Alps or to the whole Alpine region exist. *Table 1* presents the values of the parameters that were used for the Passo del Monte Moro site, along with the references which correspond to studies done in the Italian Alps. The new snow density for fresh snow is expected to have low values and it is found in literature to vary between 50 to 200 kg/m$^3$ in cold climatic areas (Heilig et al., 2009). A value of 81 kg/m$^3$ is the default of the model and was found to be applicable for the Italian Alps region. As for the maximum possible density value, the range among which it can vary is around 300 to 600 kg/m$^3$. In the Swiss and Italian Alps, Jonas et al. (2009) performed density measurements which resulted in a maximum density value around 350 kg/m$^3$, which is thus used for this case. The rest of the variables are taken as default of the model as they are found to be suitable for the Passo del Monte Moro site.

Table 1 DeltaSnow model parameter values

| Parameter | Value | Unit | Reference |
|---|---|---|---|
| $\boldsymbol{\rho_0}$ | 81 | kg/m$^3$ | Guyennon et al., 2019 |
| $\boldsymbol{\rho_{max}}$ | 350 | kg/m$^3$ | Jonas et al., 2009 |
| $\boldsymbol{\eta_0}$ | 8.5 | $10^6$ Pa.s | Guyennon et al., 2019 |
| **k** | 0.03 | m$^3$/kg | Jordan et al., 2008 |
| $\tau$ | 2.4 | cm | Winkler et el., 2021 |
| $\mathbf{c_{ov}}$ | 5.1 | $10^{-4}$ Pa$^{-1}$ | |
| $\mathbf{k_{ov}}$ | 0.38 | - | |

The resulting SWE data are used for assessing the quality of precipitation data. Another useful inference that can be made from the SWE computed is the density of fresh snow, which can be calculated as using equation [ *13* ]. This is done considering only days where snow has actually fallen (HN>0), which means also for SWE values different than zero.

The probability density function (PDF) of the density timeseries calculated is shown in *Figure 6*, done by dividing the dataset into 30 classes. The PDF shows the values over which the density of fresh snow varied over the study period, as well as the minimum and maximum possible values. The mode of fresh snow density timeseries is equal to 147.2, the mean is equal to 201.4 and the median is 160.9. The minimum possible value of density seen is around 50 kg/m$^3$ and the maximum is around 500 kg/m$^3$. These values are in line with fresh snow measured density values that can be found in literature. In specific, a study by Jonas et al. (2009) shows that the density of fresh snow in the Swiss Alps ranges between 50 and 600 kg/m$^3$, and another study by Guyennon et al. (2019) shows similar results in specific foe the Italian Alps. This implies that values of SWE and the corresponding calculated density timeseries can be used for further correction of the precipitation data, as they appropriately resemble the snowfall conditions in the Italian Alps and in the specific site in hand. For the purposes of this research, the mode value of the density distribution is chosen to be used, considering that it is the most frequently occurring value over the whole period.

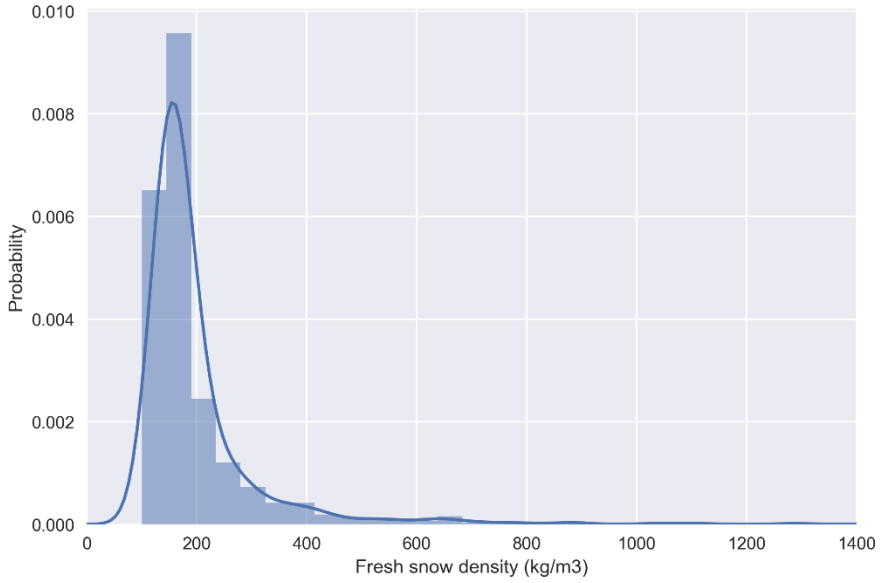


Figure 6 Probability density function of fresh snow density calculated from SWE

### 3.4.3 Catch Ratio Correction Method

The first step in the pre-processing of meteorological data was to check the correctness of these observed datasets and their compliance with the climatic conditions at the study site. In the results *section 4.4.1* it is demonstrated that the precipitation measurements underestimate the real snowfall that occurs especially during the winter season. It is realized that the observed precipitation data might have errors due to several reasons. Causes of errors in rain gauge measurements include wind, heating, and wetting effects. In this section, the correction method applied to the available precipitation measurements is explained. The evaluation of the precipitation results, and the resulting simulations done using GEOtop are presented in *sections 4.4 and 4.5*.

The wind-induced undercatch of snowfall is a very common phenomenon in remote high elevation mountains. In the case of the Italian Alps, it is expected to have an important impact on the precipitation measurements by the heated rain gauge. For this reason, the precipitation correction method that is used here to improve the precipitation data tackles the wind-induced undercatch of precipitation. The method to be applied is called the Catch Ratio (CR) method which was developed by Masuda et al. (2019). The method is based on a ratio called the catch ratio which is calculate using the formula in equation *[ 14 ]*:

$$CR = \frac{1}{1 + mU}$$

[ 14 ]

where U is the wind speed in m/s, taken at the height of the rain gauge, and m is a correction coefficient that is used to discriminate between snowfall and rainfall, and its value is based on the type of the rain gauge used for the precipitation measurements.

The wind speed in the equation of the CR, U, is computed using the formula in equation *[ 15 ]*:

$$U = U_{obs} \frac{lnZ_1 - lnZ_0}{lnZ_2 - lnZ_0}$$

[ 15 ]

where $U_{obs}$ is the observed wind speed at the height of the anemometer, $Z_0$ is the relative roughness of the surface, $Z_1$ is the rain gauge height in meters and $Z_2$ is the anemometer height in meters. The

value of the relative roughness for a snow surface is taken as 0.003 (Koussa et al., 2014). The height of the rain gauge used at Passo del Monte Moro is 6 m, while the height of the anemometer is 8 m.

As for the value of the correction coefficient *m*, the rain gauge used is a heated rain gauge with no wind shield used. According to Yokoyama et al. (2003), for this type of rain gauge the value of *m* for cases of snowfall is taken as 0.346, while for the cases of rainfall the value of m is 0.0856. Since the precipitation from a heated rain gauge is a result of the sum of snowfall and rainfall with no indicator of which phase is falling, it is essential to discriminate between snowfall and rainfall. A method proposed by Yasutomi et al. (2011) allows to distinguish solid precipitation from liquid precipitation according to the temperature and relative humidity values at the same location. A linear relationship between critical relative humidity ($RH_{cri}$ in %) and temperature (T in °C) allows to realize if the precipitation is melting, which means that it falls in liquid form, or if it is non-melting, which means it precipitates as snowfall. The equation of the linear relation is as shown in equation *[ 16 ]* (Yasutomi et al., 2011):

$$RH_{cri} = 92.5 - 6.7\,T \qquad [16]$$

The distinguishing between rain and snow is done by comparing to the melting/non-melting condition. Using equation *[ 16 ]*, the critical relative humidity values are calculates using the temperature hourly data available at Passo del Monte Moro site. The plot in *Figure 7* shows the linear relation between these 2 parameters, forming the discrimination line, below which all precipitation is assumed to be snowfall, and above which all precipitation is said to be liquid. Using this plot, the observed RH values allow to decide whether liquid or solid precipitation has occurred during each hour.

Discriminating between snow and rain cases in the hourly precipitation timeseries allows to calculate the CR using the corresponding value of *m* and the wind speed timeseries. In order to apply the correction to the observed precipitation value $P_g$, equation *[ 17 ]* is used. The resulting hourly timeseries of $P_{corr}$ is hereafter referred to as CR corrected precipitation.

$$P_{corr} = \frac{P_g}{CR} \qquad [17]$$

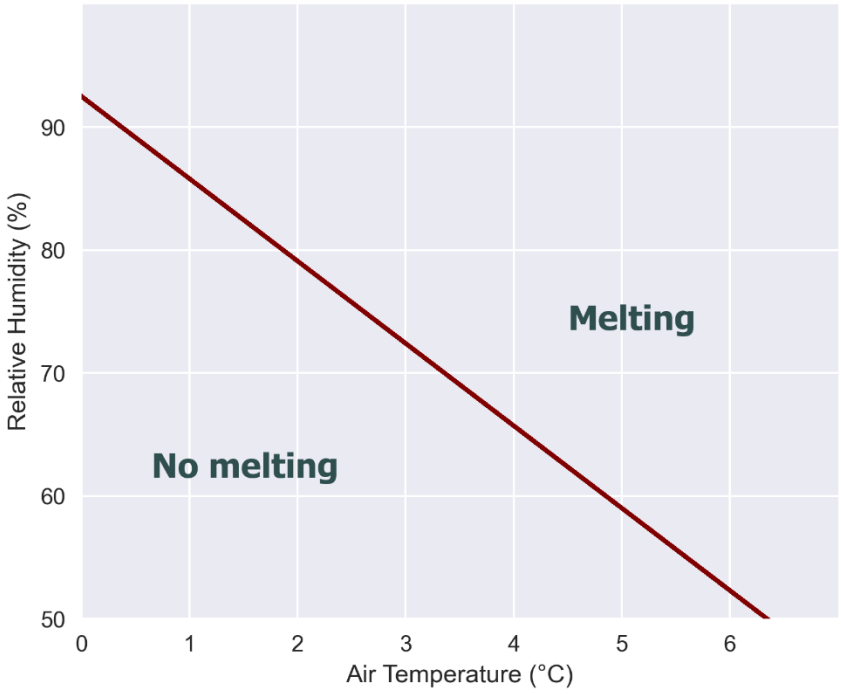


Figure 7 Snowfall/rain discrimination according to melting/non-melting conditions

### 3.4.4 Extended Catch Ratio Method

Considering the fact that the errors in precipitation data are not only caused by wind effects, it is expected that the resulting precipitation hourly timeseries $P_{corr}$ is not yet properly able to represent the actual conditions of precipitation at the monitoring site. For this reason, a further step is taken to improve the precipitation data in order for it to be used as input to simulate the snow cover and GST using GEOtop model. This is also essential since the CR corrected precipitation still does not comply perfectly with the SWE of freshly fallen snow that was calculated using ΔSnow model. The main idea of this final improvement step is to try matching the CR corrected precipitation with the actual snowfall conditions at the site. This method, which will be hereafter referred to as the extended CR method, allows to 1) overcome the fact that the precipitation data are always not in great compliance with the actual snowfall occurring at each timestep, 2) render the CR corrected precipitation data more in coherence with the fresh snowfall (HN), and 3) avoid directly using the SWE as input to the model since it is available at a daily and not hourly timescale as the model requires.

The proposed method is to perform this improvement through multiplying the CR corrected precipitation by a dimensionless factor. For computing this factor, it is necessary first to obtain an SWE hourly timeseries that represents in an indirect way the HN at each hour. The SWE series is computed using the formula in equation *[ 18 ]*:

$$SWE(t) = \rho_{HN,m} \cdot HN(t)$$

[ 18 ]

where SWE(t) (kg/m$^2$) is the computed SWE timeseries, $\rho_{HN,m}$ (kg/m$^3$) is the mode of the PDF (shown in *Figure 6*) of the density of freshly fallen snow which is rounded and taken as 150 kg/m$^3$, and HN(t) (m) is the fresh snow depth at time t. The factor is then obtained as the ratio between this SWE(t) and the CR corrected precipitation. The SWE data are available at a daily timescale and the CR corrected precipitation data are aggregated to a daily scale to match them. The computation of the factor is done according to equation *[ 19 ]* where f(t) is the dimensionless factor that varies in time along with the precipitation occurring, SWE(t) is the SWE of freshly fallen snow at same time t, $P_{corr}(t)$ is the CR corrected precipitation at time t, and t is the time in days. The resulting factor is a timeseries of daily values of this ratio. For all hours of each day, this factor is used to multiply the CR corrected precipitation in order to produce a final hourly timeseries of precipitation measurements, hereafter referred to as extended CR corrected precipitation. Since this factor is used for correcting the precipitation data only in cases of snow, the factor is applied only at temperatures below -1 °C, assuming only snow has occurred at these times.

$$f(t) = \frac{SWE(t)}{P_{corr}(t)}$$

[ 19 ]

# Chapter 4

## Results and Discussion

This chapter focuses on presenting and discussing the results of the methods performed in order to properly utilize GEOtop model to simulate the snow depth and GST profiles at Passo del Monte Moro monitoring location. As a first step the initial simulation results of GEOtop are presented. The calibration of GEOtop modules: topography, surface energy fluxes and snow characterization is explained and the results are presented and discussed. Furthermore, the outcomes of the precipitation correction methods are analysed and the results of the simulations using these datasets are shown and interpreted. The model outcomes including elements of the solar radiation and components of the surface energy balance equation are shown as well. Finally, a sensitivity analysis is done to evaluate the most impactful parameters that can be changed in GEOtop model, that have an effect on its outcomes.

## 4.1 Meteorological Characteristics

For performing simulations using GEOtop, it is essential to critically observe the Passo del Monte Moro site meteorological characteristics to get an overview about the climatic conditions in that area. The site-specific input data to the model include the observed air temperature (°C), shortwave global solar radiation ($W/m^2$), precipitation (mm), wind speed (m/s), wind direction (°) and relative humidity (%). Other characteristic variables of the site are the snow depth and the ground surface temperature (GST), which will be employed later to assess the model results. The ranges of each of these variables, after aggregating them into daily means, are presented in *Table 2*, along with the overall mean, minimum, maximum and standard deviation of the datasets. The numbers represent the general meteorological conditions prevailing at Passo del Monte Moro site in the Italian Alps over the years between 2012 till 2018. The daily means of air temperature, GST, wind speed and relative humidity are calculated, and their profiles are presented in *Figure 8*. The duration over which the plots are presented is between August 2014 and August 2014, since the observed GST data are available only over this period, and these years are considered to be representative of the general situation over all the study period.

Table 2 Daily mean ranges of Passo del Monte Moro meteorological characteristics

| Variable | Units | Mean | Minimum Value | Maximum Value | Standard Deviation |
|---|---|---|---|---|---|
| **Air Temperature** | °C | -1.4 | -21.9 | 16.4 | 6.6 |
| **Relative Humidity** | % | 75.8 | 6.8 | 100 | 20.7 |
| **Wind Speed** | m/s | 2.6 | 0 | 11.3 | 1.4 |
| **Precipitation** | mm/d | 2.3 | 0 | 62.8 | 5.5 |
| **Shortwave Solar Global Radiation** | $W/m^2$ | 181.9 | 0 | 783.5 | 119.4 |
| **Snow Depth** | mm | 1292.7 | 0 | 4090 | 1140.3 |
| **GST at 2 cm** | °C | 0.5 | -4.7 | 19 | 3.9 |

The daily mean of the air temperature over the study period varies between around -22 °C during winter months and 16.4 °C during summer months, with an annual mean of -1.4 °C (*Figure 8a*). The

GST at 2 cm depth in soil varies between -4.7 °C and a maximum of 19 °C, which occurred mostly during the summer of the year 2012. The mean value of the GST falls at around 0.5 °C, which implies that most of the time a snow layer exists above the surface, that is normal in the Alps region.


Figure 8 Daily means of observed a) air and surface ground temperature (°C), b) solar global radiation (W/m²) and c) reflected solar radiation (W/m²)

The solar global radiation and solar reflected radiation profiles are shown in *Figure 8b* and *Figure 8c* respectively. The solar global radiation goes up to a maximum of around 780 W/m² during summer times, and the amount of reflected radiation reaches a bit more than 250 W/m² at those times. It is noticeable that the global and reflected radiations in some years are different than in others, and this surely has an impact on the snow depth and its melting phase during the spring.

*Figure 9* presents another set of the meteorological parameters measured at the site. All these parameters are available over all the study period thus the plot includes the years from 2012 till 2018. The precipitation at Passo del Monte Moro site is plotted in *Figure 9a*, along with the corresponding accumulated snow depth over the study period. The maximum precipitation values seen is around 68 mm/day, with an average over all the years equal to 2.3 mm/day, considering summer days as well.

As for the snow depth, a maximum accumulated snow depth of around 4000 mm is reached during the winter of 2013. The snow cover in this region disappears during the months of August and September of approximately all the studied years.

The precipitation measured by the heated rain gauge is a mix of solid and liquid precipitation. This explains some discrepancy between the snow depth and the precipitation recorded. In addition, as mentioned before and will be discussed more in depth in later sections, the rain gauge measurements are highly erroneous and require several corrections before being properly provided to GEOtop to simulate the snow depth. The corrected precipitation profiles are presented and discussed further on.

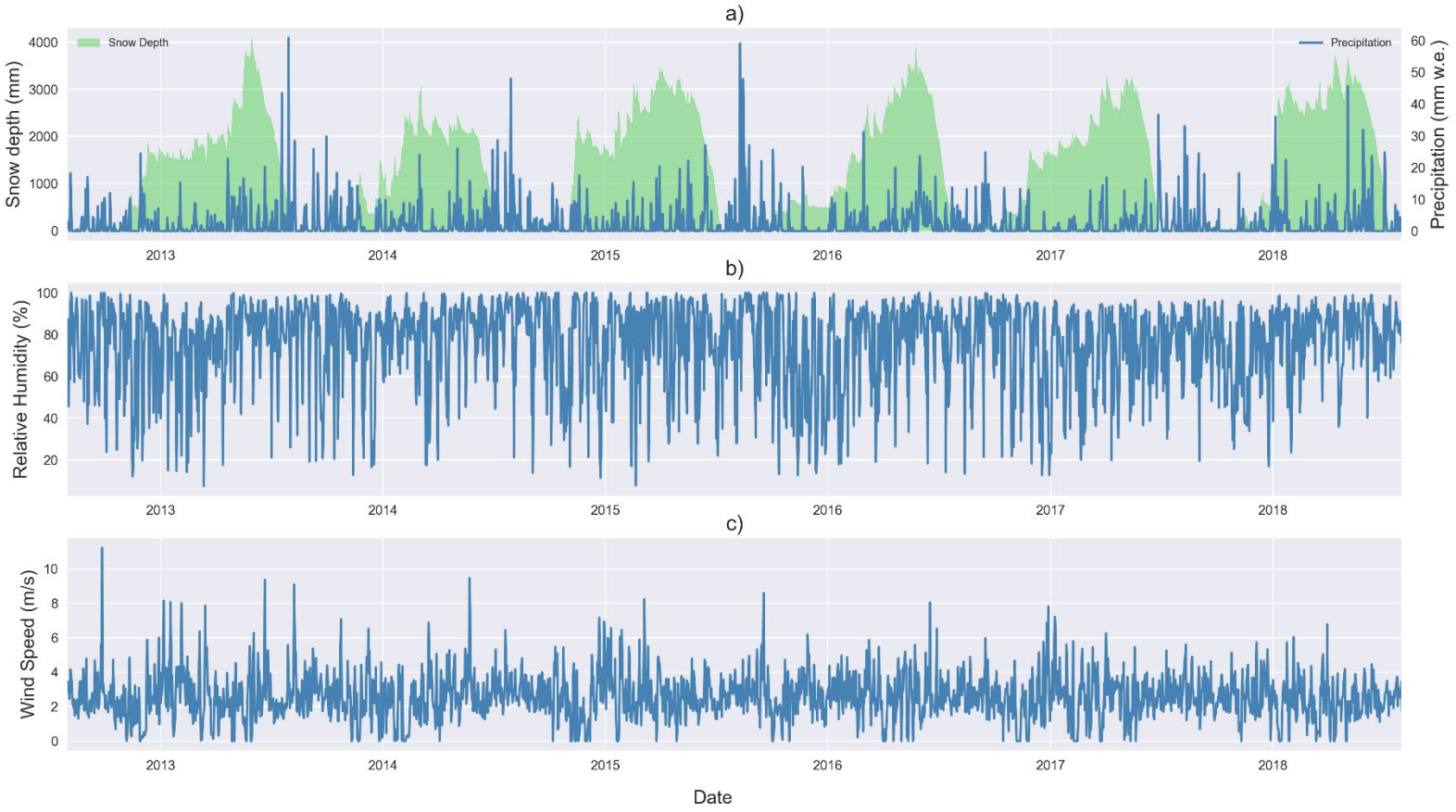


Figure 9 Daily means of observed a) precipitation (mm w.e.) and snow depth (mm) b) relative humidity (%) and c) wind speed (m/s)

Observing the accumulation and melting patterns of the snow layer, along with the incoming radiation and the temperature profiles, the cold seasons can be said to range from the end of September till the mid or end of April, whereas the hotter seasons including summer extend over the rest of the year. The model GEOtop requires also timeseries of relative humidity and wind speed, both of which profiles are shown in *Figure 9b* and *Figure 9c*. The relative humidity at the site ranges over all the possible

values, with higher values concentrated during the summer period and lower ones during the winter period.

## 4.2 Default Simulation Results

A first attempt of running the GEOtop model at the Passo del Monte Moro location is performed using default parameters of the model as reported in Endirizzi et al. (2014), Gubler et al. (2012) and Engel et al. (2017). The major parameters of which some will be calibrated, assessed and/or discussed are mainly related to the 1) complex site topography, 2) surface energy fluxes module and 3) snow characterization module. The snow characterization parameters are presented in *Table 3* along with their default values from Gubler et al. (2012) and Engel et al. (2017). The location of the simulation point, that coincides with the meteorological station location, is specified to the model through the longitude and latitude values, as well as the site elevation which is 2823 m s.l.m. Specifications related to the meteorological station sensors, such as the heights of the anemometer and the thermometer are given to the model as well. The simulations are performed at an hourly time-step, which is in line with the timestep of the meteorological data input to the model and the output from the simulations as well. The simulation is performed over the period from August 2012 till August 2018.

Table 3 Snow characterization default parameters for GEOtop model simulations

| Parameter | Description | Value | Unit |
|---|---|---|---|
| **DewTempOrNormTemp** | Use of either air temperature (0) or dew point temperature (1) to discriminate snow from rainfall | 0 | - |
| **ThresTempRain** | Threshold temperature above which all input precipitation is liquid | 3 | °C |
| **ThresTempSnow** | Threshold temperature below which all input precipitation is snow | -1 | °C |
| **AlbExtParSnow** | Threshold snow depth below which the surface albedo is interpolated between snow and soil | 10 | mm |
| **MaxSnowPorosity** | Maximum allowable snow porosity | 0.7 | - |
| **IrreducibleWatSat** | Snow irreducible water saturation | 0.02 | - |
| **FreshSnowRefVis/NIR** | Visible and infrared fresh snow reflectance | 0.9/0.65 | - |

Using the meteorological input data presented in *section 4.1* and the default parameters reported previously, the model GEOtop was run over the period from August 2012 till August 2018. The resulting snow depth and the GST simulated are plotted to evaluate the model results. Both parameters are assessed by comparing them to the measured corresponding parameter at Passo del Monte Moro monitoring station. The plot of simulated and observed snow depths at Passo del Monte Moro is shown in *Figure 10*. The snow depth profiles show a high discrepancy between the simulated and observed snow depth data. The maximum value reached by the simulated snow depth over the study period is around 1000 mm, while that of the observed snow depth is around 4000 mm. This is a typical result that falls in line with expectations and with preliminary results of simulations done using GEOtop in literature (Wani et al., 2021).

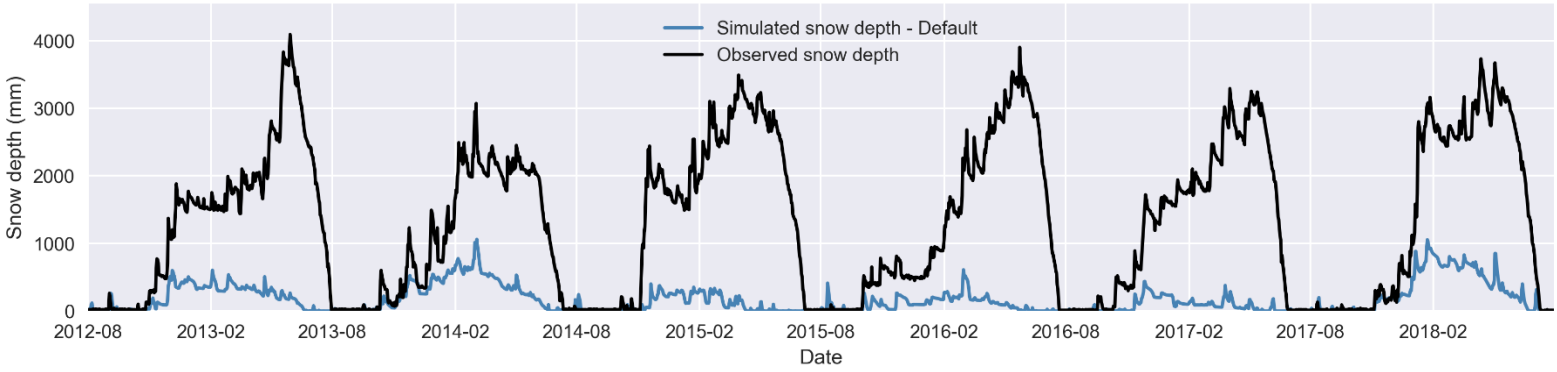


Figure 10 Plot of observed and simulated (GEOtop) snow depth at Passo del Monte Moro location

The misinterpretation of the snow depth by the model can be linked first to having not calibrated the model parameters to the specific site in hand, and also to the fact that, as discussed before, the meteorological input data to the model (precipitation in specific) require correction as they do not represent the real precipitation conditions.

Another parameter that this research work aims to model using GEOtop is the ground surface temperature (GST). This parameter can be measured at various depths in the soil at the site location. GEOtop allows to model the soil temperature at several depths in the ground as well. The available observed data from Passo del Monte Moro monitoring location are taken at a depth of 2 cm below the soil surface, and the measurements extend over a period of around 2 years, 2012-13 and 2013-14. For the purposes of this work the results of GST observed and simulated are presented over the period from August 2012 till October 2013. The default parameterization of GEOtop is used to simulate the GST at 2 cm depth (°C). The results of the simulation of GST are plot and compared to the observed GST, as shown in *Figure 11*.

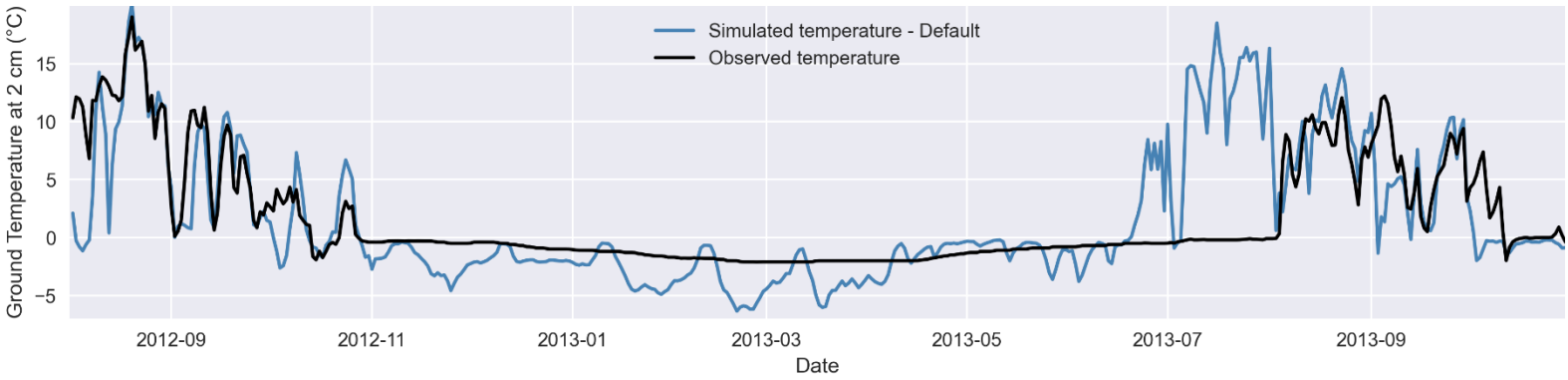


Figure 11 Default GEOtop output of GST compared to observed GST at 2 cm depth

The results of the simulated GST at 2 cm depth show different values as compared to the GST measured at the site. This is in line with what would be expected, considering the snow depth results seen previously, and the impact that the snow cover has on the soil conditions. The default simulated GST exhibits an earlier increase of temperature than that occurring in fact. This is due to the fact that in the simulation the snow cover did not build-up as required and thus there was a very thin layer of snow covering the soil during the month of July. Thus, the increase of atmospheric temperature during this month lead to an early increase of the GST. The simulation of GST result is expected to improve when the model calibration is done, and when correction of input meteorological data is applied, especially since it is highly affected by the snow cover conditions.

## 4.3 GEOtop Model Calibration Results

### 4.3.1 Complex Topography Calibration

As one of the initial steps for setting up the model for the specific Passo del Monte Moro site, the complex topography at the simulation point is accounted for through the topographic variables $V_f$ and the horizon elevations with corresponding azimuth. The 'svf' package in R is used, by setting the location at the simulation point, which is the same point as the meteorological station, having longitude 45° 59' 49,90" N and latitude 7° 58' 34,50" E. The resulting $V_f$ value is 0.9. As for the horizon elevation and corresponding azimuth, the resulting values that were input to the model through the horizon file are shown in *Table 4*.

Table 4 Horizon elevation and azimuth values of Passo del Monte Moro monitoring location

| **Azimuth (°)** | 0 | 45 | 90 | 135 | 180 | 225 | 270 | 315 |
|---|---|---|---|---|---|---|---|---|
| **Elevation (m)** | 30.7 | 30.7 | 14.2 | 0 | 0 | 0 | 14.83 | 14.83 |

The default value of $V_f$ in GEOtop is 1, and the topography is assumed to be flat if no horizon data are given to the model. Forcing the correct $V_f$ value into GEOtop and using the horizon data that correctly represent the complex topography of the site location is done. The model is then run in order to check the resulting snow depth simulated. *Figure 12* shows the simulated snow depth after this calibration step as compared to the simulated depth resulting from default parameters. A slight difference can be observed between the two plots; however, it is still essential to force the model with accurate data regarding the topography.

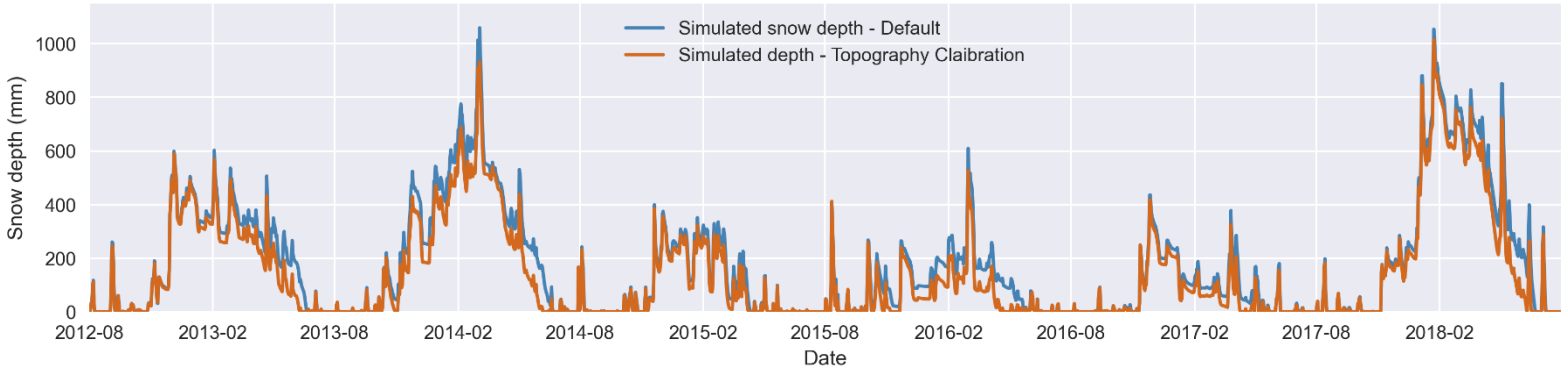


Figure 12 GEOtop simulated snow depth before and after calibration for complex topography

### 4.3.2 Surface Fluxes Calibration

The surface energy exchanges play an integral role in the moderating the climate and microclimate in the Alps. Modelling the snow cover requires solving the coupled energy and water balances at the simulation point to derive the corresponding relation with the snow depth. The surface fluxes module in GEOtop can be calibrated through some parameters including most importantly the $LW_{in}$ parameterization and the Monin-Obukhov atmospherical stability parameter.

The $LW_{in}$ parameterization is expressed by choosing the formula to be used for incoming longwave radiation calculation by GEOtop. Among the available formulas are ones by Brutsaert (1975), Idso (1981), Satterlund (1979), Idso (1981), Idso and Hodges, Koenig-Langlo & Augstein (1994), Andreas and Ackley (1982), Konzelmann (1994) and Dilley (1998). The equation choice can be given to the model through defining the parameter LWinParameterization with the formula's corresponding number. According to literature, the choice of the Lwin parameterization parameter can be done by finding the most suitable one that allows a better representation of the snow cover (Wani et al., 2021). The default formula used by GEOtop is the one by Dilley (1998). Several simulations are done by choosing different formulas for the calculation of $LW_{in}$, in order to choose the most suitable one for

this case, and the results are shown in *Figure 13*. The meteorological input data to the model are kept the same, and the complex topography calibrated parameters are from now on used as the case to compare with. This means that the default case in the plot is one were the $V_f$ and horizon files are correctly forced to the model, and the $LW_{in}$ parameterization parameter uses the formula by Dilley (1998).

The plots in *Figure 13* are shown in terms of each study year separately, to provide more clarity on the differences between the formulas available. It can be interpreted from the plots, specifically looking at the years 2013-14 and 2017-18, that the formula by Idso (1981) produces results with a faster melting during months of May through July, which coincides more with the observed snow depth seen in previous plots. The default formula, by Dilley (1998), shows more of a delay in the melting of snow. For this reason, the choice is made to proceed while using the formula of Idso (1981).

Another important parameter for the energy fluxes module calibration is the Monin-Obukhov stability parameter. This parameter represents the buoyancy effects in the lower atmospheric boundary layer and their impacts on turbulent fluxes (Grachev and Fairall, 1997). This parameter in GEOtop can be set as either accounting for both stability and instability in the atmosphere, accounting for only stability, only instability or considering only atmospheric stability. The default case in GEOtop is set as considering both stability and instability.

Simulations using GEOtop are performed to compare the 4 options for the Monin-Obukhov parameter calibration. The results in terms of snow depth are presented in *Figure 14*. The snow depth profiles of the default case simulation and the case of considering only atmospheric stability coincide with each other. The snow depth profiles of the case of neutrality and the case of only considering instability also approximately coincide. This shows that in this particular case the atmospheric instability has no impact on the snow accumulated over the study period. The atmospherical stability is the acting parameter in regard to Monin-Obukhov parameter calibration. Focusing also here on the melting pattern of the snow accumulated, the results with a steeper melting trend are more representative of the observed snow depth. Thus, it is deemed suitable to choose the atmospherical neutrality using the Monin-Obukhov parameter.

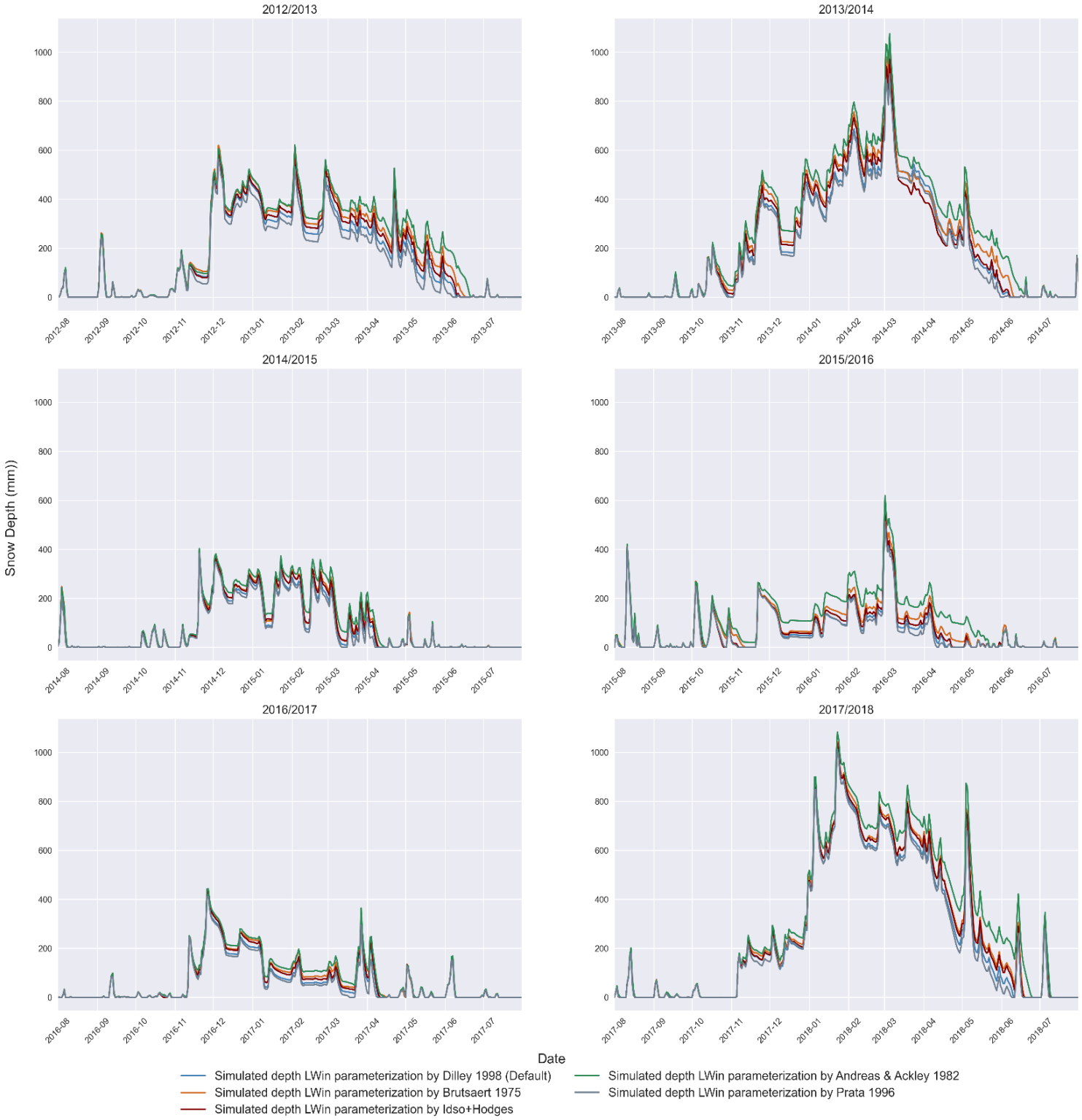


Figure 13 Snow depth simulation results for LWin parameterization calibration using formulas for LWin calculation

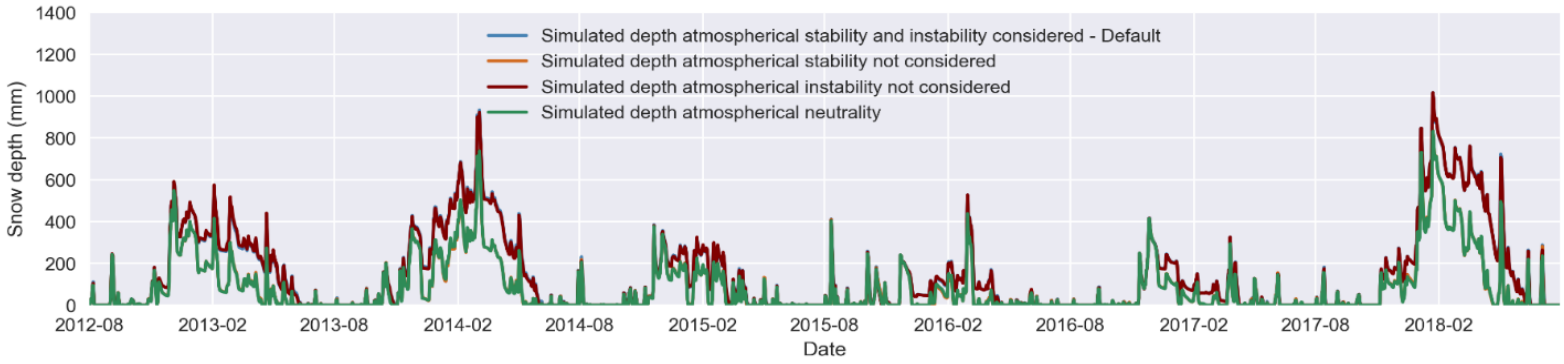


Figure 14 Snow depth simulation results comparing different Monin-Obukhov parameter options

The final result of the surface fluxes calibration is shown in *Figure 15* as compared to the initial (default case) run. The snow depth profile resembles a simulation that considers the topography calibration done in section *4.3.1*, along with applying the choice of $LW_{in}$ parameterization formula, which is Idso (1981), and the Monin-Obukhov parameter that allows the model to operate with atmospherical neutrality. The result of these 2 initial calibration steps mainly improved the melting phase in the simulated snow cover profile. This is explainable by the fact that the parameterization of the outgoing longwave radiation is an integral part of the energy fluxes at the surface, which in run has a high impact on the building up of the snow cover, as well as on its melting. On another hand, the atmospherical parameter Monin-Obukhov also interferes in the interactions between the atmosphere and the surface layer impacting the change patterns in the snow cover. The impact of the complex topography in this case are not so high, yet it is important to force the model with correct topography information.

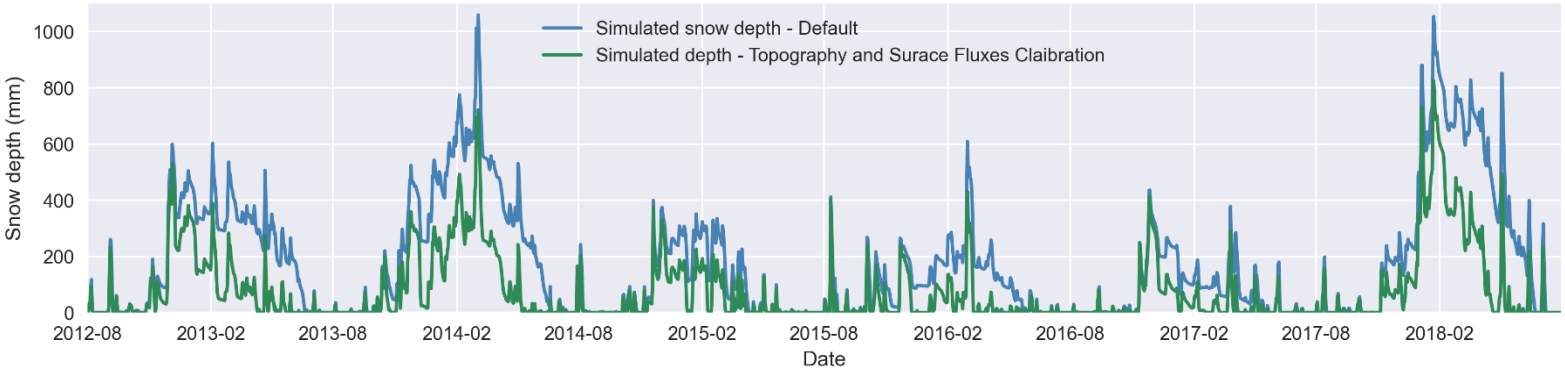


Figure 15 GEOtop simulated snow depth before and after calibration for complex topography and surface energy fluxes

### 4.3.3 Snow Module Calibration

The calibration of the snow module is done by tuning the snow characterization parameters to meet the site conditions. The values of some default parameters are changed into values that are more accurate for the Passo del Monte Moro site. Snow characterization parameters include the irreducible water saturation, the maximum snow porosity, and the visible and infrared fresh snow reflectance. The default value of the irreducible water saturation in GEOtop is 0.02. According to Engel et al. (2017), this value in the Alps can be considered to be equal to 0.07, so it is applied here. As for the maximum snow porosity value, the default value found in the model is equal to 0.7. According to a study by Zanotti et al. (2004), which describes in detail the snow module in GEOtop, the value of the maximum snow porosity can be set as 0.6. A study by Wani et al. (2021) that uses GEOtop at a site with climatic characteristics similar to the Italian Alps, the visible reflectance of fresh snow value can be used as 0.93, while the infrared reflectance of fresh snow can be assumed to be the same as the default values, which is 0.65.

Calibrating these parameters to meet the simulation point snow cover conditions is an integral step towards reasonable snow depth results, and corresponding soil surface temperature simulations. Forcing these parameters into the model GEOtop, and using the meteorological data used in the previous section, along with implementing the previous calibration of the topography and surface fluxes modules, the model is run to simulate the snow depth results. The resulting snow depth profile is shown in *Figure 16*. and the resulting case is hereafter referred to as the snow depth considering the calibrated GEOtop model.

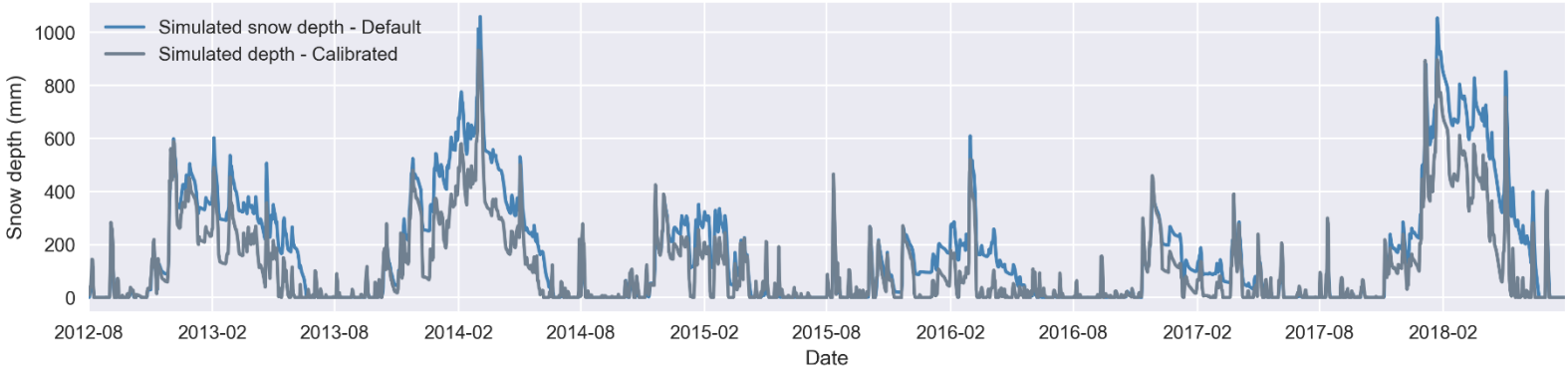


Figure 16 GEOtop simulated snow depth before and after calibration for complex topography, surface energy fluxes and snow characterization

The final result of the snow module calibration shown in *Figure 16* is compared to the simulation default case run. The snow depth profile resembles a parameterization of the model that considers the topography calibration as well as the surface energy fluxes calibration. The calibration of the modules mentioned improved the melting phase of the snow cover mainly. This advancement is essential since the melting phase of snow is one of the most impactful phenomena that occur and have an effect on the hydrological cycle, the infrastructure stability and the economy. This final result will be hereafter used as the reference case that the scenarios presented in future sections will be compared to. All the scenarios will follow the same calibration.

It is also essential to observe the changes in the simulated GST at 2 cm depth after the snow cover has been modified and the calibration of the model is done. *Figure 17* show the comparison of the plots of GST before and after calibration. The simulation is performed accounting for all the changes done in the 3 stages of calibration presented previously. Considering the slight decrease of the snow depth profile after the calibration, the GST at 2 cm depth is expected to change as well, being more affected by the atmospheric temperature than before. During the winter months, the air temperatures are constantly low, and this results in lower GST in the calibrated case as compared to the default one. As for the spring months, melting of snow occurs due to increase of solar radiation incoming and

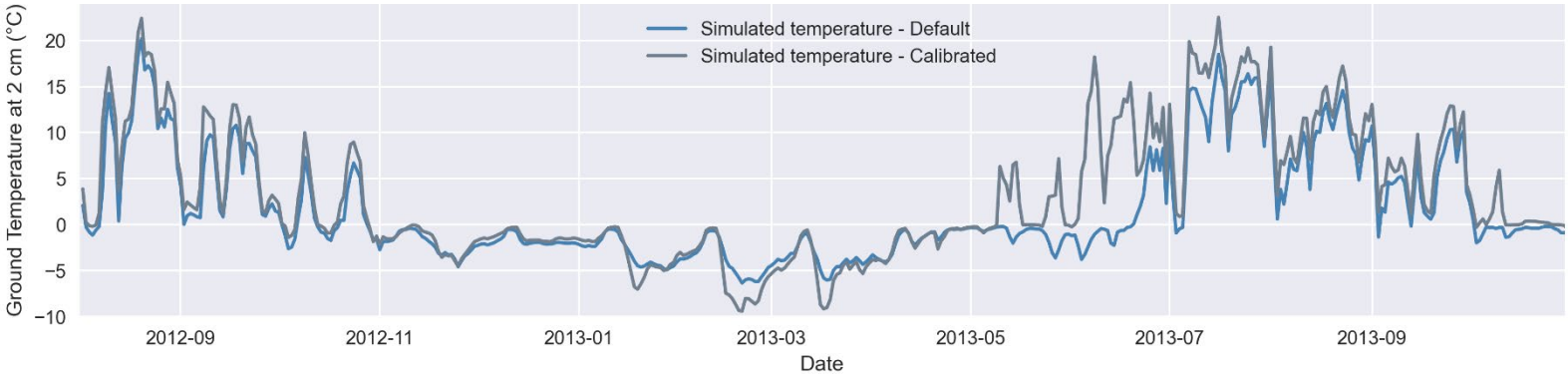


Figure 17 GEPtop simulated GST at 2 cm depth: before and after calibration

increase of air temperature. Calibrating the model improved the melting phase in the simulated snow depth profile allowing faster melting and a sharper decrease in snow depth. This is reflected on the GST by more shifting of the high temperature trend into earlier times during the year. Although this does not reflect the actual situation, however this can be improved upon fixing the snow depth profile to match the observed one, which will be done in the following sections.

## 4.4 Precipitation Correction Results

### 4.4.1 Observed Precipitation Evaluation

As mentioned in *section 3.4.2*, SWE timeseries is produced using the model ΔSnow in R. It is then used as the 'true precipitation' to which the observed precipitation is compared in order to assess whether it is underestimated and to get an approximation on the correction needed. This 'true precipitation' applies only at times when only snowfall is said to have occurred. This is assumed to be at all temperatures below -4 °C, taking a margin of error to avoid accounting for any water precipitation. The resulting SWE timeseries is computed over the period from August 2012 till August 2018 and corresponds to the accumulated daily snow depth at Passo del Monte Moro site over that period. The SWE corresponding to freshly fallen snow is calculated by computing the daily differences of the SWE for the cumulative snow depth. The observed precipitation data over the same years is aggregated into a daily timeseries and compared to the SWE calculated. The two timeseries are compared at days when the temperature values were below -4 °C.

The result of the scatter plot of observed precipitation vs SWE calculated by ΔSnow model, for days at temperatures below -4 °C, is shown in *Figure 18a*. Comparing the observed precipitation range of values, which falls between 0 and 35 mm w.e., to that of the SWE, which falls between 0 and around 100 mm w.e., a large factor of difference between the two exists. The slope of the linear fit of the two timeseries, forced to pass through zero, is equal to 0.256. In addition, as can be seen, the data are highly scattered around the linear plot and do not show a proper trend among each other. This shows that even while taking a conservative number of days where only snow is assumed to have fallen, the precipitation measured by the rain gauge does not correspond to the actual change in height of snow that was observed on the same day. The heated rain gauge used at the Passo del Monte Moro monitoring station, which is located in a remote, cold and highly elevated area, appears to produce precipitation measurements that are not perfectly reliable. Some of the causes for this unreliability are errors induced by wind effects that reduce the amount of snowfall caught by rain gauge, in addition to evaporation possibility due to heating of the rain gauge. The risk of underestimation of precipitation in cold and elevated environments is high, and correction methods are usually applied before utilizing the precipitation timeseries.

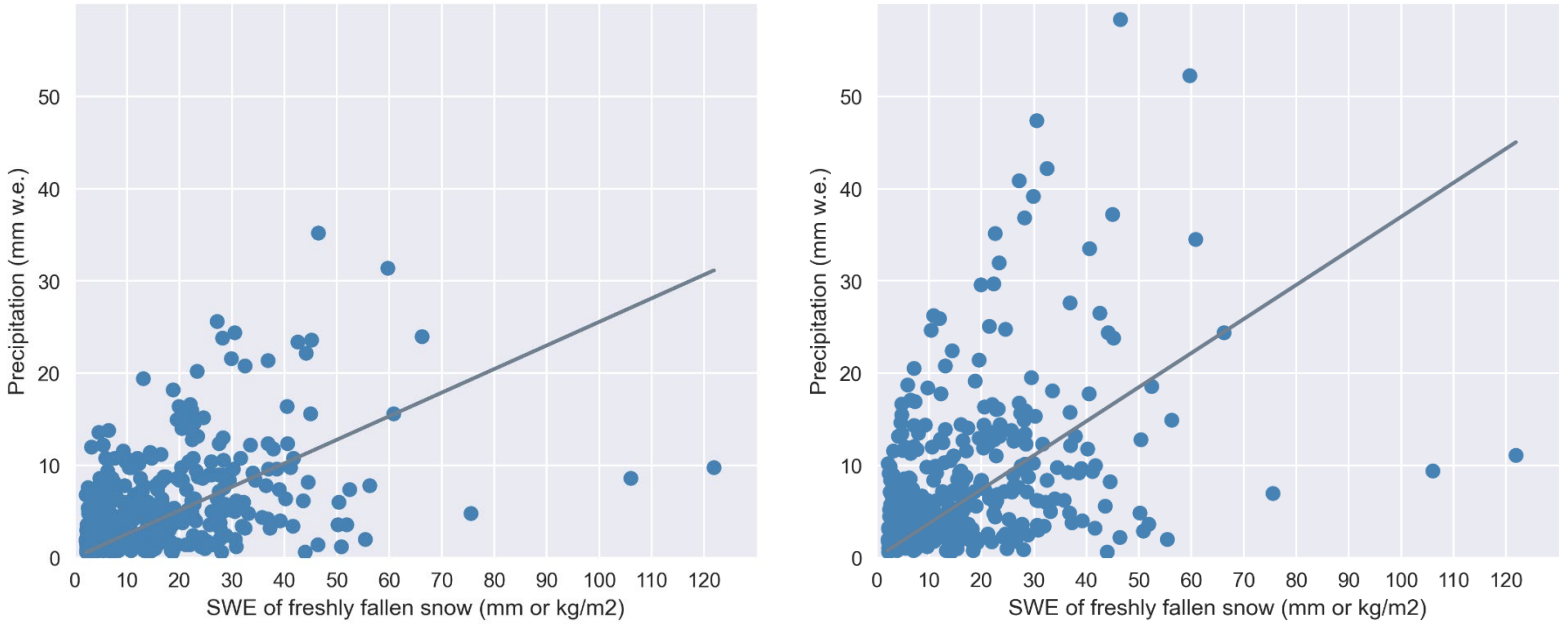


Figure 18 Plots of a) observed precipitation vs SWE calculated using DeltaSnow model, b) corrected precipitation (using CR correction method) vs SWE of freshly fallen snow

### 4.4.2 Catch Ratio Method Evaluation

It is essential to evaluate the precipitation after it has been corrected using the CR method, which accounts mainly for the wind-induced errors in the rain gauge. The corrected precipitation is a timeseries of hourly precipitation values over the period from August 2012 till August 2018, which is similar to the observed precipitation timeseries. In order to compare them, which in turn allows to evaluate the CR correction method, both datasets are aggregated over an hourly temporal scale. To assess the quality of the correction method, it is possible to compare the corrected precipitation timeseries to the SWE of freshly fallen snow, which as mentioned before can be considered as the 'true precipitation' of snow at temperatures below -4 °C. The plot of the corrected precipitation using the CR correction method against the SWE of freshly fallen snow is presented in *Figure 18b*. As can be seen, comparing the plot in *Figure 18b* to *Figure 18a*, the correction allowed the data to be more aligned along the diagonal, which shows improvement in the compatibility with the freshly fallen snow. The slope of the line in this plot is equal to 0.37, which is considerably higher than that of the previous plot that was 0.256. Grossi et al. (2017) perform a similar procedure where a precipitation timeseries from a region in the Alps is corrected and evaluated against the SWE of freshly fallen snow

in the same area. The results show a slope of around 0.4 in one of the cases. The CR correction method produces results in line with these in literature.

As a next step to compare the two timeseries, the corrected precipitation is plotted against the observed precipitation, as shown in *Figure 19*. A considerable increase in the values of the precipitation data can be seen, whereby the main bulk of data points show a factor of nearly 2 between the corrected and observed precipitations. The CR method is based on corrections related to wind, while accounting for temperature and relative humidity in order to discriminate snowfall and rainfall. This implies that the hours with low temperatures and correlated low RH values are corrected differently and more extensively. It is also noticeable that a small portion of the plotted points falls along the diagonal, which probably correspond to hours with a very low wind speed, thus not corrected by the CR method.

In order to overcome the issue of the remaining disagreement between the CR corrected precipitation data and the SWE of freshly fallen snow, the calculation of a correction factor is suggested, and the formulation of this factor was explained in *section 3.4.4*. This factor is based on the actual values of snowfall, imbedded in the SWE value, which ensures a better compliance with the actual occurring precipitation and is expected to result in better snow cover simulations.

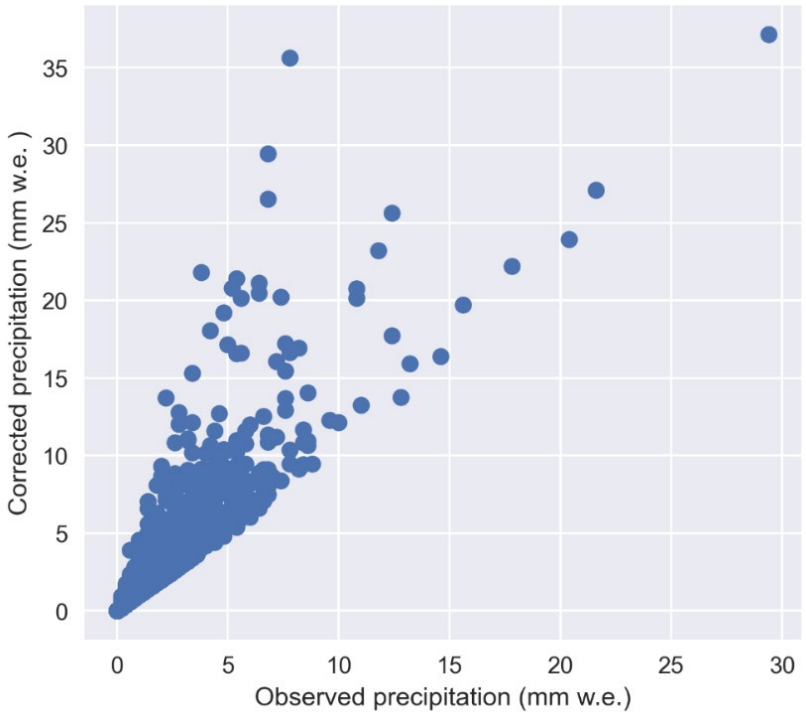


Figure 19 Plot of corrected precipitation using CR method vs observed precipitation

Table 5 Annual sums of observed precipitation and CR corrected precipitation between 2012 and 2018

| Year | Annual Sum | |
|---|---|---|
| | Observed Precipitation (mm w.e.) | CR corrected Precipitation (mm w.e.) |
| **2012** | 834 | 1350 |
| **2013** | 937 | 1325 |
| **2014** | 884 | 1284 |
| **2015** | 985 | 1445 |
| **2016** | 903 | 1344 |
| **2017** | 743 | 1098 |
| **2018** | 882 | 1360 |

*Figure 20* presents both timeseries of observed and corrected precipitation, after being aggregated into a daily timescale over the period of study. The profiles show good agreement when considering heavy precipitation events, and times at which precipitation is very low. It is also noticeable that corrected precipitation values slightly exceed the observed precipitation values at some times. The annual sums of the observed and CR corrected precipitation are shown in *Table 5*.

It is important to note that the remaining disagreement between the corrected precipitation and the SWE of freshly fallen snow, which is evident in the plot in *Figure 18b*, which has a slope less than 0.5 between the 2 datasets. In this regard, it is worth mentioning that the CR correction method corrects the data for errors related to wind effects. This means that the corrected data still does not align with the actual precipitation, which is due to other errors of rain gauges such as the heating of the snowfall which could lead to evaporation of some amounts, in addition to the effects of water wetting the instrument, that lead to losses of water amounts as well. Some other error sources which are less impactful are dents in the instrument or the tube connected to it.

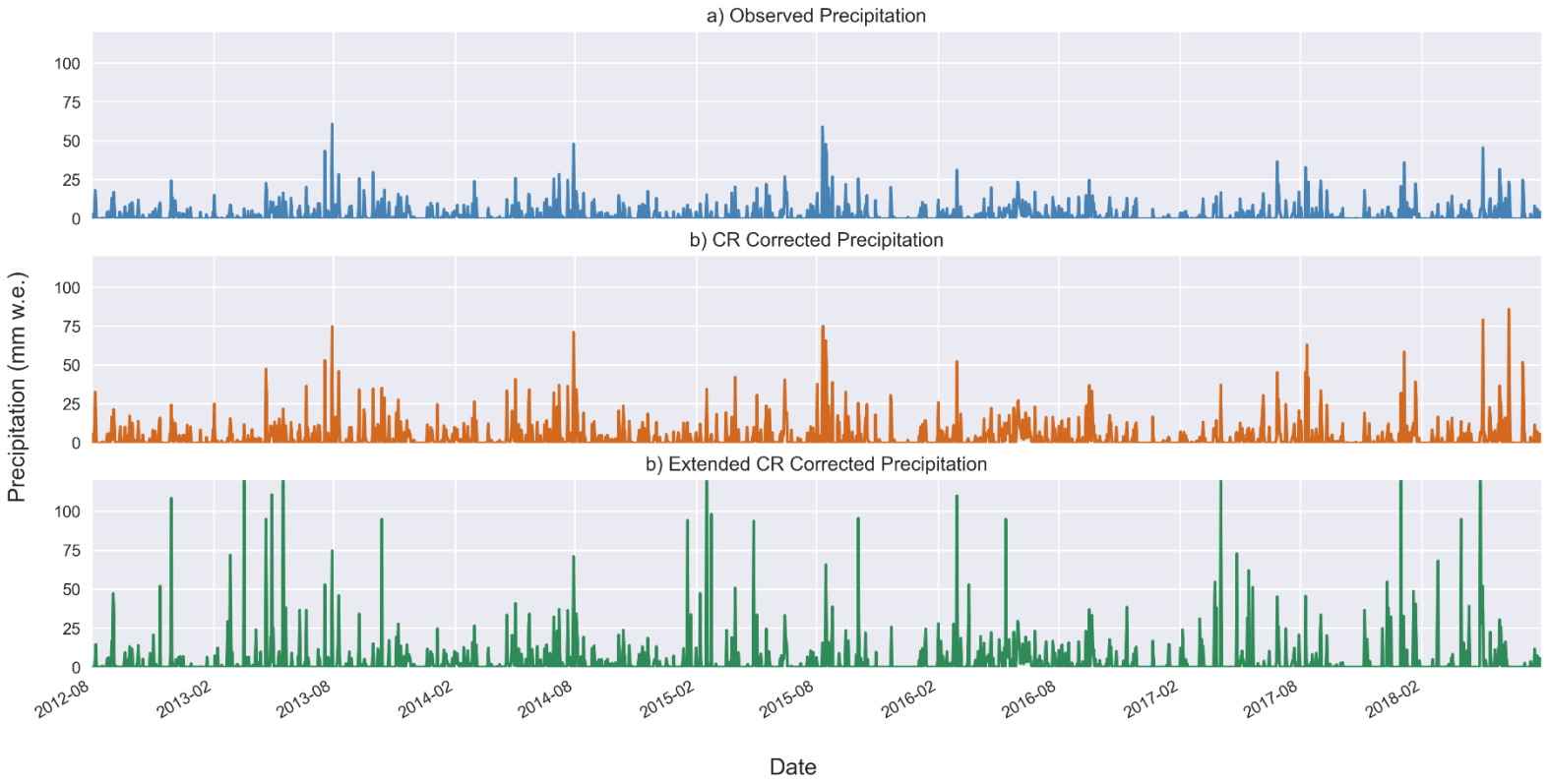


Figure 20 Timeseries of observed, CR corrected and extended CR corrected precipitation

*Figure 20c* presents the timeseries of precipitation after correction by the extended CR method. As compared to the other 2 timeseries in the figure, this one has the highest values which correspond to the true snowfall values seen at the site at those days. The 3 options for precipitation series, that are the observed original precipitation, the CR corrected precipitation and the extended CR corrected precipitation will be input to the model in order to compare the impact of these improvements on the snow depth and to realize which one is most suitable for the proper simulation of snow depth.

A further step is taken to evaluate the parameters used in the extended CR correction method, which are mainly the fresh snow density and the factor that is used. These two variables are available as a timeseries at a daily timescale but are discontinuous. The density data are available only on days when snowfall has actually occurred, as they are calculated using *equation [ 13 ]*. The factor *f(t)* is available during days when precipitation has occurred, as it is calculated in terms of SWE of freshly fallen snow and the CR corrected precipitation. The timeseries of each of these 2 parameters are shown in *Figure 21*. As can be seen, values of the density considerably fluctuate within each year and differ from year to year as well. The value of the factor is dependent on SWE of freshly fallen snow, and on the amount

of precipitation falling during each day. The value of the factor also highly fluctuates over the study period, showing the importance of considering a time-dependant factor rather than a constant one.

As discussed before, from this density timeseries, the mode which is equivalent to 150 kg/m$^3$ has been used for proceeding with the method calculations. It is worth noting that taking a constant value of density for all the years could be one reason of uncertainty in the final results, since it has been presented that the density in fact fluctuates and differs from year to year. This also means that the timeseries of the factor f(t) is independent from the actual density value seen on the same day, as it is calculated using the constant value of the density distribution mode. However, adopting such simplification is useful for applying this research methodology for modelling future snow depth profiles where a density timeseries is not available and cannot be easily approximated.

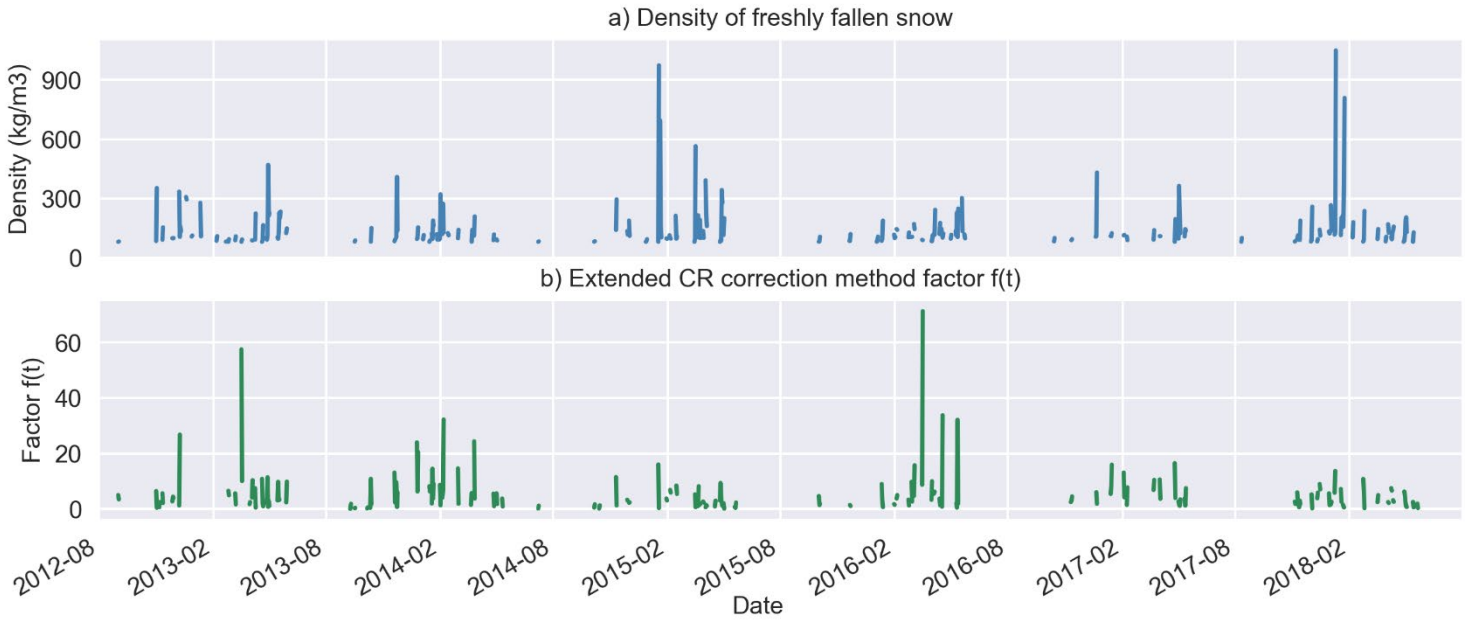


Figure 21 Timeseries of freshly fallen snow density and extended CR correction method f(t)

## 4.5 GEOtop Output Evaluation

### 4.5.1 Snow Depth

In the previous sections, an initial calibration of GEOtop mode to the Passo del Monte Moro site was done. The input data forced to the model were also pre-processed in order to become accurate enough to produce acceptable outputs from the model that could meet the measured snow depth profile available. In the current section, 3 main scenarios for simulating the snow depth are presented and interpreted. The 3 scenarios involve the precipitation corrections that have been applied, and they are as follows:

1) Default scenario having the observed original precipitation as the input precipitation, while applying the calibrations done for the complex topography parameters, the surface energy fluxes module and the snow module
2) Scenario where the input precipitation given to the model is the precipitation corrected using the Catch Ratio method, which is hereafter referred to as CR corrected precipitation. This scenario is also simulated after applying the calibrations done for the complex topography parameters, the surface energy fluxes module and the snow module
3) Scenario where the input precipitation is the precipitation multiplied by the correction factor after being corrected using the Catch Ratio method, which is the extended CR corrected precipitation case. This scenario is also simulated after applying the calibrations done for the complex topography parameters, the surface energy fluxes module and the snow module

The 3 resulting snow cover profiles are compared to the reference snow depth which is the one measured on site. This allows to evaluate which correction method is most appropriate to be used, that allows to produce results of snow depth as close as possible to the observed ones on site. In order to plot the snow cover profiles using the model output data which are in hourly timescale, all the data are aggregated over daily timescales. *Figure 22* presents the output snow depth results from simulation performed using GEOtop model. The graph shows a comparison plot between the snow depth profiles resulting from the 3 suggested scenarios and the observed snow depth profile. A more extensive presentation of the snow depth profiles for the 6 years of simulation period is shown in *Figure 23*, that allows a clearer comparison between the scenarios and with the observed snow depth profile.

The default scenario which was seen in a previous plot possesses a high difference from the actual snow depth profile. The maximum snow depth reached by the default scenario is around 1000 mm while the observed snow depth reaches a maximum value of 4000 mm over the study period. This can be explained by a major causing factor which is the erroneous precipitation data that is given as input to the model. As discussed before, the precipitation measured by the heated rain gauge includes several errors related to wind effects, heating effects and wetting complications. The dataset has failed to align with the SWE of freshly fallen snow and this is evident in the current results simulated by GEOtop.

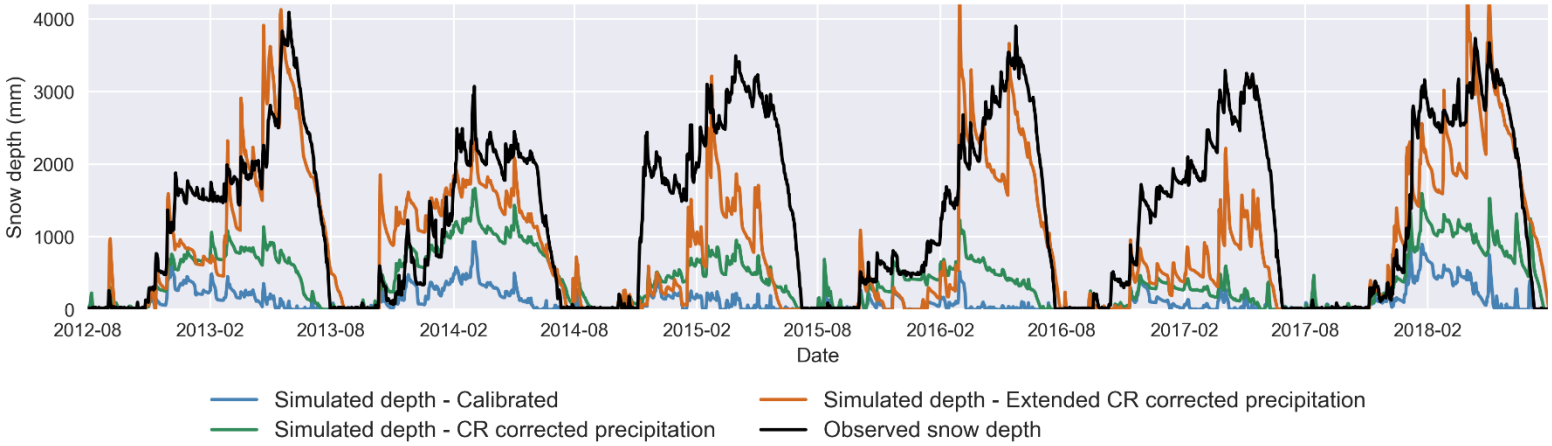


Figure 22 GEOtop output snow depth profiles from 3 different scenarios

As for the scenario that is simulated using the CR corrected precipitation, the results are considerably improved, although not yet properly aligning with the observed snow depth profile. The maximum snow depth reached during the year 2014 is around 1800 mm, which is still far below the maximum depth reached by the observed snow depth in that year. Other years show even greater differences between the 2 depth profiles. The Catch Ratio method corrects the precipitation data only for wind-induced undercatch situations. In remote mountain areas, as is the case at Passo del Monte Moro station, other factors can be behind the underestimation of fallen precipitation at the site. After the correction of the precipitation data for wind effects, the precipitation still does not meet the actual snowfall and/or rainfall that actually occurred. GEOtop model solves the mass and energy balance equations explained in *section 2.2* in order to model the snow depth. The importance of the precipitation data is immense for the mass balance part of the solution. The law of mass conservation simply explains that no additional mass can be created by the model when it simulates, which means that any underestimation of the precipitation data would lead to lower mass input to the model, consequently resulting in lower mass created, which is the snow cover mainly. Therefore, the

remaining errors in the precipitation data allow only a limited part of the actual precipitation to be given to the model in this case, leading to underestimation of the snow depth by the model.

The extended CR correction method scenario is implemented to overcome the remaining errors in the precipitation timeseries. The results of this scenario are also shown in Figure *22* and *Figure 23*. This scenario results in a snow depth profile that is much more in compliance with the observed snow depth, thus deemed properly representative of the snow depth. During the winter season of the years 2013, 2014, 2016 and 2018, the model is able to simulate the snow depth with high accuracy, and the melting phase during the spring months is well represented. A proper melting phase is reached because of the surface energy fluxes' calibration in the model. The main actors that were tuned were the parameterization of the outgoing longwave radiation and the Monin-Obukhov atmospherical parameter. Overall, the results of snow depth simulated by the model in this scenario can be considered to be properly representative of the snow cover, as compared to studies in literature that have used GEOtop and other models as well (Terzago et al., 2020). The major disagreement between the extended CR scenario and the observed snow depth profile during the years 2015 and 2017 may be hypothesized to be a result of an inaccurate assumption of the fresh snowfall density value. As mentioned before, fixing the mass balance in the model GEOtop was based on the use of the mode value of the probability density function of density of fresh snowfall. Taking a common value for all years could be a reason for inaccuracies in modelling the snow depth in some of the years, which could have experienced a different type of snowfall. *Figure 21*, which presents the timeseries of the density used, indeed show a different behaviour of the density of fresh snow in the year 2015, which means that the approximation of the density as its mode value might not be so accurate for this year in specific. Thus, the inaccuracy that might have occurred when fixing the mass balance in the mode GEOtop could be an explanation for the disagreement of the model results with the observed snow depth during this year.

It is worth noting that the rapid increase in snow depth simulated data between one day and the other at some points is thought to be caused by sudden and high intensity snowfall events. Observing the hourly timeseries produced by the model for snow depth values shows that some events of snowfall increase the snow depth from 300 mm during day hours of the first day, to a cumulative value of 1000 mm during the next day. An example of such case is during the month of April 2013 and 2018. Such

results appear in this manner in the plots because of the aggregation of hourly data into a daily timescale for clarity.

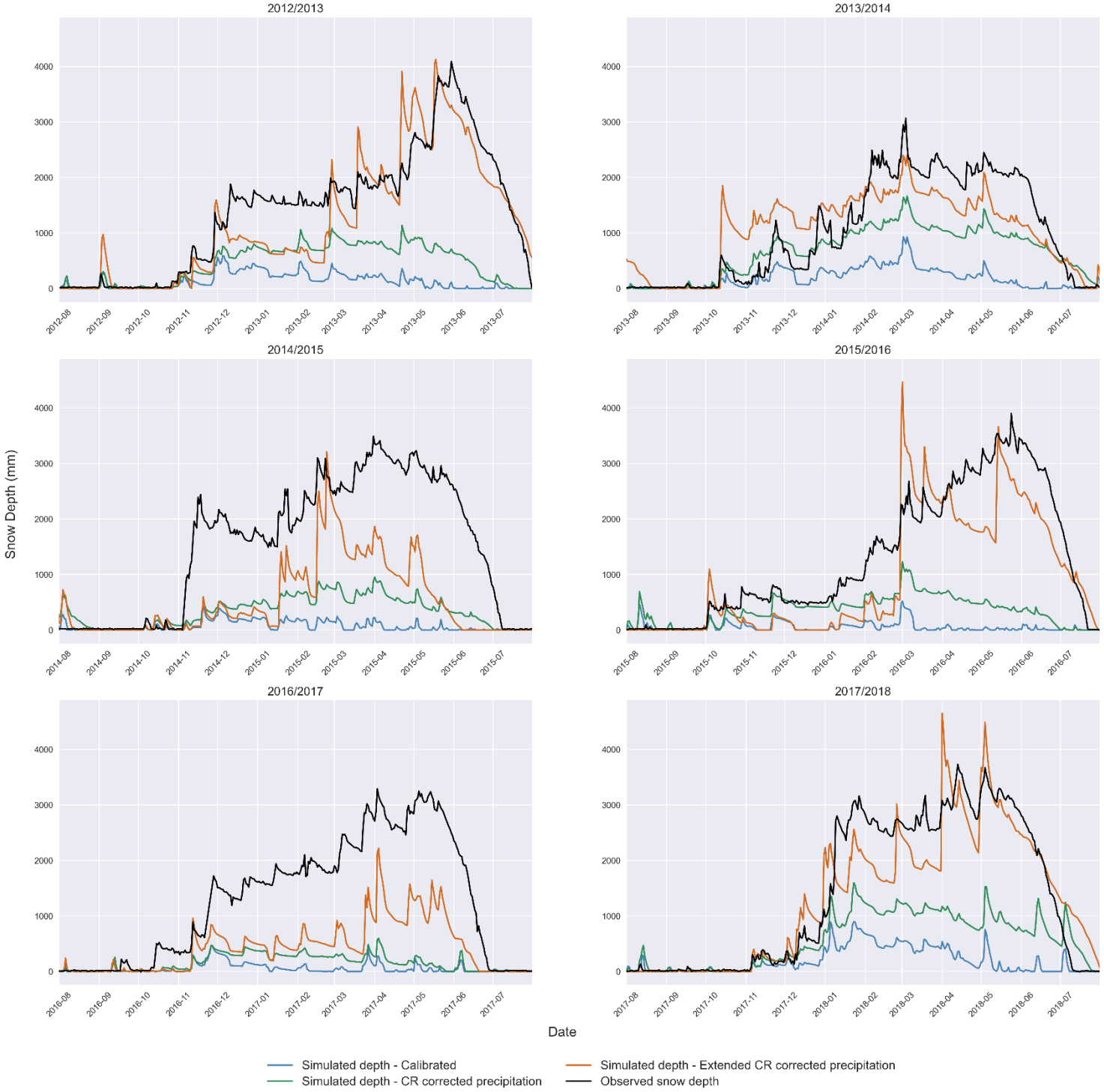


Figure 23 GEOtop year-by-year output snow depth profiles from 3 different scenarios

### 4.5.2 Ground Surface Temperature

The ground surface temperature results after the application of the 3 scenarios of precipitation input data is simulated as well. One of the goals is to be able to simulate the GST at 2 cm depth properly using the model GEOtop, while having performed model calibration and utilizing the corrected precipitation data. For simulating the GST at 2 cm depth using GEOtop, the calibration done for the complex topography module, the surface fluxes module and the snow module is applied. The precipitation scenarios that have been simulated to produce the snow depth profile are used as well to give the GST at 2 cm depth. The GST at 2 cm depth is an output timeseries from GEOtop model, which is at an hourly timescale. The duration of the simulation period is from August 2012 until October 2013, in order to meet the duration over which measurements of GST are available.

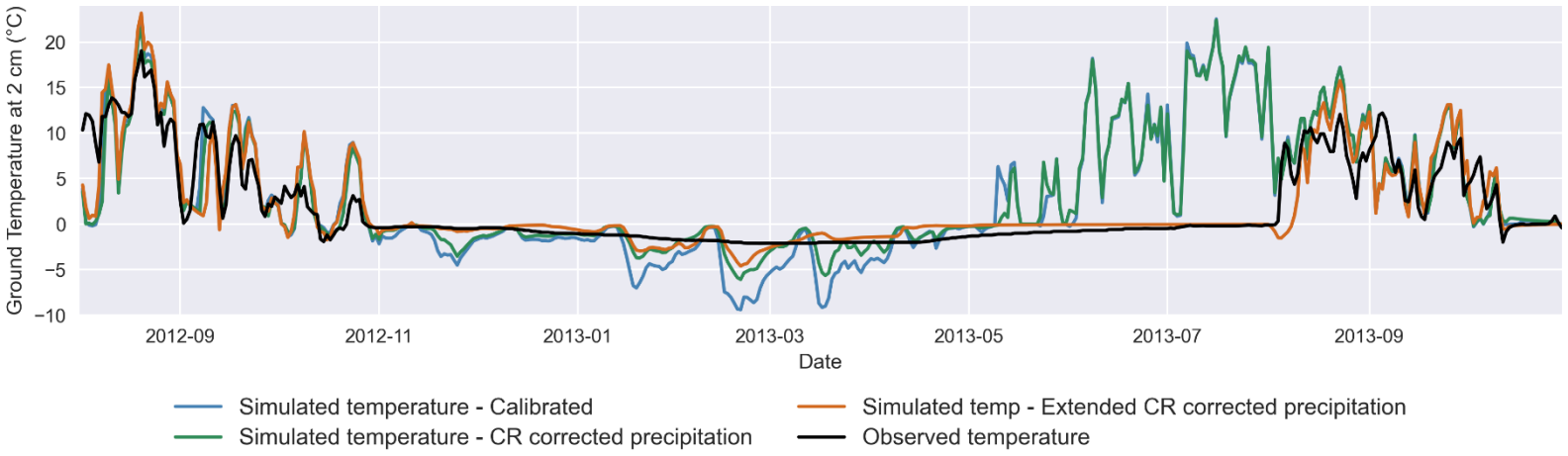


Figure 24 GEOtop output: GST at 2 cm depth profiles for the 3 scenarios

The results of the GST simulated by GEOtop using the 3 scenarios previously mentioned are presented in *Figure 24*. The 3 temperature profiles are compared to the observed GST at 2 cm depth profile, obtained from Passo del Monte Moro monitoring station. The first scenario represents the calibrated modules while forcing the model with observed precipitation data without pre-processing. The result of this scenario has been previously presented and is not properly compliant with the observed GST profile. As for the CR corrected precipitation scenario, not much change is seen as compared to the calibrated model case. This is expected because the snow depth profile of this scenario did not improve much. However, slight improvement appears during the winter months where the temperature is represented a bit better. Finally, the third scenario which includes the model calibration improvements as well as the extended CR corrected precipitation input data, the results show great improvement and good agreement with the GST observed profile. During the winter

season, the minimum values agree with the minimum temperatures of the GST observed. As for the spring and summer seasons, the increase in GST in this scenario is slightly delayed as compared to the observed one. This can be due to the slightly preceding melting phase by the model than that actually occurring. On the other hand, the maximum reached GST during these seasons matches the observed one, at a value of around 13 °C. Thus, after the improvements that have been done, this scenario can be considered as representative of the conditions seen at the simulation point for both the snow depth and the GST at 2 cm depth.

### 4.5.3 Surface Energy Balance Components

GEOtop computes the solar radiation components, including the incoming and outgoing shortwave and longwave radiations. The net SW and LW are also calculated by GEOtop. These variables can be set as output data from GEOtop along with the snow depth and other parameters. The output radiation data from GEOtop are a timeseries of hourly data over the simulation period. In order to view these timeseries, they are aggregated into a daily timescale. The incoming and outgoing shortwave and longwave daily timeseries are plotted along with the net results, as shown in *Figure 25*. Since the data exhibit high variations, it is preferable to view only a couple of years, which is here taken from August 2012 till July 2014, for more clarity. These 2 years are considered representative of the study period, and the snow depth simulated in these years matches the measured one at site.

As shown in *Figure 25*, the daily mean values of $SW_{in}$ range between 7 W/m$^2$ to 386 W/m$^2$. From *Figure 23*, it can be seen that the snow cover persists during the winter months, which is translated into more reflection of the $SW_{in}$ during these months (*Figure 25a*). During the month of October in both years shown, the $SW_{out}$ mean exhibits a fairly constant value, which is considered a period with no snowfall occurring. $LW_{out}$ has a pattern of lower daily mean variations than that of $LW_{in}$ over the whole year (*Figure 25b*). The net value of SW falls around zero, which is considered to be due to the high reflectance of snow as compared to the total incoming radiation. The net value LW has a mean over the whole year of around -80 W/m$^2$.

In *Figure 26* the daily mean variability of the components of the surface energy balance equation (shown in *equation [ 1 ]*) resulting from the GEOtop simulations are plotted over the same years as the previous plot. The components are the net radiation $R_n$, the sensible heat flux SH, the latent heat LE, and the ground heat flux G. The net radiation varies seasonally, showing high daily means during hot


Figure 25 Plots of GEOtop outputs: daily mean values of SW and LW (in, out and net)

months and low daily means during colder ones. Maximum $R_n$ daily mean value is around 150 W/m$^2$, and the minimum reached is -28 W/m$^2$. The daily means of SH vary seasonally, showing the highest values during months when the snow cover has accumulated, and negative values during other months. LE show a wider variability in the daily mean than SH. During the months when the snow cover is barely existing, the daily mean values of LE vary around zero, which can be caused by the freezing of soil during these months. Other months have negative values of LE, especially during evaporation periods. The ground heat conduction G has a rather constant profile during all months except September and beginning of October, where it shows high variations. The overall mean of this value is close to zero and thus it is considered to have little impact in the energy balance equation.


Figure 26 Plots of GEOtop outputs: daily mean values of SEB components

In order to better interpret the seasonality of the SEB components, along with the hourly changes during the day, Figure *27* is created from the GEOtop output data of the SEB components. Hourly mean values of each SEB components are calculated over 4 different seasons, using the output data of the 6-year-study period. The seasons are divided as follows: pre-winter is considered September and October, Winter is December and January, Post-winter includes March and April, and Summer is July and August. During pre-winter and summer seasons, the $R_n$ shows relatively high values as compared to the other 2 seasons, where $R_n$ during post-winter season is slightly lower, and during winter season it is much lower. Also, during pre-winter and summer seasons the value of G is slightly negative especially mid-day and positive during night, while it varies around zero during the other

months. LE and H values are much lower than the other components during all seasons. They vary slightly below zero during pre-winter and summer, while during winter and post-winter they go slightly above zero in the mean.

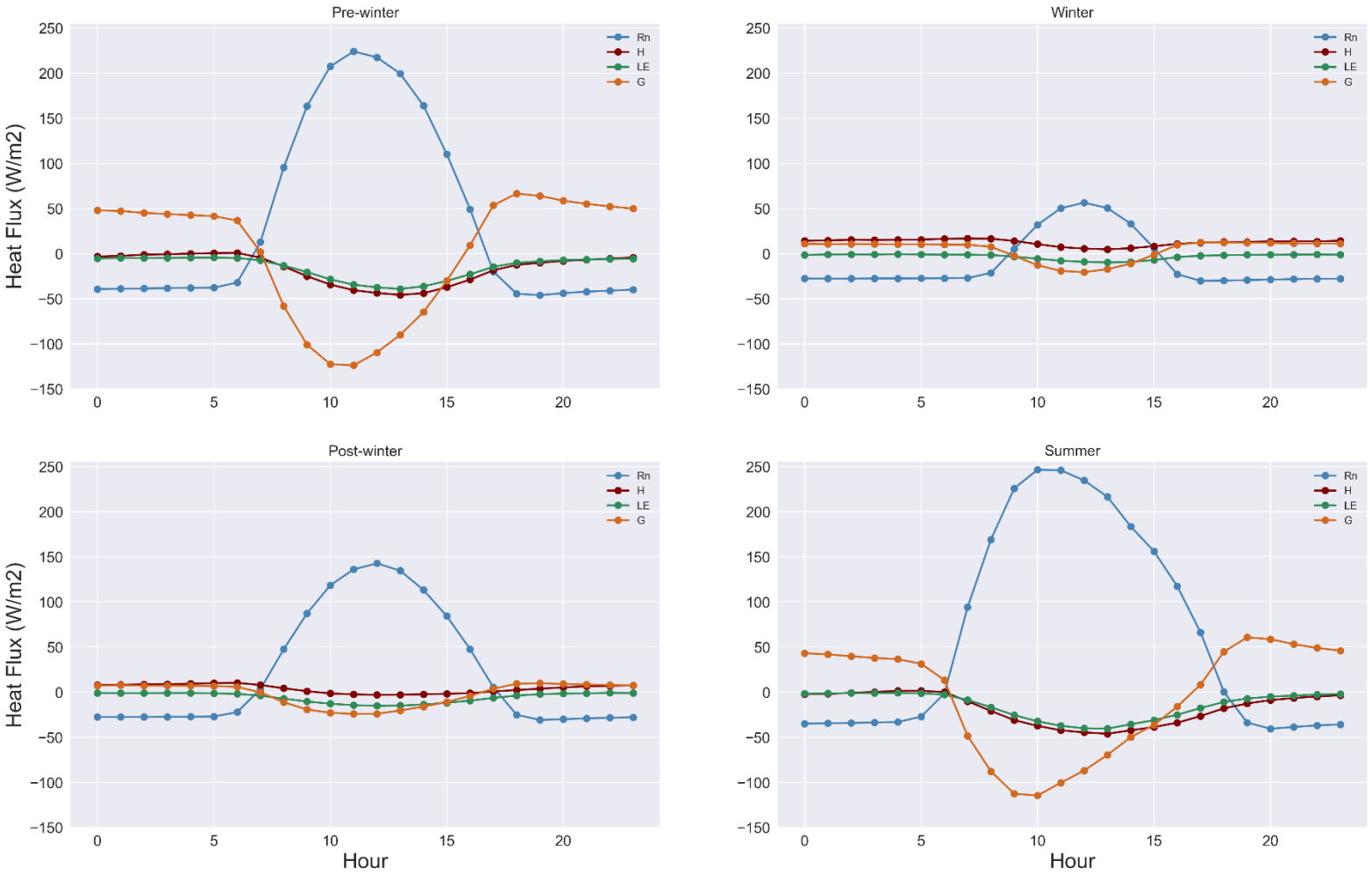


Figure 27 Plots of GEOtop outputs: Hourly variations in SEB components during 4 seasons

## 4.6 Sensitivity Analysis

The last phase of this research work deals with performing a sensitivity analysis on parameters of the snow module in GEOtop. The snow module parameters are impactful in governing the simulated snow depth, which in turn controls the simulated ground surface temperature. The importance of the snow characteristics is that they play an important role in controlling the water and energy balances. The sensitivity analysis is done for the purpose of highlighting the main and most impactful snow characteristics that are expressed through parameters that can be changed by the modeler in GEOtop.

The baseline of all the sensitivities done is by applying all calibrations already suggested to the model and using the extended CR corrected precipitation as the precipitation in the input meteorological data file. The sensitivity analysis performed in this section handles mainly 3 parameters from GEOtop that are mentioned below, and the range of these parameters used to perform the sensitivity analysis is adopted from Engel et al. (2017).:

1) SnowCorrFactor: is the snow correction factor, a factor that is implemented in the model that allows to overcome errors of rain gauge measurements. The default value in GEOtop is 1, which indicates no correction of precipitation.
2) ThresTempRain, ThresTempSnow and DewTempOrNormTemp: are considered as one parameter since they operate together. The model allows selecting either the dew point or air temperature to be used in order to discriminate between snowfall and rainfall. The modeler can also choose the threshold temperature below which all precipitation is snowfall, and another, or same, threshold above which all precipitation is rainfall. The default values in GEOtop are -3 °C for snow threshold and 1°C for rain threshold, using air temperatures.
3) FreshSnowRefVis: represents the reflectance of fresh snow in the visible band. The default value in GEOtop is 0.65.

*Figure 28* presents the sensitivity done on the snow correction factor (SCF). This parameters functions by modifying the input precipitation data to correct for errors caused by rain gauges. The value 1 which is the default one performs no corrections. The SCF is varied over the values 1.4 and 1.8 adopted from Engel et al. (2017) and Wani et al. (2021) respectively. As can be seen, the snow depth profile shifts upward as the SCF is increased. However, the disadvantages of the used of this factor can be seen through the shift of the depth profiles during the summer times as well, where the snow depth is supposed to reach values close to 0. This means that the melting phase of the snow is altered,

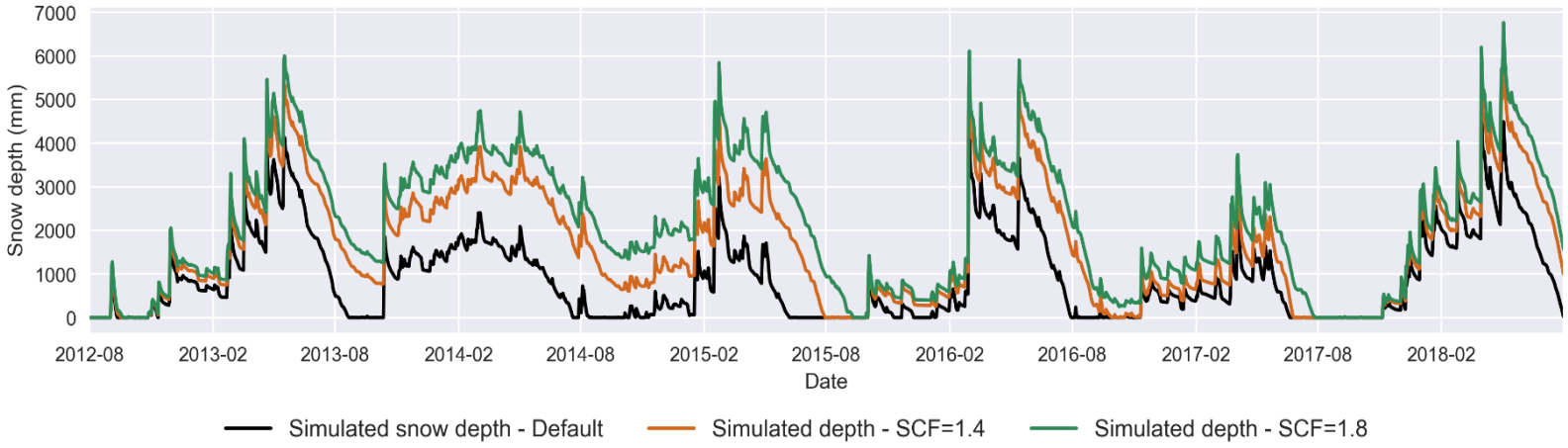


Figure 28 Sensitivity analysis on snow sorrection factor in GEOtop

which in turn would render the simulation not very compliant with the observed snow depth in this case. In general, the improvement of the snow depth upon the use of the SCF is noticeable, yet in some cases might not be accurate.

The second set of parameters that sensitivity analysis is performed on is related to the threshold temperature used to distinguish snowfall from rainfall by the model. The default values in GEOtop are -3 °C for snow threshold and 1°C for rain threshold, using air temperatures. These will be varied according to Engel et al. (2017) work, by choosing the values of snow/rain thresholds as: -0.5/0.5, -3.5/7, 1/3, and 1.5/1.5 (°C). The results of snow depth after the changes of this parameter are shown in *Figure 29*. The impact of changing this set of parameters is lower than that of the SCF. The slight changes seen mainly cause increases in the snow amounts considered by the model from the input data, represented by an increase in the snow depth profile, and delay in melting process.

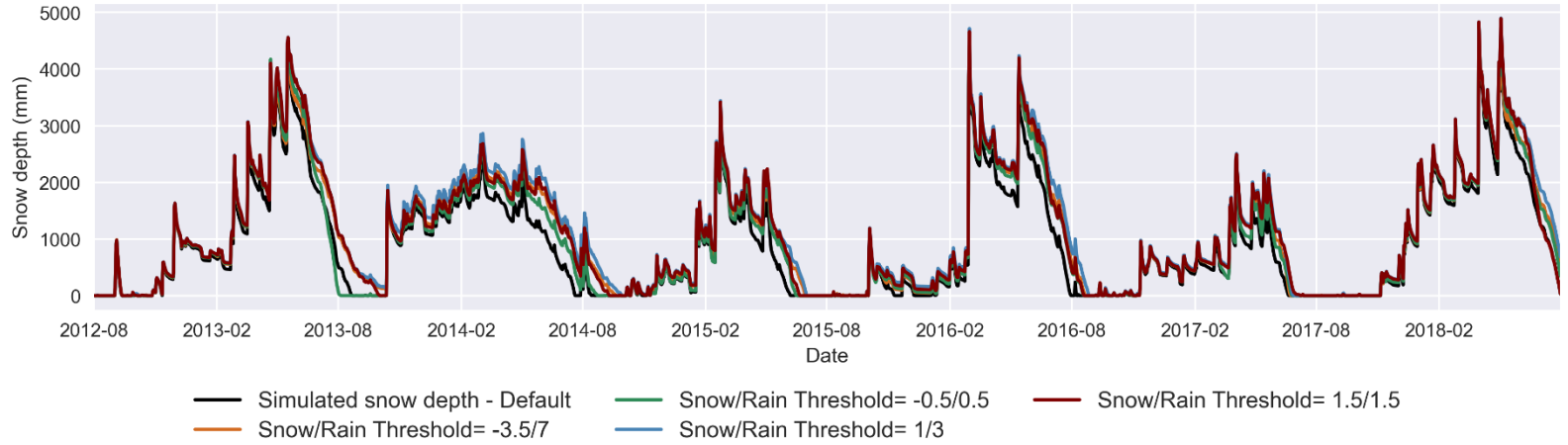


Figure 29 Sensitivity analysis on snow/rain thresholds air temperature in GEOtop

The third and final parameter undergoing the sensitivity analysis the fresh snow reflectance in the visible band (FSRV). The default value in GEOtop is 0.9 and the parameter is varied here over the values 0.75 and 0.96. The results of the snow depth profiles are shown in *Figure 30*. As would be expected, an increase in the reflectance value leads to the increase of the snow depth on each day, caused by lower melting rates of snow; on the other hand, the decrease of the reflectance causes a decrease in the snow depth as a consequence of higher melting rates, and leads to a sharper melting phase profile.

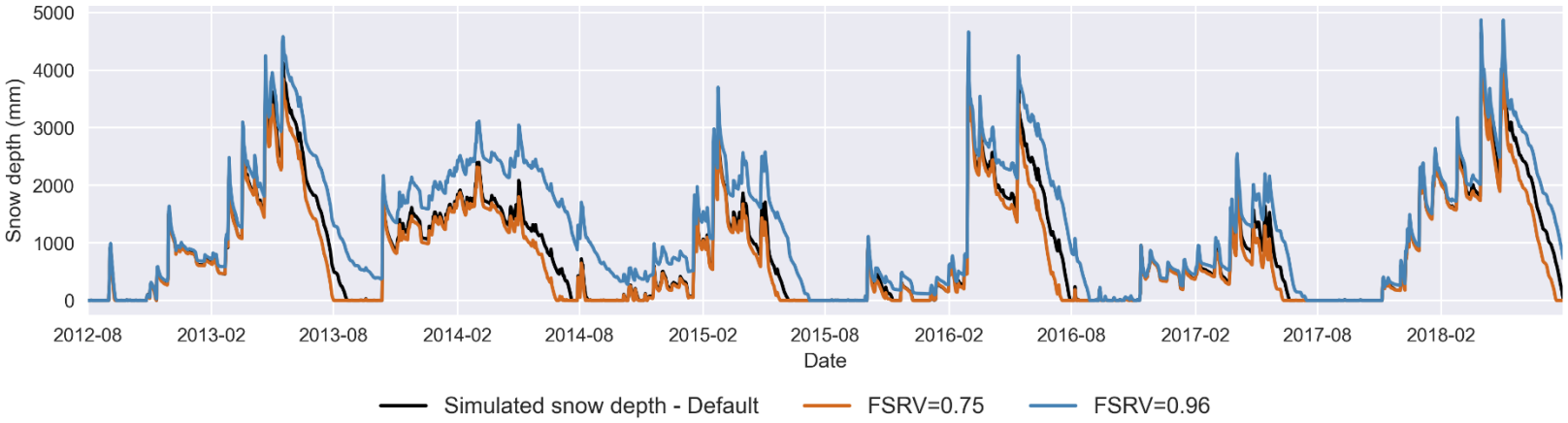


Figure 30 Sensitivity analysis on fresh snow visible reflectance in GEOtop

# Chapter 5

# Conclusions

Surface energy fluxes in high-mountain areas play a crucial role in defining the permafrost thermal state (Noetzli et al., 2007). The surface layer conditions, atmospheric air temperatures and turbulent fluxes are all important factors that govern the permafrost situation and its evolution in regions like the European Alps. In order to understand the evolution of permafrost over time, information about the temperature at and below the ground surface is required. Thus, a major part of the knowledge of the permafrost thermal conditions depends on knowledge of the ground temperature, which in turn moderates the soil freeze and thaw processes. Another essential factor that interferes in the surface heat fluxes is the type of surface that overarches the permafrost layer. The existence of a snow cover over the permafrost underlain ground is very frequent in high elevation Alpine areas. The characteristics of this layer are some of the essential factors that regulate the SEB, especially its depth. This provokes the need to monitor the snow depth in permafrost areas and to be able to simulate the snow depth in order to get future estimations and get insights on the permafrost future conditions.

The goal of this research work was to be able to appropriately model the thermodynamical processes governing the evolution of the cryosphere, namely the snow layer, to investigate its role in defining the ground temperature in the presence of permafrost. The focus was to provide a better understanding of the role of the surface energy balance in a permafrost-dominated area. The importance of being able to model the snow cover in highly elevated areas is mainly due to the vital role that this layer plays in the hydrological cycle. The hydrological cycle in areas including mountains with snow has immense impacts on many sectors including agriculture and the economy. The safety issues that are faced due to the impacts of climate change on the cryosphere is also a great motive for this field of research.

During this research work, the site used was Passo del Monte Moro located in the Italian Alps. The hydrological model GEOtop with coupled water and surface energy balances was employed. The model was calibrated and tuned over several steps and using multiple approaches. The aim is to be able to properly model the snow depth profile and the ground surface temperature at the simulation point. The results of the work highlight the important actors in the definition of the snow cover and the corresponding ground surface temperature. It was found that the parameterization of the SEB

components is a very impactful parameter for modelling the snow depth. The model GEOtop has a snow module where the characteristics of the snow layer can be set by the modeler.

The results of the work also show the importance of tuning these parameters in the model in order to obtain proper results that are compliant with the observed snow depth at site. An important part of the work tackled the correction of input meteorological data to the model. The precipitation measurements in specific were found to be highly erroneous and led to false results of simulated snow depth and soil surface temperature. For the aim of correcting the precipitation timeseries to match the actual rain and snowfall, the Catch Ration correction method was employed. Further correction was needed to handle errors other than wind-induced undercatch and so an extended version of the method was applied. The results of the corrections applied to the precipitation showed good agreement with the actual precipitation at the site, approximated as the SWE of freshly fallen snow. The evaluation of the correction method showed an important parameter which is the density of the fresh snow, which is used for the correction calculations. The density of fresh snow highly varies, and a challenge is that no measured data for it are usually available in mountainous sites. Calculating the density using several methods is possible yet causes some inaccuracies. For the purposes of this work the mode of the density distribution was used, although it has been shown that the density could vary from year to year. Adopting such simplification is useful for applying this research methodology for modelling future snow depth profiles where a density timeseries is not available and cannot be easily approximated. The median or the mean can also be suitable for similar research work.

Combining the model calibration and tuning with the corrected precipitation input data, a final simulation of the snow depth and ground surface temperature was done using GEOtop. The results rendered showed good agreement with the site measurements for most of the 6 years over which study was done. This conclusion allows future successful use of GEOtop model at Passo del Monte Moro site, and also at nearby sites with similar climatic conditions. It provides a set of calibrated parameters along with a suggested method to be used to correct the meteorological input data to the model.

Research work in general is faced with several possible limitations. The limitations of this research work could be mainly the data availability such as values of fresh snow density. In this context the fact that the site chosen is a remote high mountain area, it is common that some datasets are difficult to find. Literature provides several solutions that allow to approximate missing parameters and some of

these were applied here as well. Another challenge to this field of research is the difficulty to discriminate between snowfall and liquid precipitation, which has a major impact on the results of a hydrological model. Several methods attempt to discriminate between the two phases, yet not always fully sufficient in describing the actual scenario.

## 5.1 Future Work

The research work provided can be a baseline for several future work related to permafrost, high mountain areas and hydrological modelling, using the model GEOtop in specific. Based in the calibration and tuning of the model done in this work, the model GEOtop can be used for performing future predictions for the snow layer profile and ground surface temperature. This requires the availability of data from regional or global climatic models. The use of GEOtop for these purposes can be applied for the site Passo del Monte Moro and other sites as well. The prediction of the future situation of the snow cover in this area would give important data to policy makers on which the economy and the safety of this region in the future would be based.

In addition to that, the model GEOtop can be extended to be applied over a grid instead of a single simulation point. Modeling the snow layer and the ground surface temperature over a grid provides more impactful information for studying the changes in permafrost caused by climate changes. With the current rapid increase of temperatures and of climatic condition all over the world, the value of such research work grows more and more, and it becomes inevitable to apply modelling techniques along with other technologies for measurements for the purposes of monitoring and decision making.

# Bibliography


Adler, C., Huggel, C., Orlove, B. and Nolin, A., 2019. Climate change in the mountain cryosphere: impacts and responses.

Anders, K., Marx, S., Boike, J., Herfort, B., Wilcox, E.J., Langer, M., Marsh, P. and Höfle, B., 2020. Multitemporal terrestrial laser scanning point clouds for thaw subsidence observation at Arctic permafrost monitoring sites. *Earth Surface Processes and Landforms*, *45*(7), pp.1589-1600.

Atkinson, D.E., Brown, R., Alt, B., Agnew, T., Bourgeois, J., Burgess, M., Duguay, C., Henry, G., Jeffers, S., Koerner, R. and Lewkowicz, A.G., 2006. Canadian cryospheric response to an anomalous warm summer: a synthesis of the climate change action fund project "The state of the arctic cryosphere during the extreme warm summer of 1998". *Atmosphere-Ocean*, *44*(4), pp.347-375.

Auer, I., Böhm, R., Jurkovic, A., Lipa, W., Orlik, A., Potzmann, R., Schöner, W., Ungersböck, M., Matulla, C., Briffa, K. and Jones, P., 2007. HISTALP—historical instrumental climatological surface time series of the Greater Alpine Region. *International Journal of Climatology: A Journal of the Royal Meteorological Society*, *27*(1), pp.17-46.

Awan, N.K. and Formayer, H., 2017. Cutoff low systems and their relevance to large-scale extreme precipitation in the European Alps. *Theoretical and Applied Climatology*, *129*(1), pp.149-158.

Barry, R.G., 1985. The cryosphere and climate change. *Detecting the Climatic Effects of Increasing Carbon Dioxide*, *109*, p.148.

Bednorz, E., 2004. Snow cover in eastern Europe in relation to temperature, precipitation and circulation. *International Journal of Climatology: A Journal of the Royal Meteorological Society*, *24*(5), pp.591-601.

Beniston, M., 2007. Entering into the "greenhouse century": recent record temperatures in Switzerland are comparable to the upper temperature quantiles in a greenhouse climate. *Geophysical Research Letters*, *34*(16).

Beniston, M., Farinotti, D., Stoffel, M., Andreassen, L.M., Coppola, E., Eckert, N., Fantini, A., Giacona, F., Hauck, C., Huss, M. and Huwald, H., 2018. The European mountain cryosphere: a review of its current state, trends, and future challenges. *The Cryosphere*, *12*(2), pp.759-794.

Bocchiola, D. and Rosso, R., 2007. The distribution of daily snow water equivalent in the central Italian Alps. *Advances in water resources*, *30*(1), pp.135-147.

Bommer, C., Phillips, M. and Arenson, L.U., 2010. Practical recommendations for planning, constructing and maintaining infrastructure in mountain permafrost. *Permafrost and Periglacial Processes*, *21*(1), pp.97-104.

Brönnimann, S., Rajczak, J., Fischer, E.M., Raible, C.C., Rohrer, M. and Schär, C., 2018. Changing seasonality of moderate and extreme precipitation events in the Alps. *Natural Hazards and Earth System Sciences*, *18*(7), pp.2047-2056.

Brooks, K.N., Ffolliott, P.F. and Magner, J.A., 2012. *Hydrology and the Management of Watersheds*. John Wiley & Sons.

Brunetti, M., Maugeri, M., Nanni, T., Auer, I., Böhm, R. and Schöner, W., 2006. Precipitation variability and changes in the greater Alpine region over the 1800–2003 period. *Journal of Geophysical Research: Atmospheres*, *111*(D11).

Bui, M.T., Lu, J. and Nie, L., 2020. A Review of Hydrological Models Applied in the Permafrost-Dominated Arctic Region. *Geosciences*, *10*(10), p.401.

Cess, R.O., Potter, G.L., Zhang, M.H., Blanchet, J.P., Chalita, S., Colman, R., Dazlich, D.A., Del Genio, A.D., Dymnikov, V., Galin, V. and Jerrett, D., 1991. Interpretation of snow-climate feedback as produced by 17 general circulation models. *Science*, *253*(5022), pp.888-892.

Chen, Y., Liu, A. and Moore, J.C., 2020. Mitigation of Arctic permafrost carbon loss through stratospheric aerosol geoengineering. *Nature communications*, *11*(1), pp.1-10.

Chiarle, M., Geertsema, M., Mortara, G. and Clague, J.J., 2021. Relations between climate change and mass movement: Perspectives from the Canadian Cordillera and the European Alps. *Global and Planetary Change*, p.103499.

Colombo, N., Salerno, F., Martin, M., Malandrino, M., Giardino, M., Serra, E., Godone, D., Said-Pullicino, D., Fratianni, S., Paro, L. and Tartari, G., 2019. Influence of permafrost, rock and ice glaciers on chemistry of high-elevation ponds (NW Italian Alps). *Science of the Total Environment*, *685*, pp.886-901.

Coon, E.T., 2016. ATS: The Advanced Terrestrial Simulator. *Github, avaialble at: https://github. com/amanzi/ats (last access: October 2019)*.

Coppola, E., Nogherotto, R., Ciarlo', J.M., Giorgi, F., van Meijgaard, E., Kadygrov, N., Iles, C., Corre, L., Sandstad, M., Somot, S. and Nabat, P., 2021. Assessment of the European climate projections as simulated by the large EURO-CORDEX regional and global climate model ensemble. *Journal of Geophysical Research: Atmospheres*, *126*(4), p.e2019JD032356.

Cunderlik, J., 2003. *Hydrologic model selection for the CFCAS project: assessment of water resources risk and vulnerability to changing climatic conditions*. Department of Civil and Environmental Engineering, The University of Western Ontario.

Dall'Amico, M., Endrizzi, S., Gruber, S. and Rigon, R.J.T.C., 2011. A robust and energy-conserving model of freezing variably-saturated soil. *The Cryosphere*, *5*(2), pp.469-484.

Dhami, B.S. and Pandey, A., 2013. Comparative review of recently developed hydrologic models. *J. Indian Water Resour. Soc*, *33*(3), pp.34-41.

Dickinson, R.E., 1993. Biosphere atmosphere transfer scheme (BATS) version 1e as coupled to the NCAR community climate model. *NCAR Tech. Note TH-387+ STR*.

Dingman, S.L., 2015. *Physical hydrology*. Waveland press.

Dong, C., 2018. Remote sensing, hydrological modeling and in situ observations in snow cover research: A review. *Journal of Hydrology*, *561*, pp.573-583.

Doré, G., Niu, F. and Brooks, H., 2016. Adaptation methods for transportation infrastructure built on degrading permafrost. *Permafrost and Periglacial Processes*, *27*(4), pp.352-364.

Dramis, F., Govi, M., Guglielmin, M. and Mortara, G., 1995. Mountain permafrost and slope instability in the Italian Alps: the Val Pola landslide. *Permafrost and Periglacial Processes*, *6*(1), pp.73-81.

Duvillard, P.A., Ravanel, L., Marcer, M. and Schoeneich, P., 2019. Recent evolution of damage to infrastructure on permafrost in the French Alps. *Regional Environmental Change*, *19*(5), pp.1281-1293.

Endrizzi, S., 2007. Snow cover modelling at a local and distributed scale over complex terrain. *University of Trento, Trento, Italy*.

Endrizzi, S., Gruber, S., Dall'Amico, M. and Rigon, R., 2014. GEOtop 2.0: simulating the combined energy and water balance at and below the land surface accounting for soil freezing, snow cover and terrain effects. *Geoscientific Model Development*, *7*(6), pp.2831-2857.

Engel, M., Notarnicola, C., Endrizzi, S. and Bertoldi, G., 2017. Snow model sensitivity analysis to understand spatial and temporal snow dynamics in a high-elevation catchment. *Hydrological Processes*, *31*(23), pp.4151-4168.

Erbs, D.G., Klein, S.A. and Duffie, J.A., 1982. Estimation of the diffuse radiation fraction for hourly, daily and monthly-average global radiation. *Solar energy*, *28*(4), pp.293-302.

Etzelmüller, B., Guglielmin, M., Hauck, C., Hilbich, C., Hoelzle, M., Isaksen, K., Noetzli, J., Oliva, M. and Ramos, M., 2020. Twenty years of European mountain permafrost dynamics—the PACE legacy. *Environmental Research Letters*, *15*(10), p.104070.

Fitzharris, B.N., Allison, I., Braithwaite, R.J., Brown, J., Foehn, P.M.B., Haeberli, W., Higuchi, K., Kotlyakov, V.M., Prowse, T.D., Rinaldi, C.A. and Wadhams, P., 1996. The cryosphere: changes and their impacts. In *Climate Change 1995: Impacts, Adaptations and Mitigation of Climate Change: Contribution of Working Group II to the Second Assessment Report of the Intergovernmental Panel on Climate Change* (pp. 241-266). Cambridge University Press.

Flynn, M., Ford, J.D., Labbé, J., Schrott, L. and Tagalik, S., 2019. Evaluating the effectiveness of hazard mapping as climate change adaptation for community planning in degrading permafrost terrain. *Sustainability science*, *14*(4), pp.1041-1056.

Froese, D.G., Westgate, J.A., Reyes, A.V., Enkin, R.J. and Preece, S.J., 2008. Ancient permafrost and a future, warmer Arctic. *Science*, *321*(5896), pp.1648-1648.

Gao, H., Nie, N., Zhang, W. and Chen, H., 2020. Monitoring the spatial distribution and changes in permafrost with passive microwave remote sensing. *ISPRS Journal of Photogrammetry and Remote Sensing*, *170*, pp.142-155.

Gelfan, A., Motovilov, Y., Krylenko, I., Moreido, V. and Zakharova, E., 2015. Testing the robustness of the physically-based ECOMAG model with respect to changing conditions. *Hydrological Sciences Journal*, *60*(7-8), pp.1266-1285.

Gobiet, A., Kotlarski, S., Beniston, M., Heinrich, G., Rajczak, J. and Stoffel, M., 2014. 21st century climate change in the European Alps—A review. *Science of the Total Environment*, *493*, pp.1138-1151.

Goodison, B.E., Brown, R.D., Crane, R.G., Alley, R., Bales, R., Barber, D., Barry, R., Bentley, C., Carrol, T., Cline, D. and Duguay, C.R., 1999. Cryospheric systems. *EOS Science Plan: The State of Science in the EOS Program*, pp.261-307.

Gottardi, F., Obled, C., Gailhard, J. and Paquet, E., 2012. Statistical reanalysis of precipitation fields based on ground network data and weather patterns: Application over French mountains. *Journal of Hydrology*, *432*, pp.154-167.

Grachev, A.A. and Fairall, C.W., 1997. Dependence of the Monin–Obukhov stability parameter on the bulk Richardson number over the ocean. *Journal of Applied Meteorology*, *36*(4), pp.406-414.

Granberg, H.B. and Vachon, P.W., 1998, June. Delineation of discontinuous permafrost at Schefferville using RADARSAT in interferometric mode. In *Proceedings 7th International Conference on Permafrost, Yellowknife, Canada* (pp. 341-345).

Grossi, G., Lendvai, A., Peretti, G. and Ranzi, R., 2017. Snow precipitation measured by gauges: Systematic error estimation and data series correction in the central Italian Alps. *Water*, *9*(7), p.461.

Gruber, S. and Haeberli, W., 2007. Permafrost in steep bedrock slopes and its temperature-related destabilization following climate change. *Journal of Geophysical Research: Earth Surface*, *112*(F2).

Gruber, S. and Haeberli, W., 2009. Mountain permafrost. In *Permafrost soils* (pp. 33-44). Springer, Berlin, Heidelberg.

Gruber, S., 2012. Derivation and analysis of a high-resolution estimate of global permafrost zonation. *The Cryosphere*, *6*(1), pp.221-233.

Gubler, S., Gruber, S. and Purves, R.S., 2012. Uncertainties of parameterized surface downward clear-sky shortwave and all-sky longwave radiation. *Atmospheric chemistry and physics*, *12*(11), pp.5077-5098.

Güntner, A., 2008. Improvement of global hydrological models using GRACE data. *Surveys in geophysics*, *29*(4-5), pp.375-397.

Guyennon, N., Valt, M., Salerno, F., Petrangeli, A.B. and Romano, E., 2019. Estimating the snow water equivalent from snow depth measurements in the Italian Alps. *Cold Regions Science and Technology*, *167*, p.102859.

Haeberli, W. and Beniston, M., 1998. Climate change and its impacts on glaciers and permafrost in the Alps. *Ambio*, pp.258-265.

Haeberli, W., Schaub, Y. and Huggel, C., 2017. Increasing risks related to landslides from degrading permafrost into new lakes in de-glaciating mountain ranges. *Geomorphology*, *293*, pp.405-417.

Hall, D.K., 1988. Assessment of polar climate change using satellite technology. *Reviews of Geophysics*, *26*(1), pp.26-39.

Hauck, C., 2013. New concepts in geophysical surveying and data interpretation for permafrost terrain. *Permafrost and Periglacial Processes*, *24*(2), pp.131-137.

Hay, L.E., Clark, M.P., Pagowski, M., Leavesley, G.H. and Gutowski, W.J., 2006. One-way coupling of an atmospheric and a hydrologic model in Colorado. *Journal of Hydrometeorology*, *7*(4), pp.569-589.

Hayashi, M., Goeller, N., Quinton, W.L. and Wright, N., 2007. A simple heat-conduction method for simulating the frost-table depth in hydrological models. *Hydrological Processes: An International Journal*, *21*(19), pp.2610-2622.

He, H., Zhang, Q., Zhou, J., Fei, J. and Xie, X., 2009. Coupling climate change with hydrological dynamic in Qinling Mountains, China. *Climatic change*, *94*(3), pp.409-427.

Heilig, A., Schneebeli, M. and Eisen, O., 2009. Upward-looking ground-penetrating radar for monitoring snowpack stratigraphy. *Cold Regions Science and Technology*, *59*(2-3), pp.152-162.

Hock, R., 2003. Temperature index melt modelling in mountain areas. *Journal of hydrology*, *282*(1-4), pp.104-115.

Huscroft, C.A., Lipovsky, P., Bond, J.D., Emond, D.S. and Lewis, L.L., 2003. Permafrost and landslide activity: Case studies from southwestern Yukon Territory. *Yukon exploration and geology*, pp.107-119.

Iqbal, M., 2012. *An introduction to solar radiation*. Elsevier.

Jajarmizadeh, M., Harun, S. and Salarpour, M., 2012. A review on theoretical consideration and types of models in hydrology. *Journal of Environmental Science and Technology*, *5*(5), pp.249-261.

Jin X, Jin H, Wu X, Luo D, Yu S, Li X, He R, Wang Q, Knops JM. Permafrost degradation leads to biomass and species richness decreases on the Northeastern Qinghai-Tibet Plateau. Plants. 2020 Nov;9(11):1453.

Jonas, T., Marty, C. and Magnusson, J., 2009. Estimating the snow water equivalent from snow depth measurements in the Swiss Alps. *Journal of Hydrology*, *378*(1-2), pp.161-167.

Jordan, R., Albert, M. and Brun, E., 2008. Physical processes within the snow cover and their parameterization. *Snow and Climate: Physical Processes, Surface Energy Exchange and Modeling*, pp.12-69.

Jorgenson, M.T., Racine, C.H., Walters, J.C. and Osterkamp, T.E., 2001. Permafrost degradation and ecological changes associated with a warmingclimate in central Alaska. *Climatic change*, *48*(4), pp.551-579.

Jorgenson, M.T., Romanovsky, V., Harden, J., Shur, Y., O'Donnell, J., Schuur, E.A., Kanevskiy, M. and Marchenko, S., 2010. Resilience and vulnerability of permafrost to climate change. *Canadian Journal of Forest Research*, *40*(7), pp.1219-1236.

Kääb, A., 2008. Remote sensing of permafrost-related problems and hazards. *Permafrost and periglacial processes*, *19*(2), pp.107-136.

Kääb, A., Huggel, C., Fischer, L., Guex, S., Paul, F., Roer, I., Salzmann, N., Schlaefli, S., Schmutz, K., Schneider, D. and Strozzi, T., 2005. Remote sensing of glacier-and permafrost-related hazards in high mountains: an overview. *Natural Hazards and Earth System Sciences*, *5*(4), pp.527-554.

Kittler, F., Heimann, M., Kolle, O., Zimov, N., Zimov, S. and Göckede, M., 2017. Long-term drainage reduces CO2 uptake and CH4 emissions in a Siberian permafrost ecosystem. *Global Biogeochemical Cycles*, *31*(12), pp.1704-1717.

Kneisel, C., Hauck, C., Fortier, R. and Moorman, B., 2008. Advances in geophysical methods for permafrost investigations. *Permafrost and periglacial processes*, *19*(2), pp.157-178.

Kollet, S., Sulis, M., Maxwell, R.M., Paniconi, C., Putti, M., Bertoldi, G., Coon, E.T., Cordano, E., Endrizzi, S., Kikinzon, E. and Mouche, E., 2017. The integrated hydrologic model intercomparison project, IH-MIP2: A second set of benchmark results to diagnose integrated hydrology and feedbacks. *Water Resources Research*, *53*(1), pp.867-890.

Kotak, Y., Gul, M.S., Muneer, T. and Ivanova, S.M., 2015, April. Investigating the impact of ground albedo on the performance of PV systems. In *Proceedings of the CIBSE Technical Symposium, London, UK* (pp. 16-17).

Koussa, D.S., Koussa, M. and Hadji, S., 2014, March. Technical and economic study of a stand-alone wind energy system for mountainous rural area electrification in Algeria. In *2014 5th International Renewable Energy Congress (IREC)* (pp. 1-6). IEEE.

Li, F., Peng, Y., Natali, S.M., Chen, K., Han, T., Yang, G., Ding, J., Zhang, D., Wang, G., Wang, J. and Yu, J., 2017. Warming effects on permafrost ecosystem carbon fluxes associated with plant nutrients. *Ecology*, *98*(11), pp.2851-2859.

Lindner, F., Wassermann, J. and Igel, H., 2021. Seasonal freeze-thaw cycles and permafrost degradation on Mt. Zugspitze (German/Austrian Alps) revealed by single-station seismic monitoring. *Earth and Space Science Open Archive ESSOAr*.

Liston, G.E., 1999. Interrelationships among snow distribution, snowmelt, and snow cover depletion: Implications for atmospheric, hydrologic, and ecologic modeling. *Journal of Applied Meteorology and Climatology*, *38* (10), pp.1474-1487.

Luetschg, M., Lehning, M. and Haeberli, W., 2008. A sensitivity study of factors influencing warm/thin permafrost in the Swiss Alps. *Journal of Glaciology*, *54*(187), pp.696-704.

Lunardini, V.J., Heat Transfer in Cold Climates, 1981.

Mair, E., Leitinger, G., Della Chiesa, S., Niedrist, G., Tappeiner, U. and Bertoldi, G., 2016. A simple method to combine snow height and meteorological observations to estimate winter precipitation at sub-daily resolution. *Hydrological Sciences Journal*, *61*(11), pp.2050-2060.

Marty, C., 2008. Regime shift of snow days in Switzerland. *Geophysical research letters*, *35*(12).

Masuda, M., Yatagai, A., Kamiguchi, K. and Tanaka, K., 2019. Daily adjustment for wind-induced precipitation undercatch of daily gridded precipitation in Japan. *Earth and Space Science*, *6*(8), pp.1469-1479.

Matiu, M., Crespi, A., Bertoldi, G., Carmagnola, C.M., Marty, C., Morin, S., Schöner, W., Cat Berro, D., Chiogna, G., De Gregorio, L. and Kotlarski, S., 2021. Observed snow depth trends in the European Alps: 1971 to 2019. *The Cryosphere*, *15*(3), pp.1343-1382.

McGuire, A.D., Lawrence, D.M., Koven, C., Clein, J.S., Burke, E., Chen, G., Jafarov, E., MacDougall, A.H., Marchenko, S., Nicolsky, D. and Peng, S., 2018. Dependence of the evolution of carbon dynamics in the northern permafrost region on the trajectory of climate change. *Proceedings of the National Academy of Sciences*, *115*(15), pp.3882-3887.

Mewes, B., Hilbich, C., Delaloye, R. and Hauck, C., 2017. Resolution capacity of geophysical monitoring regarding permafrost degradation induced by hydrological processes. *The Cryosphere*, *11*(6), pp.2957-2974.

Meyer, C.R., Keegan, K.M., Baker, I. and Hawley, R.L., 2020. A model for French-press experiments of dry snow compaction. *The Cryosphere*, *14*(5), pp.1449-1458.

Motovilov, Y.G., Gottschalk, L., Engeland, K. and Belokurov, A., 1999. ECOMAG-regional model of hydrological cycle. Application to the NOPEX region.

Mulvany, T.J., 1850. On the use of self-registering rain and flood gauges. *Making Observations of the Relations of Rain Fall and Flood Discharges in a Given Catchment. Transactions and Minutes of the Proceedings of the Institute of Civil Engineers of Ireland, Dublin, Ireland, Session*, *1*.

Murton, J.B., 2021. Permafrost and climate change. In *Climate Change* (pp. 281-326). Elsevier.

Nan, Z.T., Li, S.X. and Liu, Y.Z., 2002. Mean annual ground temperature distribution on the Tibetan Plateau: permafrost distribution mapping and further application. *J. Glaciol. Geocryol*, *24*(2), pp.142-148.

Natali, S.M., Holdren, J.P., Rogers, B.M., Treharne, R., Duffy, P.B., Pomerance, R. and MacDonald, E., 2021. Permafrost carbon feedbacks threaten global climate goals. *Proceedings of the National Academy of Sciences*, *118*(21).

National Snow and Ice Data Center, 2020. *https://nsidc.org/cryosphere/snow/climate.html.* Accessed 10 September 2021.

Nelson, F.E. and Outcalt, S.I., 1987. A computational method for prediction and regionalization of permafrost. *Arctic and alpine research*, *19*(3), pp.279-288.

Noetzli, J., Gruber, S., Kohl, T., Salzmann, N. and Haeberli, W., 2007. Three-dimensional distribution and evolution of permafrost temperatures in idealized high-mountain topography. *Journal of Geophysical Research: Earth Surface*, *112*(F2).

Norbiato, D., Borga, M., Sangati, M. and Zanon, F., 2007. Regional frequency analysis of extreme precipitation in the eastern Italian Alps and the August 29, 2003 flash flood. *Journal of hydrology*, *345*(3-4), pp.149-166.

Oke, T.R., 2002. *Boundary layer climates*. Routledge.

Oldenborger, G.A. and LeBlanc, A.M., 2018. Monitoring changes in unfrozen water content with electrical resistivity surveys in cold continuous permafrost. *Geophysical Journal International*, *215*(2), pp.965-977.

Overduin, P.P., Westermann, S., Yoshikawa, K., Haberlau, T., Romanovsky, V. and Wetterich, S., 2012. Geoelectric observations of the degradation of nearshore submarine permafrost at Barrow (Alaskan Beaufort Sea). *Journal of Geophysical Research: Earth Surface*, *117*(F2).

Pall, P., Allen, M.R. and Stone, D.A., 2007. Testing the Clausius–Clapeyron constraint on changes in extreme precipitation under CO 2 warming. *Climate Dynamics*, *28*(4), pp.351-363.

Park, H., Fedorov, A.N., Zheleznyak, M.N., Konstantinov, P.Y. and Walsh, J.E., 2015. Effect of snow cover on pan-Arctic permafrost thermal regimes. *Climate Dynamics*, *44*(9), pp.2873-2895.

Park, H., Kim, Y. and Kimball, J.S., 2016. Widespread permafrost vulnerability and soil active layer increases over the high northern latitudes inferred from satellite remote sensing and process model assessments. *Remote Sensing of Environment*, *175*, pp.349-358.

Patton, A.I., Rathburn, S.L. and Capps, D.M., 2019. Landslide response to climate change in permafrost regions. *Geomorphology*, *340*, pp.116-128.

PermaNET Alpine Space, 2021. *http://www.permanet-alpinespace.eu/project.html.* Accessed 6 October 2021.

Pistocchi, A., 2016. Simple estimation of snow density in an Alpine region. *Journal of Hydrology: Regional Studies*, *6*, pp.82-89.

Qin, Z.Y., Xie, W.Z., Tong, B.L. and Xie, Y.Q., 1987. The relationship between plateau plants and melting soil-layer in the frozen season in Tnmen, Prefecture Xizang. *Journal of Glaciology and Geocryology*, *9*(2), pp.149-156.

Rasmussen, R., Baker, B., Kochendorfer, J., Meyers, T., Landolt, S., Fischer, A.P., Black, J., Thériault, J.M., Kucera, P., Gochis, D. and Smith, C., 2012. How well are we measuring snow: The NOAA/FAA/NCAR winter precipitation test bed. *Bulletin of the American Meteorological Society*, *93*(6), pp.811-829.

Rigon, R., Bertoldi, G. and Over, T.M., 2006. GEOtop: A distributed hydrological model with coupled water and energy budgets. *Journal of Hydrometeorology*, *7*(3), pp.371-388.

Robinson, D.A., Dewey, K.F. and Heim Jr, R.R., 1993. Global snow cover monitoring: An update. *Bulletin of the American Meteorological Society*, *74*(9), pp.1689-1696.

Romanovsky, V., Burgess, M., Smith, S., Yoshikawa, K. and Brown, J., 2002. Permafrost temperature records: Indicators of climate change. *EOS, Transactions American Geophysical Union*, *83*(50), pp.589-594.

Runyan, C.W. and D'Odorico, P., 2012. Ecohydrological feedbacks between permafrost and vegetation dynamics. *Advances in Water Resources*, *49*, pp.1-12.

Scherrer, S.C., Wüthrich, C., Croci-Maspoli, M., Weingartner, R. and Appenzeller, C., 2013. Snow variability in the Swiss Alps 1864–2009. *International journal of climatology*, *33*(15), pp.3162-3173.

Schneider, S., Hoelzle, M. and Hauck, C., 2012. Influence of surface and subsurface heterogeneity on observed borehole temperatures at a mountain permafrost site in the Upper Engadine, Swiss Alps. *The Cryosphere*, *6*(2), pp.517-531.

Schramm, I., Boike, J., Bolton, W.R. and Hinzman, L.D., 2007. Application of TopoFlow, a spatially distributed hydrological model, to the Imnavait Creek watershed, Alaska. *Journal of Geophysical Research: Biogeosciences*, *112*(G4).

Schuur, E.A., McGuire, A.D., Schädel, C., Grosse, G., Harden, J.W., Hayes, D.J., Hugelius, G., Koven, C.D., Kuhry, P., Lawrence, D.M. and Natali, S.M., 2015. Climate change and the permafrost carbon feedback. *Nature*, *520*(7546), pp.171-179.

Sebben, M.L., Werner, A.D., Liggett, J.E., Partington, D. and Simmons, C.T., 2013. On the testing of fully integrated surface–subsurface hydrological models. *Hydrological Processes*, *27*(8), pp.1276-1285.

Sellman, P.V., Chamberlain, E.J., Delaney, A.J. and Neave, K.G., 1980. *Delineation and engineering characteristics of permafrost beneath the Beaufort Sea*. US Army Corps of Engineers, Cold Regions Research and Engineering Laboratory.

Seppi, R., Carturan, L., Carton, A., Zanoner, T., Zumiani, M., Cazorzi, F., Bertone, A., Baroni, C. and Salvatore, M.C., 2019. Decoupled kinematics of two neighbouring permafrost creeping landforms in the Eastern Italian Alps. *Earth Surface Processes and Landforms*, *44*(13), pp.2703-2719.

Serreze, M.C., Bromwich, D.H., Clark, M.P., Etringer, A.J., Zhang, T. and Lammers, R., 2002. Large-scale hydro-climatology of the terrestrial Arctic drainage system. *Journal of Geophysical Research: Atmospheres*, *107*(D2), pp.ALT-1.

Shaw, E., 2005. *Hydrology in practice*. CRC press.

Shi, Y., Davis, K.J., Duffy, C.J. and Yu, X., 2013. Development of a coupled land surface hydrologic model and evaluation at a critical zone observatory. *Journal of Hydrometeorology*, *14*(5), pp.1401-1420.

Smith, M.W. and Riseborough, D.W., 1996. Permafrost monitoring and detection of climate change. *Permafrost and periglacial processes*, *7*(4), pp.301-309.

Sommer, C., Malz, P., Seehaus, T.C., Lippl, S., Zemp, M. and Braun, M.H., 2020. Rapid glacier retreat and downwasting throughout the European Alps in the early 21 st century. *Nature communications*, *11*(1), pp.1-10.

Stocker-Mittaz, C., Hoelzle, M. and Haeberli, W., 2002. Modelling alpine permafrost distribution based on energy-balance data: a first step. *Permafrost and Periglacial Processes*, *13*(4), pp.271-282.

Stoffel, M., Tiranti, D. and Huggel, C., 2014. Climate change impacts on mass movements—case studies from the European Alps. *Science of the Total Environment*, *493*, pp.1255-1266.

Sturm, M., Holmgren, J., König, M. and Morris, K., 1997. The thermal conductivity of seasonal snow. *Journal of Glaciology*, *43*(143), pp.26-41.

Sudakova, M., Sadurtdinov, M., Skvortsov, A., Tsarev, A., Malkova, G., Molokitina, N. and Romanovsky, V., 2021. Using Ground Penetrating Radar for Permafrost Monitoring from 2015–2017 at CALM Sites in the Pechora River Delta. *Remote Sensing*, *13*(16), p.3271.

Swenson, S.C., Lawrence, D.M. and Lee, H., 2012. Improved simulation of the terrestrial hydrological cycle in permafrost regions by the Community Land Model. *Journal of Advances in Modeling Earth Systems*, *4*(3).

Terzago, S., Andreoli, V., Arduini, G., Balsamo, G., Campo, L., Cassardo, C., Cremonese, E., Dolia, D., Gabellani, S., von Hardenberg, J. and Morra di Cella, U., 2020. Sensitivity of snow models to the accuracy of meteorological forcings in mountain environments. *Hydrology and Earth System Sciences*, *24*(8), pp.4061-4090.

Turco, M., Zollo, A.L., Ronchi, C., Luigi, C.D. and Mercogliano, P., 2013. Assessing gridded observations for daily precipitation extremes in the Alps with a focus on northwest Italy. *Natural Hazards and Earth System Sciences*, *13*(6), pp.1457-1468.

Van Doninck, 2018. *https://rdrr.io/cran/horizon/man/horizon-package.html.* Accessed 3 June 2021.

Vautard, R., Yiou, P., D'andrea, F., De Noblet, N., Viovy, N., Cassou, C., Polcher, J., Ciais, P., Kageyama, M. and Fan, Y., 2007. Summertime European heat and drought waves induced by wintertime Mediterranean rainfall deficit. *Geophysical Research Letters*, *34*(7).

Vonk, J.E., Tank, S.E., Bowden, W.B., Laurion, I., Vincent, W.F., Alekseychik, P., Amyot, M., Billet, M.F., Canário, J., Cory, R.M. and Deshpande, B.N., 2015. Reviews and syntheses: Effects of permafrost thaw on Arctic aquatic ecosystems. *Biogeosciences*, *12*(23), pp.7129-7167.

Vorosmarty, C.J., Hinzman, L., Peterson, B., Bromwich, D., Hamilton, L.C., Morison, J., Romanovsky, V., Sturm, M. and Webb, R., 2001. The hydrologic cycle and its role in arctic and global environmental change: a rationale and strategy for synthesis study.

Vuille, M., Francou, B., Wagnon, P., Juen, I., Kaser, G., Mark, B.G. and Bradley, R.S., 2008. Climate change and tropical Andean glaciers: Past, present and future. *Earth-science reviews*, *89*(3-4), pp.79-96.

Walker, D.A., Jia, G.J., Epstein, H.E., Raynolds, M.K., Chapin Iii, F.S., Copass, C., Hinzman, L.D., Knudson, J.A., Maier, H.A., Michaelson, G.J. and Nelson, F., 2003. Vegetation-soil-thaw-depth relationships along a low-Arctic bioclimate gradient, Alaska: Synthesis of information from the ATLAS studies. *Permafrost and Periglacial Processes*, *14*(2), pp.103-123.

Walvoord, M.A. and Kurylyk, B.L., 2016. Hydrologic impacts of thawing permafrost—A review. *Vadose Zone Journal*, *15*(6), pp.vzj2016-01.

Walvoord, M.A., Voss, C.I. and Wellman, T.P., 2012. Influence of permafrost distribution on groundwater flow in the context of climate-driven permafrost thaw: Example from Yukon Flats Basin, Alaska, United States. *Water Resources Research*, *48*(7).

Wani, J.M., Thayyen, R.J., Ojha, C.S.P. and Gruber, S., 2021. The surface energy balance in a cold and arid permafrost environment, Ladakh, Himalayas, India. *The Cryosphere*, *15*(5), pp.2273-2293.

Westermann, S., Lüers, J., Langer, M., Piel, K. and Boike, J., 2009. The annual surface energy budget of a high-arctic permafrost site on Svalbard, Norway. *The Cryosphere*, *3*(2), pp.245-263.

Winkler, M., Schellander, H. and Gruber, S., 2021. Snow water equivalents exclusively from snow depths and their temporal changes: the Δ snow model. *Hydrology and Earth System Sciences*, *25*(3), pp.1165-1187.

Winkler, M., Schellander, H., 2021. *https://cran.r-project.org/web/packages/nixmass/index.html.* Accessed 2 October 2021.

Woo, M.K., Kane, D.L., Carey, S.K. and Yang, D., 2008. Progress in permafrost hydrology in the new millennium. *Permafrost and Periglacial Processes*, *19*(2), pp.237-254.

Yang, Z.P., Ou, Y.H., Xu, X.L., Zhao, L., Song, M.H. and Zhou, C.P., 2010. Effects of permafrost degradation on ecosystems. *Acta Ecologica Sinica*, *30*(1), pp.33-39.

Yasutomi, N., Hamada, A. and Yatagai, A., 2011. Development of a long-term daily gridded temperature dataset and its application to rain/snow discrimination of daily precipitation. *Global Environmental Research*, *15*(2), pp.165-172.

Yi, S., Woo, M.K. and Arain, M.A., 2007. Impacts of peat and vegetation on permafrost degradation under climate warming. *Geophysical Research Letters*, *34*(16).

Yokoyama, K., Ohno, H., Kominami, Y., Inoue, S. and Kawakata, T., 2003. Performance of Japanese precipitation gauges in winter. Seppyo, 65, 303-316. In *Japanese with English abstract*.

Yu, Z., Pollard, D. and Cheng, L., 2006. On continental-scale hydrologic simulations with a coupled hydrologic model. *Journal of Hydrology*, *331*(1-2), pp.110-124.

Zanotti, F., Endrizzi, S., Bertoldi, G. and Rigon, R., 2004. The GEOTOP snow module. *Hydrological Processes*, *18*(18), pp.3667-3679.

Zappa, M. and Kan, C., 2007. Extreme heat and runoff extremes in the Swiss Alps. *Natural Hazards and Earth System Sciences*, *7*(3), pp.375-389.

Zeinivand, H. and De Smedt, F., 2009. Hydrological modeling of snow accumulation and melting on river basin scale. *Water resources management*, *23*(11), pp.2271-2287.

Zeinivand, H. and De Smedt, F., 2010. Prediction of snowmelt floods with a distributed hydrological model using a physical snow mass and energy balance approach. *Natural hazards*, *54*(2), pp.451-468.

Zhang, T., Frauenfeld, O.W., Serreze, M.C., Etringer, A., Oelke, C., McCreight, J., Barry, R.G., Gilichinsky, D., Yang, D., Ye, H. and Ling, F., 2005. Spatial and temporal variability in active layer thickness over the Russian Arctic drainage basin. *Journal of Geophysical Research: Atmospheres*, *110*(D16).

Zhang, T., Heginbottom, J.A., Barry, R.G. and Brown, J., 2000. Further statistics on the distribution of permafrost and ground ice in the Northern Hemisphere. *Polar geography*, *24*(2), pp.126-131.

Zhang, Y., Chen, W. and Cihlar, J., 2003. A process-based model for quantifying the impact of climate change on permafrost thermal regimes. *Journal of Geophysical Research: Atmospheres*, *108*(D22).